University of Bayreuth,
Dept. of Micrometeorology

Research Institute of
Organic Agriculture,
Dept. of Soil Sciences

Master thesis in Geoecology

Application of ^{15}N labelled slurry in a microplot field study: Ammonia volatilization and plot N balance

by
Michael Cormann

Bayreuth, 29th January 2020

First Supervisor: Dr. Wolfgang Babel, Micrometeorology, University of Bayreuth
Second Supervisor: Dr. Else Bünemann, Soil Sciences, FiBL
                     Hanna Frick, Soil Sciences, FiBL

Figure 0.1: An overview of the experimental setup at 31/07/2018 during the third NH$_3$ sampling sequence (G3) on the grass-clover field (Field B)

Abstract

Understanding the dynamics and losses of fertilizer N in agroecosystems is crucial to optimize efficieny and reduce environmental impacts conventional and organic cropping systems. Leaching of excess NO_3^--N below the rooting depth can endanger ground- and drinking water resources. Volatilization of NH_3-N contributes to the formation of fine particulate matter, and impacts plant diversity and community structure when deposited on vulnerable ecosystems. In a microplot field experiment in the canton of Solothurn, Switzerland, NH_3 losses after five applications of cattle slurry or ammonia nitrate fertilizer, as well as from a $0\,N$ control, on a maize and a grass-clover field were measured using the Standard Comparison Method (SCM). Transport of NH_3 after volatilization, being represented by the SCM transfer factors, is dependent on the meteorological conditions. It was tested if linear models based on standard meteorological parameters can map and temporarily replace SCM transfer factors in order to reduce the effort of simultaneous Standard Flux Reference (SFR) measurements. Further, it was assessed if adding data on gaseous NH_3 losses to tracing the fate of ^{15}N-labelled fertilizer can contribute to closing the plot N balance. For two sampling sequences following slurry application, SCM transfer factor data gaps had to be closed by meteorology-based model predictions. Resulting NH_3 fluxes and cumulative losses were comparable to values reported in the literature and to the recent ALFAM2 model. Parameter sets and their p-values as well as accuracy and predictive power, evaluated by the Nash-Sutcliffe model efficiency coefficient (NSE), strongly differed between optimized model fits. Models calibrated on a combination of data from multiple sampling sequences could, according to the NSE and with one exception, not successfully predict transfer factors of the respective test sampling sequences. These results indicate that we did not use enough or the right type of calibration data, or that linear models are not suited to represent the meteorological processed driving SCM transfer factor dynamics. For the grass-clover-field, measured gaseous losses of NH_3 reduced the amount of fertilizer N not accounted for by ^{15}N recoveries. For the maize field, NH_3 losses overcompensated the N balance gap of slurry-fertilized plots, which could be explained by systematic overestimation of soil ^{15}N recoveries, as an overestimation of NH_3 volatilization is unlikely.

Zusammenfassung

Das Verständnis der Umsätze und Verluste von Düngerstickstoff (N) in Agrarökosystemen ist entscheidend, um die Nährstoffnutzung in organischen und konventionellen Landbausystemen zu optimieren und ihre negativen Umweltauswirkungen zu minimieren. Die Auswaschung von NO_3^--N aus dem Wurzelbereich hinaus gefährdet Grund- und Trinkwasserressourcen. Volatilisiertes NH_3-N führt zu Feinstaubbildung und beeinflusst die Biodiversität und Pflanzengemeinschaft von gefährdeten Ökosystemen. In einem Mikroplot-Feldexperiment im Kanton Solothurn, Schweiz, wurden auf Kleegras/Kunstwiese und Mais fünf Ausbringungen von Rindergülle und Ammoniumnitrat durchgeführt. Mit der Standard Comparison Method (SCM) wurde anschließend die NH_3-Volatilisierung von gedüngten und $0\,N$-Kontrollplots gemessen. Der Transport des volatilisierten NH_3 wird in der SCM durch Transferfaktoren ausgedrückt und ist abhängig von den meteorologischen Verhältnissen. Auf meteorologischen Standardparametern basierende, optimierte lineare Modelle könnten den Verlauf der Transferfaktoren abbilden und zeitweise ersetzen, um den Aufwand für parallele Referenzmessungen zu verringern. Auch könnte die Kombination von NH_3-Volatilisierungsmessungen mit einer ^{15}N-Markierung des Düngers das Aufstellen einer geschlossenen Plot-N-Bilanz ermöglichen. Während zwei Probenahmefolgen konnten fehlende Transferfaktoren durch Modellvorhersagen aus meteorologischen Daten ersetzt werden. Die resultierenden NH_3-Flüsse und kumulative Verluste sind mit Literaturwerten und Vorhersagen aus dem ALFAM2-Modell vergleichbar. Die p-Werte und der Vorhersagequalität der Modelle, die mittels des Nash-Sutcliffe-Koeffizienten für Modelleffizienz (NSE) untersucht wurde, unterschieden sich stark. Modelle, die auf kombinierten Daten aus verschiedenen Probenahmefolgen angepasst wurden konnten die Transferfaktoren der jeweiligen Testdaten mit einer Ausnahme nicht erfolgreich vorhersagen. Diese Ergebnisse legen nahe dass die Menge oder die Art der verwendeten Daten oder die Art der Modelle nicht geeignet war um die relevanten meteorologischen Prozesse abzubilden. Für Kleegras konnten Messungen der NH_3-Verluste die nicht wieder gefundene Menge an ^{15}N kompensieren, während sie im Fall des mit Rindergülle gedüngten Mais die N-Bilanzlücke überstiegen. Da zu hohe Werte für die Volatilisierung von NH_3 unwahrscheinlich sind, ist die systematische Überschätzung der ^{15}N-Wiederfindung eine mögliche Erklärung.

Contents

List of Figures

List of Tables

List of abbreviations

Symbol	Meaning	Value	Unit
b	Model transfer parameter		
Con	0 N control treatment		
c_p	Specific heat at constant pressure	1004.834	$\mathrm{J\,K^{-1}\,kg^{-1}}$
c_x	Concentration of a quantity x		$\mathrm{mg\,L^{-1}}$
d	Passive sampler exposure time		min
D	Soil layer depth		cm
e	Euler's number	2.71828	
e	Actual vapour pressure		hPa
E	Saturation vapour pressure		hPa
f	Transfer factor		$\mathrm{mg\,L^{-2}}$
F	Gas volume flux		$\mathrm{L\,min^{-1}}$
g	Local gravity of the earth	9.81	$\mathrm{m\,s^{-2}}$
γ	Psychrometric constant	0.667	$\mathrm{hPa\,K^{-1}}$
H_2SO_4	Sulphuric acid		
I	Meteorological model input variable		
K	Potassium		
Min	Mineral fertilizer treatment		
$m_{\mathrm{NH_3/N}}$	Mass of volatilized NH_3 or NH_3-N		g
$M_{\mathrm{NH_3/N}}$	Molar or atomic mass of NH_3 or N, respectively		$\mathrm{g\,mol^{-1}}$
N/N_2	Nitrogen		
NH_3	Ammonia		
NH_4^+	Ammonium		
NO_3^-	Nitrate		
Ndff	Absolute amount of fertilizer-derived N		
%Ndff	relative fraction of fertilizer-derived N		%
p	Air pressure		hPa

P	Phosphorus		
rH	Relative humidity		%
ρ_B	Soil layer bulk density		$\mathrm{g\,cm^{-3}}$
Ri	Bulk Richardson number		°C
R_l	Gas constant for dry air	287.058	$\mathrm{J\,kg^{-1}\,K^{-1}}$
R_n	Universal gas constant	8.314 46	$\mathrm{J\,mol^{-1}\,K^{-1}}$
s	Soil layer skeletal content		%
S	Passive sampler NH$_3$ concentration flux		$\mathrm{mg\,L^{-1}\,min^{-1}}$
SCM	Standard Comparison Method		%
SFR	Standard Flux Reference		%
Slu	Slurry fertilizer treatment		
T	Temperature		K
t	Temperature		°C
TAN	Total Ammoniacal Nitrogen		
Θ	Potential temperature		°C
Θ_v	Virtual potential temperature		°C
v, u	Wind speed		$\mathrm{m\,s^{-1}}$
$\tilde{x}$	Median of quantity x		
$\bar{x}$	temporal average of quantity x		
$<x>$	spatial average of quantity x		
z	Measuring height above ground		m

1 Introduction

Naturally, reactive nitrogen (N) available for plant uptake is scarce in the environment, and thus is a limiting factor for plant growth and food production in terrestrial ecosystems (Erisman et al., 2013; Robertson and Groffman, 2015). Transformations between the various forms of reactive N in ecosystems are mostly mediated by soil microorganisms (Robertson and Groffman, 2015), which has implications for the behaviour of reactive N in the ecosystem. Some N species are mobile in soils and thus prone to leaching (nitrate, NO_3^-), while others can escape the ecosystem in a gaseous state (ammonia, NH_3 and ammonium, NH_4^+). Another part of reactive N is bound to C-rich molecules as organic N (Robertson and Vitousek, 2009).

Natural ecosystems have developed to efficiently use and re-use reactive N (Robertson and Groffman, 2015; Erisman et al., 2013). The most important natural process making the inert N_2 of the earth's atmosphere ($\sim 78\,\%$) available to organisms by converting it into reactive N is biological nitrogen fixation (Galloway, 1998). This is mostly performed by free-living microbes or plant root symbionts like the *Rhizobium* bacteria in the case of legumes, which can be used as a source of organic N in cropping systems (Robertson and Vitousek, 2009). By the invention of the Haber-Bosch process in 1908, it has become possible to industrially fix atmospheric nitrogen for the production of synthetic N fertilizers (Appl, 1982; Smil, 2004). This led to an unprecedented increase in agricultural yields, sustained by a dramatically increasing use of artificial N inputs (Galloway, 1998), while nutrient losses have increased as well. The amount of N ultimately consumed by humans as food is 10 times smaller than the amount used for its production (Robertson and Vitousek, 2009). The global N cycle is disturbed by an unintended cascade of N emissions and reactions caused by an excess of reactive N in the enviroment (Hansen et al., 2017). Pollution of aquifers as a result of leaching of excess nitrate (NO_3^-) N from agricultural land has become a common picture, which ultimately can affect human health if the groundwater is used as drinking water (Hansen et al., 2017). Drinking water resources threatened to exceed the maximum standard level of 50 mg/l in the European Union (European Parliament, 2006) and 40 mg/l in Switzerland (Schweizerische Eidgenossenschaft, 1998) pose significant economic risks to water suppliers (Oelmann et al., 2017).

In times of low energy and synthetic fertilizer prices, conventional farmers' economic incentives to increase N use efficency and reduce N losses are low (Ziesemer, 2007). Nevertheless, anticipation of rising fossil fuel prices as well as increasingly strict sustainability requirements and legislation makes closing the agricultural N cycle an important task. This is especially true for organic farmers that rely on N input from biological N fixation. For closing the N cycle, efficient recycling of N contained in lifestock excreta and organic wastes for plant uptake is the crucial step (Jensen, 2013).

Manure, composts and organic mulches contain organic and inorganic N. Applied to soil, fertilizer N enters a mineralization - immobilization turnover (MIT) cycle driven by microorganisms (Jensen, 2013; Robertson and Groffman, 2015). Inorganic N, if not directly taken up by plant roots, volatilized as ammonia (NH_3) or leached down in the soil column below the rooting depth, is for the most part immobilized in the biomass of microorganisms and thus is not available for plant growth. Simultaneously, organic fertilizer N is broken down by microorganisms according to the degradability of the fertilizer compound. By the death of microorganisms, inorganic N is released from microbial biomass. This temporary immobilization and delayed release of mineral N compromises the synchronisation between N supply and crop N demand, which makes it difficult to ensure high N use efficiency when using manure as a source of N for crops (Jensen, 2013). Late mineralization, when crop N uptake is low, may lead to leaching of NO_3^-. Understanding these transformations is crucial for sustainable management of agroecosystems (Robertson and Groffman, 2015).

Intensive use of N fertilizers also leads to an increase in NH_3 emissions. It is mainly released and volatilized during the decomposition of manure and organic matter, but also, to a lesser extent, by degradation of synthetic fertilizers (i.e. urea) after application (Schneidemesser et al., 2016). In the atmosphere, NH_3 is highly reactive and a precursor gas for the formation of secondary inorganic aerosols. NH_3 emissions from agriculture are responsible for 10 - 20% of fine particulate matter in urban areas and even more in areas with intensive lifestock farming. As secondary inorganic aerosols remain in the atmosphere for several days, they can be transported over long distances of several hundreds of kilometers (Ferm, 1998; Asman and Sutton, 1998) and deposited in remote areas. Especially plant species diversity and composition of communities adapted to nutrient-poor conditions can be affected by soil acidification, direct toxic damage to leafs, increasing plant vulnerability to external stress and outcompetition by fast-growing species adapted to high nutrient availability (Guthrie et al., 2018).

Losses of N from organic fertilizer, especially animal slurry and manure, by volatilization of NH_3 after field application are highly variable. Environmental conditions like air and soil temperature, wind speed, vegetation cover and soil properties, as well as slurry properties and application technique and management strongly influence the intensity of NH_3 losses (Asman and Sutton, 1998; Meisinger and Jokela, 2000; Sommer and Hutchings, 2001). Volatilization of NH_3 depends on the equilibrium between the concentration of NH_3 in the air close to the manured soil surface and the concentration of NH_3 dissolved in the manure as well as the time of manure exposure to the ambient air (Meisinger and Jokela, 2000). The amount of NH_3 readily available for volatilization depends on the partitioning of the total ammoniacal N (TAN) contained in the manure into NH_4^+-N and NH_3-N, which is a strongly pH-dependent equilibrium (Sommer and Hutchings, 2001). The equilibrium between these two species is shifted towards NH_3 at high pH values of the manure.

Wind speed and solar radiation are the drivers of turbulent transport and advection of the NH_3 away from the manure surface (Sommer and Hutchings, 2001; Meisinger and Jokela, 2000). At high wind speeds, often factors other than the atmospheric transport limit emission (Sommer and Hutchings, 2001). Animal species, N excess in feeding, use of bedding, and manure storage management influence the TAN content of the manure (Meisinger and Jokela, 2000). Evaporation of manure water due to high temperatures and wind speeds can increase manure TAN concentration and increase the risk of NH_3 losses. Conversely, dilution by rainfall can decrease volatilization of NH_3 at the soil surface by reducing TAN concentration and promoting transport of NH_3 into the soil matrix. Soil infiltration benefits from low soil humidity and low manure dry matter content and viscosity. The application method influences the time and extent to which the manure is exposed to the air and hence also influences the emission (Asman and Sutton, 1998). Injection, narrow band application, or cultivation after application significantly reduces NH_3 losses and can increase yields (Meisinger and Jokela, 2000). Timing of application in conditions less favorable for NH_3 volatilization like in spring or fall, in the late afternoon, or before rain can be used to reduce emissions (Asman and Sutton, 1998; Sommer and Hutchings, 2001).

In the case of cattle slurry, NH_3 volatilization frequently accounts for 35 - 70 % of TAN contained in the slurry (Meisinger and Jokela, 2000).

For investigating gaseous trace gas fluxes from the surface, micrometeorological and enclosure approaches can be distinguished. Enclosure or chamber methods sample the rise of trace gas concentration in a known and confined volume of air above the source in a known period. However, for NH_3, micrometeorological methods are preferable. This is because NH_3 is a sticky

compound towards measurement device surfaces (Pacholski et al., 2006; Sintermann et al., 2011) and chambers heavily disturb the NH_3 air-surface equilibrum that is determined by meteorological parameters such as wind speed, temperature, humidity and radiation (Loubet et al., 2018; Sommer and Hutchings, 2001; Sommer et al., 1991). Additionally, trace gas transport is dependent on the intensity of turbulence and atmospheric stratification, expressed by atmospheric stability (Foken and Napo, 2016; Baldocchi et al., 1988). Micrometeorological methods relate instantaneous or mean quantities of trace gas concentration in the air above or downwind of the source area to the trace gas flux density at the source, using information about the conditions and mechanisms of atmospheric transport (Baldocchi et al., 1988).

The disadvantage of most micrometeorological approaches is their need for expensive and complex sensor equipment, large field sizes, and in-depth micrometeorological knowledge. For example, the widely used IHF (Denmead, 1983) and ZINST (Wilson et al., 1982) approach as well as recent methods using fast-response sensors (Sintermann et al., 2016; Sintermann et al., 2011) require homogeneous field plot diameters of several dozens of meters.

Simple, micrometeorological methods for characterizing NH_3 emissions from very small plot or microplot experiments are scarce. Recently, modelling approaches using a backwards Lagrangian Stochastic Dispersion model and passive samplers have become more popular (Flesch et al., 1995; Flesch et al., 2004; Sommer et al., 2005; Yang et al., 2017), but are intensive in knowledge and equipment (Pacholski, 2016). Other approaches use the concept of calibrated transfer factors that relate qualitative passive sampler measurements on each plot to reference measurements performed on some plots of the same experiment (Vandré and Kaupenjohann, 1998; Pacholski, 2016) or to standard calibrations derived under model conditions that do not take into account local conditions of turbulent atmospheric transport (Pacholski et al., 2006). Wind tunnels can be seen as a compromise between allowing for ambient meteorological conditions and controlling the air flow over the source area (Lockyer, 1984).

The Standard Comparison Method (SCM), presented by Vandré and Kaupenjohann (1998), is a method developed to easily measure NH_3 emissions from very small plots, the authors used plot sizes of $2\,m$ by $2\,m$. It is based on the placement of passive acid diffusion samplers in the middle of each experimental plot and of equally sized standard reference plots which are equipped with an outgassing tube system providing a constant, known NH_3 flux. Fluxes from experimental plots are calculated by comparing passive sampler acid solution NH_4^+ concentrations found on standard and experimental plots, assuming homogeneity of atmospheric transport conditions for all plots. It can be easily adjusted to higher numbers of plots, does not necessarily require meteorological

measurements and does not involve extensive handling of complex micrometeorological data and theory. Adjustment to larger plot sizes, however, proved to be difficult (Gericke et al., 2011). Furthermore, the logistics of running a reference outgassing system including gas cylinders and pressure valves controlling concentrated, corrosive and hazardous NH_3 gas, maintaining the carrier gas source and tube system and ensuring a constant gas outflux includes some complexity and effort. According to Wulf et al. (2002), meteorological conditions have a direct effect on the transfer of NH_3 from the tube system to the passive sampler and explain more than 74% of the temporal variability of the transfer factors. For replicated NH_3 flux measurements at the same site, it would certainly be a relief if it was possible to calibrate the SC method for the specific meteorological conditions at the site including local inhomogeneities. By modelling the transport efficiency between the NH_3 source area and the passive sampler as a function of meteorological parameters, the use of a reference outgassing system could be restricted in time, especially for repeated measurements at the same site.

Since the 1980s, groundwater of the Gäu-Olten region in the Swiss canton of Solothurn faces NO_3^- pollution above the Swiss drinking water quality threshold of 25 mg/l (Hunkeler et al., 2015; Schweizerische Eidgenossenschaft, 1998). After the tolerance NO_3^- threshold of 40 mg/l (Schweizerische Eidgenossenschaft, 1998) was almost reached at some wells in the 1990s, the nitrate project Gäu-Olten was initiated in 1999. It is designed to reduce NO_3^- leaching from agricultural land by adopting improved management practices (Hunkeler et al., 2015). Now, after more than 15 years, the NitroGäu research project evaluates the effectiveness of these measures and aims to propose further improvements.

For one of the work packages in the NitroGäu project, a soil-system N balance including N additions from cattle slurry and mineral fertilizer, N-uptake and removal by typical crops of the region, residual N in the soil as well as N losses through NO_3^- leaching and NH_3 volatilization will be established in a microplot field study over a period of 2.5 years (Frick et al., 2018). The fate and transformations of nutrients added to the plant-soil system are evaluated using an ^{15}N isotope enrichment method (Douxchamps et al., 2011; Di et al., 2000; Dittert et al., 1998). NO_3^- leaching is tracked per cropping season by self-integrating accumulators (SIAs) buried under the rootable space of the soil column (Bischoff, 2008; Frick et al., 2018) and ^{15}N enrichment is assessed in soil and plant samples taken after and at the harvest, respectively, as well as in SIA samples in order to establish a soil-plant system N balance together with data on NH_3 volatilization (Frick et al., 2018).

Objectives

As part of a PhD thesis on manure management within the NitroGäu framework (Frick et al., 2018), the aim of this study is to provide data on gaseous N loss through volatilization of NH_3 from cattle slurry and mineral fertilizer (ammonium nitrate) in a microplot field experiment established on two field sites cropped with maize and grass-clover, respectively. This data was obtained during five field campaigns during the summer of 2018 using the SCM (Vandré and Kaupenjohann, 1998).

Further, it was assessed if for this specific field experiment, modelling of the transport efficiency between the NH_3 source area and the passive samplers is feasible. The question is which set of meteorological parameters is most reasonable to use, and if the data obtained during the field experiment is sufficient to calibrate such a model. In order to do so, models were optimized in order to be parsimonious in their parametrization but still provide a high quality of prediction. Also, it was tested if these models can successfully predict the atmospheric transport efficiency during NH_3 sampling sequences that they were or were not calibrated for.

Additionally, NH_3 volatilization from the field experiment was compared to the plot nitrogen balance during the cropping season of 2018, including inputs of slurry and mineral fertilizer N, as well as uptake by crops and removal by harvest, and incorporation into soil N pools. Collection of this data by a ^{15}N labelling approach was not part of this study, but was provided by the superordinate PhD thesis on manure management (Frick et al., 2018).

2 Hypotheses

In order to meet the objectives, I hypothesize:

1. Volatilization of NH_3 from the experimental plots as determined using the Standard Comparison Method (SCM) is greater for cattle slurry than for ammonium nitrate, and within the range reported in the available literature.

2. Efficiency of the transport of NH_3 from the plot surface into the passive diffusion sampler acid solution, expressed by the transfer factors of the SCM, can be represented by a meteorology-based model.

3. Running a standard flux reference (SFR) system during SCM measurements of NH_3 emissions can be partially replaced by predicting transfer factors by a meteorology-based model calibrated with data from the residual sampling sequences.

4. Determining NH_3 volatilization after slurry application contributes, together with data on soil N pool and plant N uptake, to closing the microplot N balance.

3 Material and methods

3.1 Field experiment

3.1.1 Field site

The field site is located in the Gäu-Olten region in the canton of Solothurn, Switzerland. A 2.5 year field experiment is conducted on two adjacent fields (see Figure 3.1) owned and used by a dairy farmer. During the cropping season of 2018, they were cropped with silage maize (Field A) and a grass clover ley in its fourth year (Field B). The crop rotation for both fields is shown in Figure 3.2. Agricultural management on the experimental plots is mainly conducted by the farmer. Otherwise, in order not to disturb the experimental setting, soil preparation was performed manually by the research team according to the practice elsewhere on the field. Three different fertilization treatments were tested in this experiment: ^{15}N-labelled cattle slurry (Slu), ^{15}N-labelled mineral fertilizer (ammonium nitrate ^{15}NH$_4$^{15}NO$_3$, Min) and a zero N fertilization control (Con). In order to track N losses of each culture by leaching of NO$_3^-$ in seepage water, three self-integrating accumulators (SIAs) intercepting percolate NO$_3^-$ by using NO$_3^-$-adsorbing resin (Bischoff, 2008) were installed under each microplot by laterally accessing the central plot area from a directly adjacent pit in a depth of 80 cm (see Figures 3.7, 3.6). The soil type on both fields is a Cambisol on alluvial clays, as determined during SIA installation. This fits with the classification as "Braunerde" according to the german soil classification by the Departement for Environment of the canton of Solothurn (Amt für Geoinformation, 2019). Soil texture is silty loam in the upper soil layers until 60 cm depth and clayey loam below until 100 cm depth. The soil pH value, measured in H$_2$O, is 6.2 on Field A and varies between 7.6 and 6.4 on Field B on an east-west gradient.

3.1.2 Surrounding landscape, meteorological and micrometeorological conditions

North and south of the flat agricultural fields situated at an altitude of 415 m, ridges of the jura mountain chain border the Dünnern valley in west-southwest to east-northeast direction
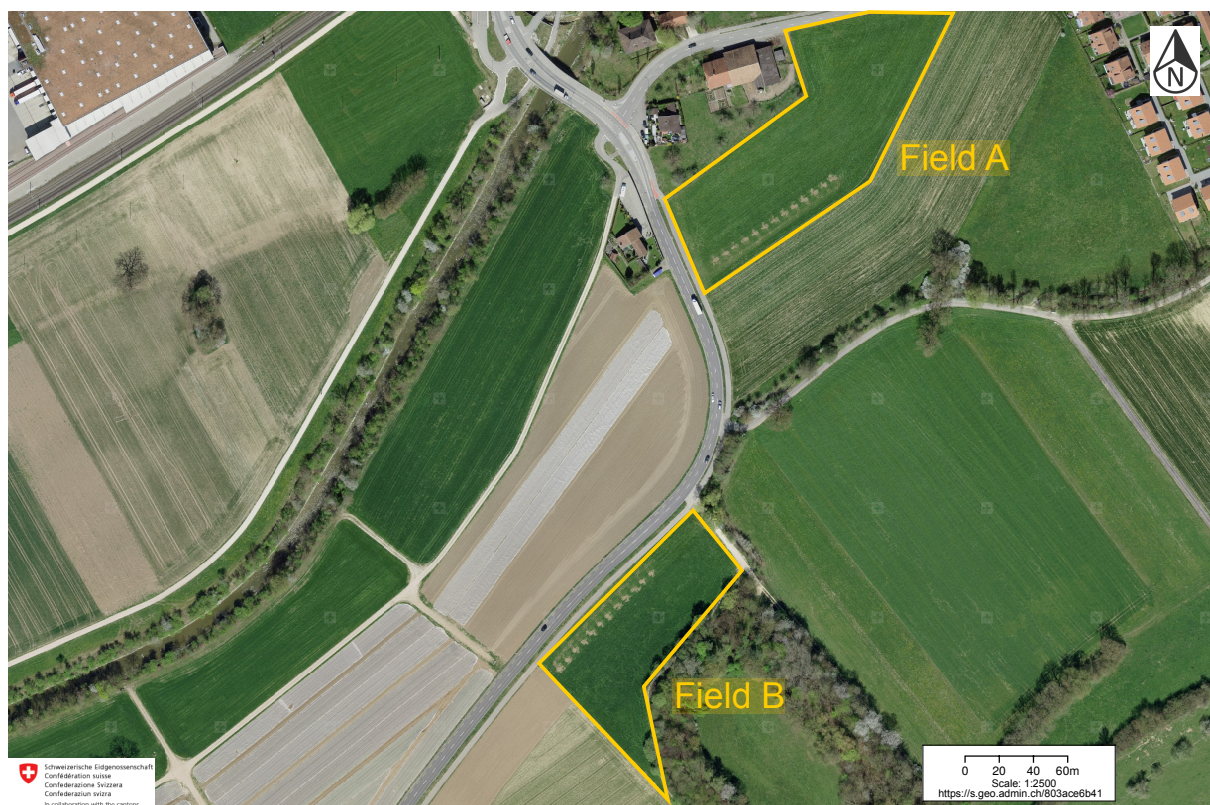
Figure 3.1: Aerial picture of the field site, showing Field A and Field B in early spring 2018. Light brown spots are traces of pits beside each microplot used to install SIA sensors for sampling seepage water NO_3^- losses. Modified after Federal Office of Topography swisstopo (2019).

with altitudes of up to 719 m in the southeast (Born) and 979 m in the northwest (Säntelhöchi). West-southwestern and east-southeastern winds are most prevailing in this region (see Figure 3.3; Bundesamt für Energie, 2018), which conforms to the orientation of the valley bottom. Fields are either directly bordering on tree lines, wood patches or buildings or these structures can be found within a distance of max. 200 m in all directions to the microplots (see Figure 3.4). Even if flow distortion is least in the main wind direction as the terrain is quite open, it can be expected that the conditions of turbulence are not the same for all plots. This makes it necessary to apply enhanced instrumentation in order to be able to check for possible hedge effects.

The general meteorological conditions during the summer 2018 in Switzerland were exceptional (MeteoSchweiz, 2019): Both the whole year and the summer term 2018 were the hottest since the beginning of records in 1864, the average summer term temperature being 2.4 °C higher than the climatologic reference period 1981 - 2010. It was the fourth of a recent series of exceptionally hot summers (2003, 2015, 2017, 2018), featuring a steep warming in spring (second-warmest April after a relatively cool March), a 10-day heat wave with mean daily maxima between 32
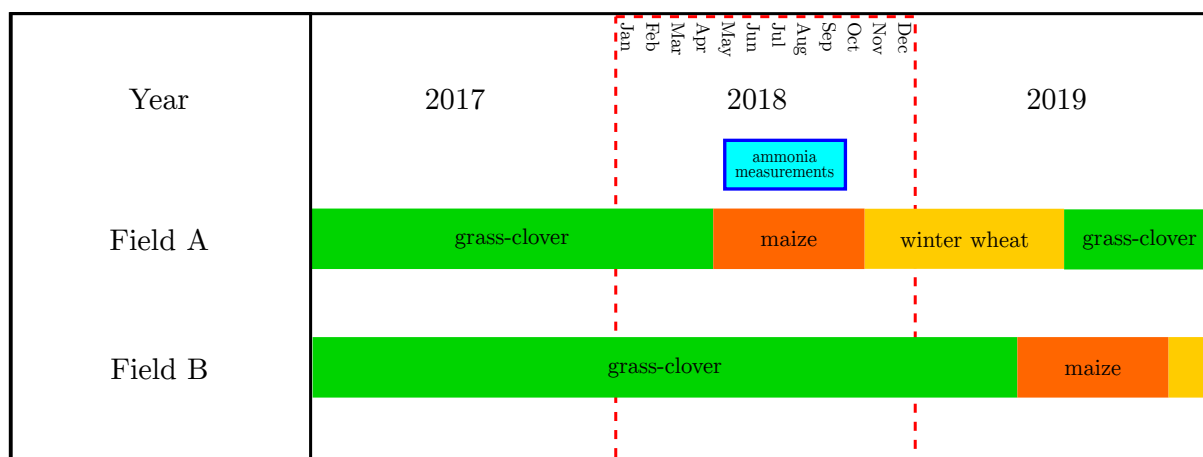
Figure 3.2: Crops being cultivated on Field A and Field B during 2017 - 2019, including the timing of NH$_3$ measurements.

and 34 °C in the beginning of August and an exceptional draught period: The period from April to November was the third-driest since the beginning of records with only 61% of the mean precipitation of the climatologic reference period 1981 - 2010. Simultaneously, an all-time record of sunshine hours was recorded for many Swiss regions.

3.1.3 Field experiment design

On each of the two field sites, plots of the three fertilization treatments (Slu, Min, Con) were marked out in fourfold replication, resulting in twelve plots. They were arranged on a 3 m wide strip, 9 m apart from the field's edge, in a semi-randomized block design in order to fit within and allow for usual field cultivation (see Figure 3.5). Plots were 2 m long and 1.5 m wide, equalling to a surface of 3 m^2, with a distance of 5 m between plots in order to avoid contaminations from neighboring plots caused by soil cultivation and in order to keep distance for NH$_3$ sampling (see Chapter 3.2). According to Jokela and Randall (1987) plots were located in a way that one corn row (in 2018 on Field A, 2019 on Field B) is located in the plot's centerline, while two of them form the plot's long edges (see Figure 3.6). In order to compensate for lateral aberrations during drilling of the maize seeds in spring 2018, the plot sizes in Field A were adjusted to 2 m x 1.75 m.

3.1.4 Fertilization

Slurry production

In the field experiment, ^{15}N-enriched cattle slurry (7.3 atom% abund.) and mineral fertilizer (^{15}N-ammonium nitrate, 8 atom% abund.) were applied to microplots in an amount and timing equivalent to the agricultural practice common for each of the crops. ^{15}N enriched cattle slurry
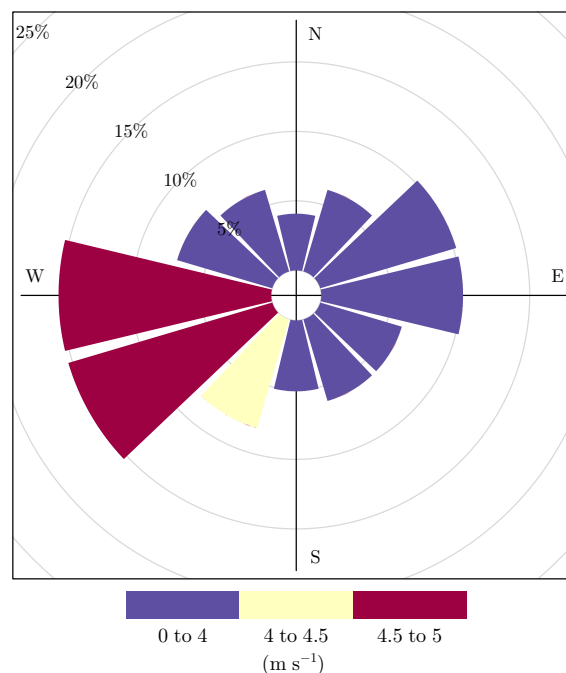
Figure 3.3: Plot of the prevailing wind directions for the field site according to a modelling approach for the assessment of wind energy potentials in Switzerland using a 100 x 100 m horizontal grid. Data: Bundesamt für Energie (2018)

was produced by feeding a young female cattle for eight days with ^{15}N enriched ryegrass (*Lolium multiflorum* L.) hay in order to ensure homogeneous ^{15}N enrichment in all fractions of the slurry. In 2017, the ^{15}N enriched hay had been produced by both growing ryegrass on artificial substrate fertilized with ^{15}N-ammonium nitrate in a greenhouse and fertilizing a pure stand designated for seed production with ^{15}N-ammonium nitrate solution. The excrements of the cow were collected daily, liquid and solid phase separately, and stored frozen at $-20\,°C$. For field application, the excrement samples with highest ^{15}N enrichment were mixed according to the sample's respective enrichment in order to ensure equal and homogeneous amounts of ^{15}N. To match common N contents of farm slurrys, it was diluted with water.

Fertilizer application

In the course of this field experiment, a total of five fertilizer applications were performed (Figure 3.8). On Field A, fertilizer was applied once on 28th May 2018. Field B was fertilized four times, once after each cut of the grass-clover biomass. Timing of these applications was dependent on biomass growth determined by weather conditions and on the farmer's planning. Slurry was applied directly from the storage canisters on the plot's surface while trying to imitate the pattern of a drag hose slurry distributer. Usually, slurry was applied in the evening between 1800 and
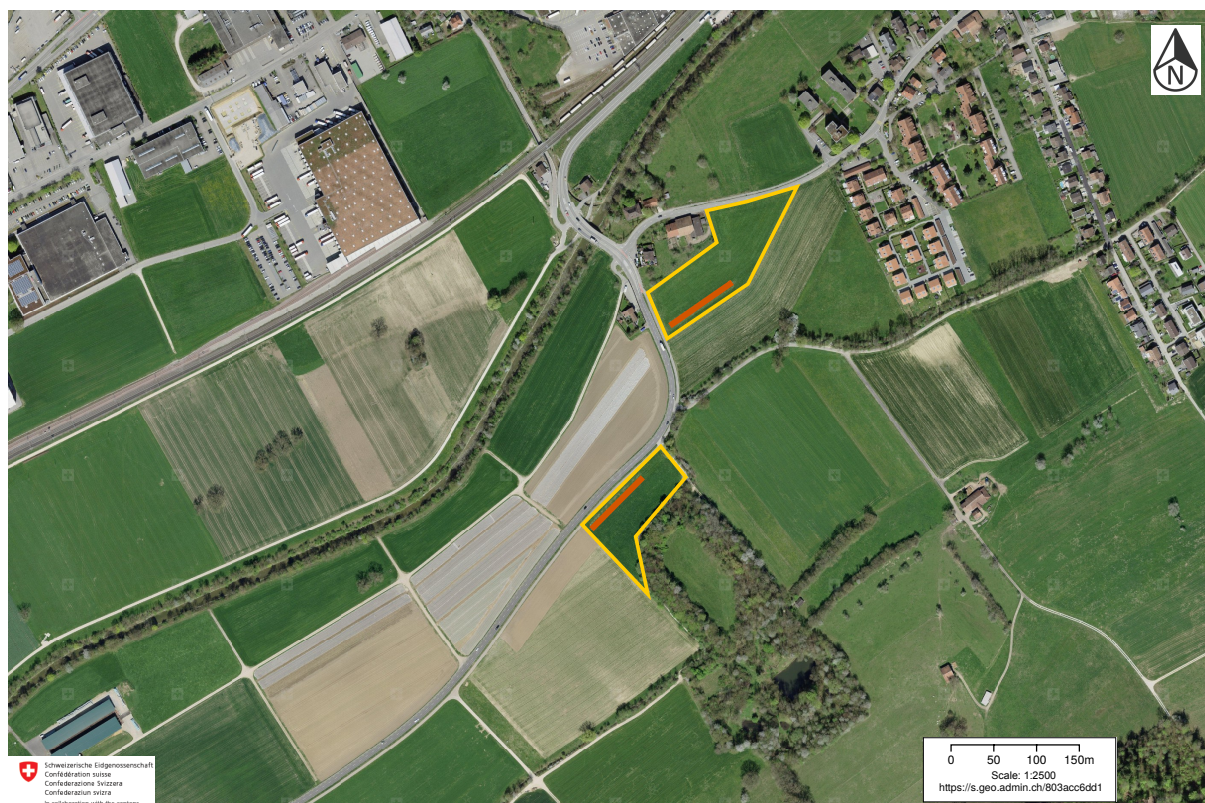
Figure 3.4: Overview aerial picture of the landscape structure surrounding the fields (yellow borders) with microplot stripes (orange). Buildings reach heights of about 15 m, trees and hedges are about 15-20 m high, with single trees reaching up to 25 m. Modified after Federal Office of Topography swisstopo (2019).

2000 hrs (see Table 3.8) in order to avoid excessive losses of NH_3 due to hot temperatures and intensive sunshine. On Field B, the Slu plots of the grass-clover lawn were fertilized after each of the four cuts in 2018 with the equivalent of 30 m^3 of ^{15}N enriched cattle slurry per hectare. On the closeby Field A, the same amount of ^{15}N enriched slurry was applied just once at the 3-4 leaf stage of the maize plants, 17 days after drilling. In the Min treatment, an amount of ^{15}N enriched ammonium nitrate equivalent to the NH_4^+-N content of the slurry was diluted in demineralized water and distributed on the plot surface from cans. Fertilizer cans were flushed with 3 L of demineralized water, which was evenly distributed on the plot surface. In the control treatment, an equivalent amount of water was taken from an adjacent stream and spread using watering cans with sprinklers. The amount of water applied to Con and Min plots equaled to the amount of water being spread with the slurry. Both Con and Min treatments were fertilized with mineral phosphorus (P) and potassium (K) fertilizer in an amount corresponding to the nutrient content in the applied slurry in order to eliminate potential effects of differences in P and K availability. On 31st July 2018, before fertilization, plots were irrigated with additional 3 mm of stream water due to the hot weather and drought situation in summer 2018. The total
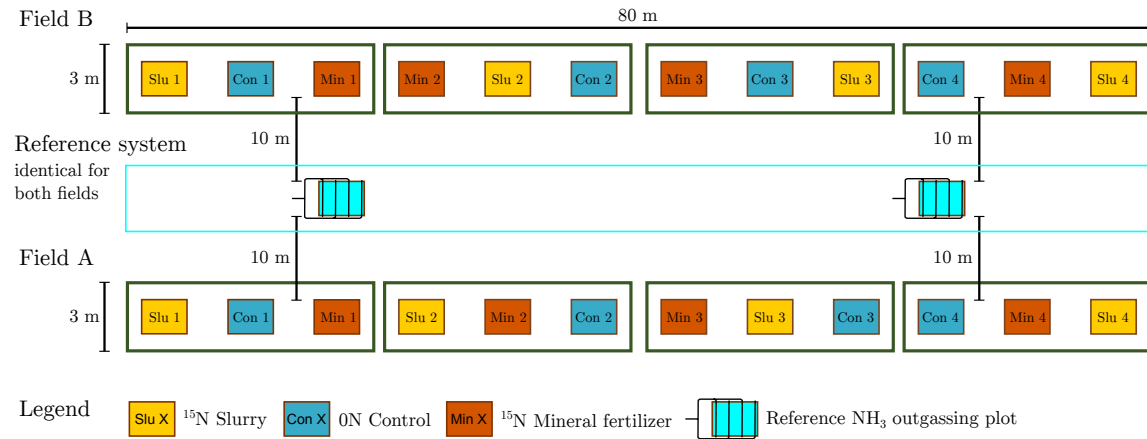
Figure 3.5: Design of the microplot strips on Field A and Field B. Figure: Hanna Frick, modified and supplemented.
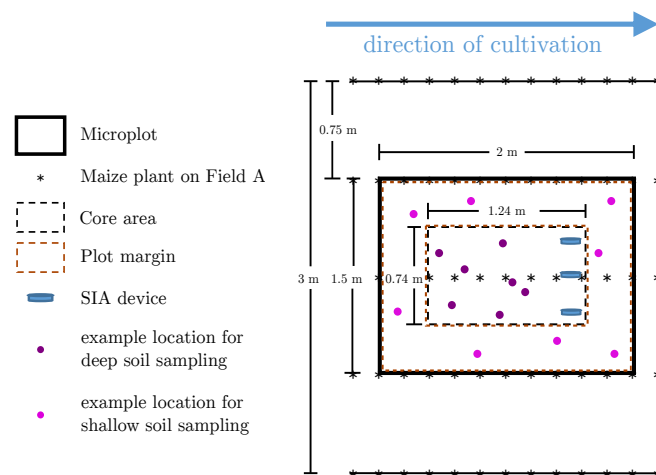
Figure 3.6: Microplot zoning and arrangement of measurement devices and sampling positions on a microplot. Figure: Hanna Frick, modified and supplemented.

volume of water applied was ensured to be equal for all plots of all treatments, including the amount contained in the slurry. Additionally, on Field A, mineral K fertilizer was applied to all plots according to the farmer's practice. P fertilizer and, at the 6-8 leaf stage of the maize, non-^{15}N enriched urea was applied by the farmer. This made it possible to trace the fate of N from a single slurry application upon drilling, which is a common practice.

3.2 NH$_3$ measurements

For measuring NH$_3$ emissions from the microplots in the 60 hours after fertilizer application, an open system according to the Standard Comparison Method (SCM) described by Vandré and Kaupenjohann (1998) was chosen. NH$_3$ being emitted from each plot was measured qualitatively
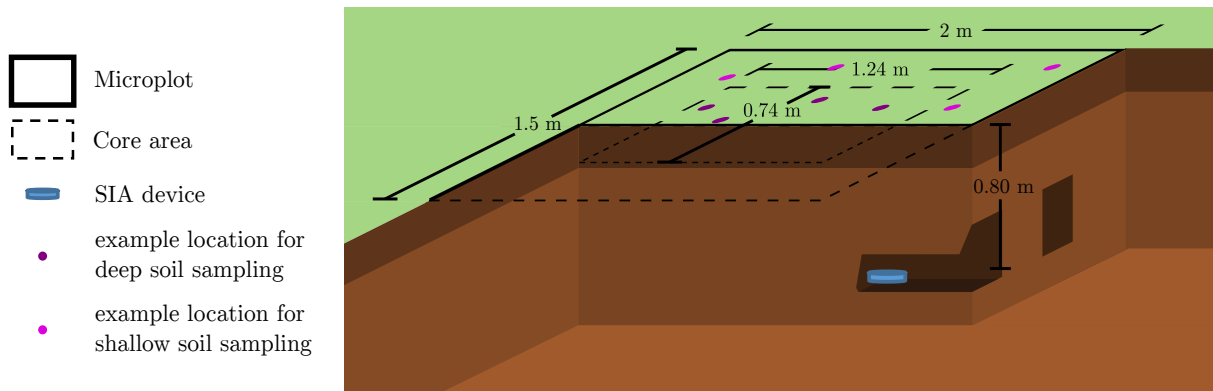
Figure 3.7: Installation and positioning of SIA seepage water NO_3^- sampling units under each experimental microplot. The soil pit for installation is excavated beside the plot itself, which is left undisturbed. SIAs are installed under the microplot core area in lateral tunnels as displayed.

using passive NH_3 samplers. Each of the five slurry applications (G1, M1, G2, G3, G4) was followed by a sampling sequence, each consisting of 6 or 7 passive sampler measurement intervals. In order to be able to transfer these qualitative into quantitative fluxes, a standard reference NH_3 outgassing system was set up and kept running during the NH_3 measurements. Compared to the method presented by Vandré and Kaupenjohann (1998), in this experiment, an extended meteorological instrumentation was used in order to be able to factor meteorological parameters known to influence NH_3 volatilization and turbulent transport into the parameterization of the transfer function, including a measure of dynamic atmospheric stability.

3.2.1 NH$_3$ trapping system

NH_3 volatilizing from the fertilized microplots was sampled by passive acid trap samplers (Figure 3.9). Into each side of 250 mL PE-HD 60x60 mm square bottles (item number 4295, Semadeni AG, Ostermundingen, Switzerland), 44 mm circular holes were drilled, 30 mm above the bottom, and covered with white fly-screen mesh to prevent insects from entering. They were installed in the field by attaching them under 20x20 cm square rain and sun protection roofs made from white 2 mm polystyrene using heavy duty hook-and-loop tape (item number 60243, Velcro Europe S.A., Barcelona, Spain). The roofs were mounted, using nuts and washers, on 8 mm threaded bars sticked in the ground. The height of the center of the holes on the side of the acid traps was adjusted to 10 cm above the bare soil surface on Field A (maize) and the cut grass-clover canopy on Field B, respectively, which is about 15 cm above ground on Field B. For trapping of NH_3, 20 mL of a 0.05 M sulphuric acid (H_2SO_4) solution (E.Merck, Darmstadt, Germany) was poured in the acid traps using an Eppendorf Multipette plus (Eppendorf AG, Hamburg, Germany).
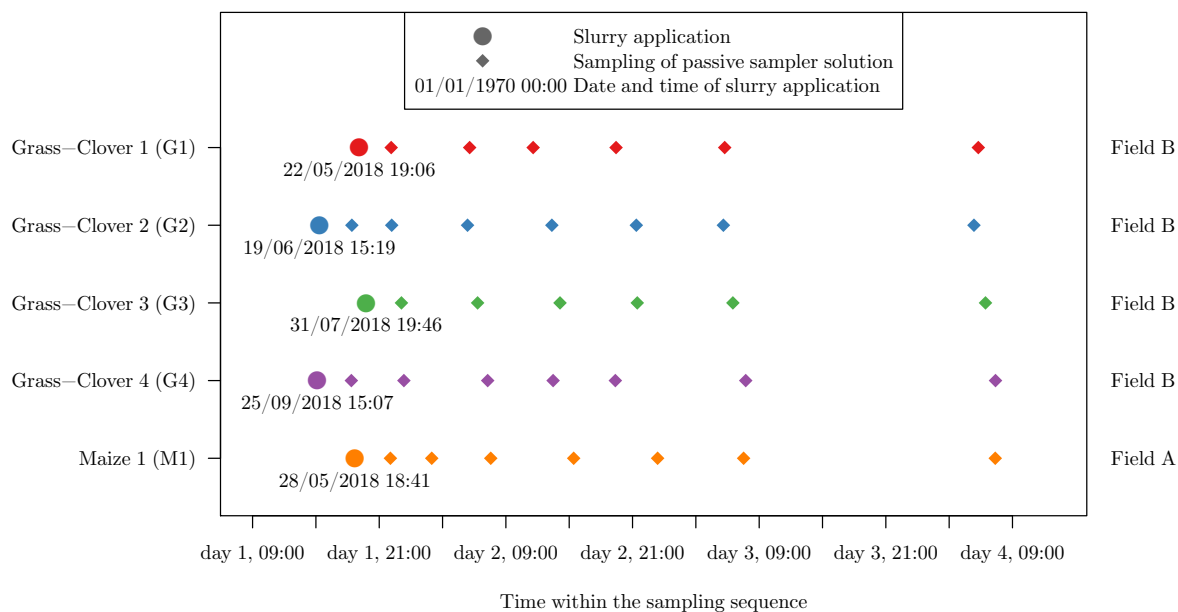
Figure 3.8: Overview of the dates of slurry applications and subsequent passive sampler measuring intervals that have been performed during the experiment.

During a measurement interval, NH_3 is transported into the acid traps by turbulent transport and dissolves in the solution (Figure 3.9) according to Henry's law. Due to the low pH, the equilibrium of the reaction:

$$NH_3 + H_3O^+ \rightleftharpoons NH_4^+ + H_2O \qquad \{1\}$$

is shifted to ammonium (NH_4^+), which can not volatilize again and NH_3 is trapped as NH_4^+ and accumulates in the solution. This happens quantitatively dependent on the NH_3 partial pressure in ambient air and the time of exposure. A $10\,ppm$ PO_4^{3-} spike was added to the H_2SO_4 sampling solution as KH_2PO_4 (E. Merck, Darmstadt, Germany) and used to track evaporation of water (or dilution by rain) during the measuring interval. For sampling at the end of each measuring interval, the bottle was removed from the protection roof, and 10 ml of the solution was pipetted into plastic tubes using plastic Pasteur pipettes. A clean bottle with fresh $0.05\,M$ H_2SO_4 + $10\,ppm$ PO_4^{3-} was attached to the roof to start a new measuring interval. Samples were stored cool in the field and frozen at $-20\,°C$ once in the lab. Remaining solution was removed, the sampling bottles were flushed with demineralized water and dried before re-use. The moment of exchange was recorded for each acid trap in steps of 30 seconds. Exchanging acid traps and sampling the contained solution took 1.5 - 2 minutes each. Additionally to the 12

acid traps installed in the center of each microplot, 2 acid traps were put in the center of each standard reference plot (see Figure 3.10) and one in each corner of the experimental area for recording background emissions (see Figure 3.11). Additionally, 2 acid traps were installed on slurry reference plots (see Chapter 3.2.2), summing up to a total of 20 acid traps. The first acid traps were put simultaneously with fertilizer application. After that, the solution was sampled in time intervals of increasing length, between 3 and 24 hours, depending on daytime and time since fertilization (see Table 3.8). Samples from the acid traps were analyzed for NH4+ and PO_4^{3-} concentration on a Skalar Aqua Pro Segmented Flow Analyzer (Skalar Analytical, 2005).

Figure 3.9: Acid trap passive sampler for cumulative air NH_3 sampling.

3.2.2 Standard flux reference (SFR) system

A known reference NH_3 flux was set free from two replicate standard reference flux outgassing systems made from 50 mm polypropylene sewage tube. Similarly to Vandré and Kaupenjohann (1998), a mix of 10% NH_3 in N_2 (Messer Schweiz AG, Lenzburg, Switzerland) was released at a rate of 0.09 and $0.18 \, l \, min^{-1}$ (corresponding to a flux of 31.0 and $62.0 \, \mu g \, s^{-1} \, m^{-2}$ per area), respectively. Gas release was regulated by a two-stage pressure valve (Messer Schweiz AG,
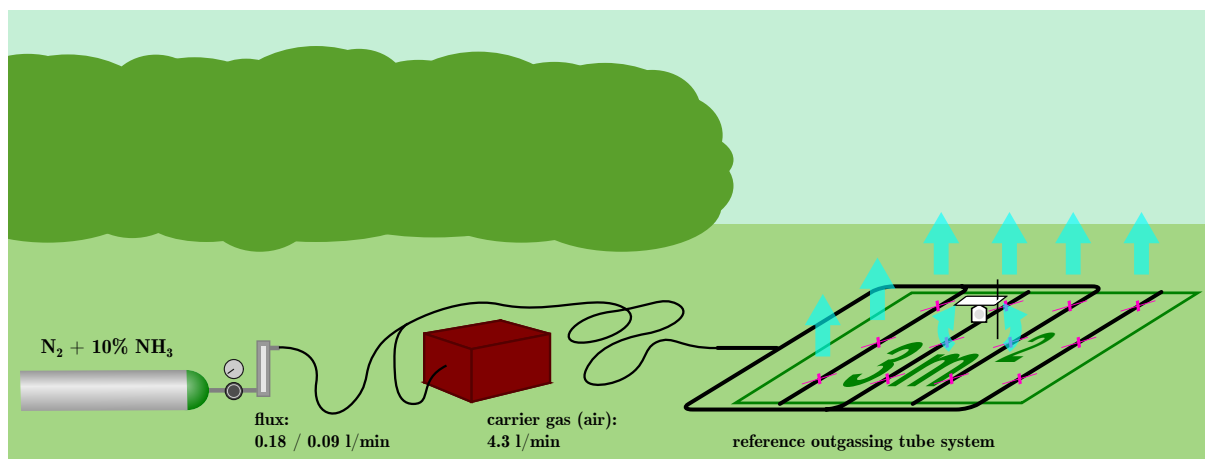
Figure 3.10: Reference NH$_3$ outgassing system including pressurized gas cylinder, pressure valve with flow meter, carrier gas stream supply, tube system and passive sampler on a 1.5x2 m plot area

Lenzburg, Switzerland) and a Q-Flow flowmeter (Vögtlin Instruments AG, Aesch, Switzerland). For each reference outgassing system, a M2K3 12V DC aquarium air pump (Schego Schemel & Goetz GmbH & Co KG, Offenbach, Germany) provided a $260 \, l \, h^{-1}$ carrier air stream, which transported the NH$_3$ gas mix to the outgassing system. Finally, it was released through 12 holes of 1mm diameter on the upper side of the tubes. They were arranged in the centers of imaginary 50x50 cm grid cells covering the imaginary microplot area of 1.5x2 m (see Figure 3.10). It can be assumed that these point sources imitate, by turbulent mixing, a continuous, laminar source on the ground. Electricity supply was ensured by two EEC100 12V lead-acid batteries with a capacity of 100 Ah (batterium GmbH, Freiberg am Neckar, Germany). Additionally, as a second reference system, cattle slurry of known N content and dry mass was equally poured into four rainwater gutters (length/width: 2 m/5 cm) arranged in a distance of 37.5 cm and replicated twice. This arrangement should, similarly to the outgassing system, imitate a two-dimensional source of NH$_3$. Together with the sampling of the acid trap solution, samples of the slurry were taken and stored together with the NH$_3$ samples. By analyzing for total N and dry matter, NH$_3$ volatilization and evaporation during the sampling interval should have been tracked. Data of this slurry reference system was ultimately not used for further calculations as it was not possible to representatively take samples due to a high undigested fiber content of the slurry and caking of the slurry during the hottest NH$_3$ sampling sequences.

3.2.3 Meteorological measurements

Wind speed and direction at 2 and 4 m height were measured using Young 05103 Wind Monitors (R.M. Young, Traverse City, Michigan, USA). Measurements at 2 m height were conducted on
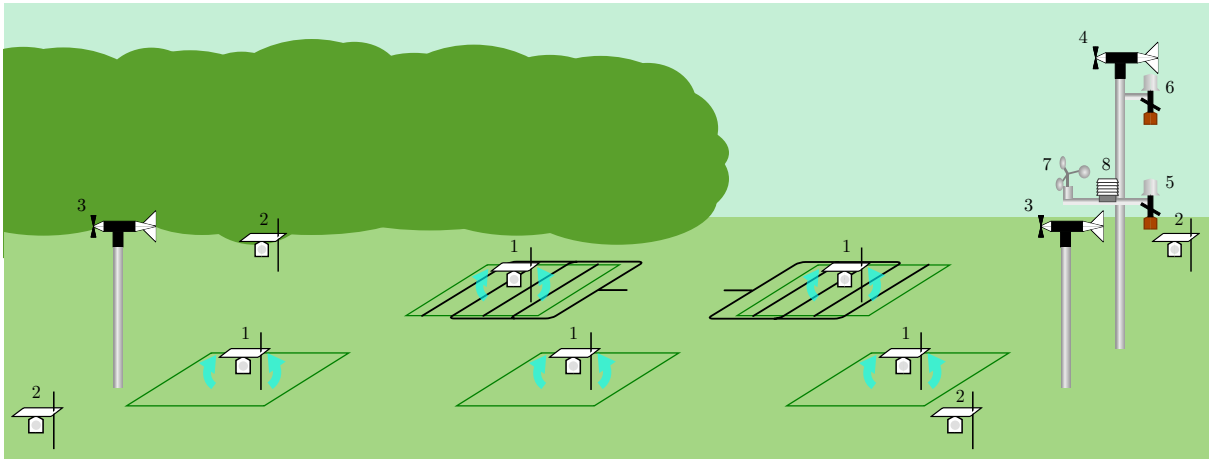
Figure 3.11: Instrumentation for NH$_3$ measurements, shown for a model microplot strip containing 3 plots: Passive samplers in the center of each microplot (1) and in 4 directions surrounding the measurement area for background concentration measurements (2); wind vanes at 2 m height on each end (3) and at 4 m height on one end of the microplot strip (4) as well as psychrometers at 2 (5) and 4 m height (6) on the 4 m pole. Additionally, at 2 m on the main pole, a cup anemometer (7) and a sheltered BME280 temperature and humidity probe (8).

both ends of the plot strip in order to cover the range of wind speeds occurring due to nearby obstacles (see Figure 3.4). The 4 m Wind Monitor was only installed on the western end. On the same mast, air temperature and relative humidity were measured using two ventilated psychrometers (Theodor Friedrichs & Co, Schenefeld, Germany) at 2 and 4 m height. For electricity supply, one of the same 100 Ah / 12V batteries installed for running the carrier air stream pump was used. Additionally, a A100R anemometer (Vector Instruments, Rhyl, North Wales, UK) and a BME280 temperature and humidity probe (Bosch Sensortec GmbH, Reutlingen, Germany), covered by a radiation shield, were installed at 2 m height on the same 4 m mast carrying psychrometers and the 4 m Wind Monitor. An overview of the meteorological instrumentation is displayed in Figure 3.11. Measured values were logged by BayEOS Low Power Boards, an Arduino clone developed by the Bayreuth Center of Ecology and Environmental Research and adapted to the sensors used in this study (BayCEER, 2019). Data for air pressure and precipitation were obtained from the Swiss Federal Office of Meteorology and Climatology MeteoSwiss for the closest meteorological station in Wynau, canton of Bern, Switzerland in a distance of 9.2 km.

3.3 Soil and biomass sampling

Soil layering, texture, pH and further soil characteristics were recorded according to the German soil mapping manual KA5 (Eckelmann et al., 2006) at the first SIA installation on 9th April 2018.

For bulk density, mean values for each field were calculated for 0 - 30 cm, 30 - 60 cm and 60 - 80 cm soil layers, respectively. For the 60 - 80 cm soil layer on Field A, values from Field B were used as soil characteristics were found to be very similar. Skeletal fraction (stones > 2 mm) of the soils was estimated at multiple spots per field.

Soil samples were taken from each plot on both fields on the 16th October 2018 using an automatic sampling unit (bodenproben.ch ag, Homburg, Switzerland). Three cores (1.5 mm diameter) per plot were separated in 0 - 30 cm, 30 - 60 cm and 60 - 80 cm soil layers and mixed. Samples were sieved to < 5 mm and stored at 4 °C until further processing and analysis.

Before, during and after each fertilizer application, several sampling activities were undertaken:

Maize biomass on Field A was sampled on the 28th August 2018 directly before the harvest of the entire field by the farmer. Only plants from the middle of the central maize row in each microplot (see Figure 3.6) were sampled for determination of fertilizer recovery. Plants from the margins of the microplot were counted and weighed in the field for determination of the total yield.

On Field B, before each harvest of the grass clover, biomass of the 1.24x0.74 m central plot area (see Figure 3.6) was cut in order to determine yield. On a 50x50 cm subarea within the central plot area, biomass was sampled and proportions of grass, leguminous and herbal biomass fractions were determined, dried and stored for chemical analysis (see Chapter 3.4). Subsequently, on Field B, the entire meadow including plots was mowed by the farmer and the biomass was removed. This was followed by fertilizer application and NH_3 emission measurements on the microplots, which is described in Chapter 3.2.

3.4 Soil and plant analyses for plot N balance

Chemical analyses of the soil and plant samples were for the most part performed by Hanna Frick as part of her PhD project. Data on leaching of NO_3^- in percolate water that had been collected using SIA samplers were provided by Hanna Frick (Frick et al., 2018, unpublished).

Composite soil samples stored at 4 °C were air-dried within two weeks at ambient temperature after removing subsamples for the determination of soil nitrogen pools. After sieving to 2 mm, a subsample was pulverized using a ball mill. Total N content and isotopic ratio of $^{15}N/^{14}N$ were determined using a Flash EA 1112 NC analyser coupled with a ConFlo IV universal continuous flow interface to a DELTA V isotope ratio mass spectrometer (ThermoFisher ScientificInc.,USA).

In order to ensure homogeneous and representative samples for the analysis of fresh and dry mass as well as N and ^{15}N content, maize plants were split in stem, leaves and ears with the

subfractions grains, husks including stigmas and cob. Each of these fractions was weighed and dried at 60 °C. Grass clover biomass samples were stored at 4 °C, split into grass, leguminous and herbal fractions as described in Chapter 3.3, weighed fresh and dried at 40 °C for 24 hours. The biomass subsamples of the middle of the central maize row and the 50x50 cm subarea on the grass-clover field were homogenized in a cutting mill. Dry matter content was determined by drying a weighed subsample at 105 °C. For chemical analysis, subsamples were further pulverized in a ball mill. Total N content and isotopic ratio of $^{15}N/^{14}N$ were determined just as in the case of the soil samples. Chemical analyses were performed on the separate subfractions of the biomass samples. By using a mass balance approach, the total N content and ^{15}N enrichment of the subfractions were recombined according to their mass share in order to determine total numbers for an entire maize plant or the whole grass-clover crop.

4 Computation and statistics

4.1 Meteorological data

For data handling, correction, calculations, statistics and plotting, the free software for statistical computing R 3.4.4 was used in the RStudio 1.1.383 environment (R Core Team, 2018). An interconnected network of R scripts containing function definitions, calculations and plot commands for different data groups was created (figure 4.1).
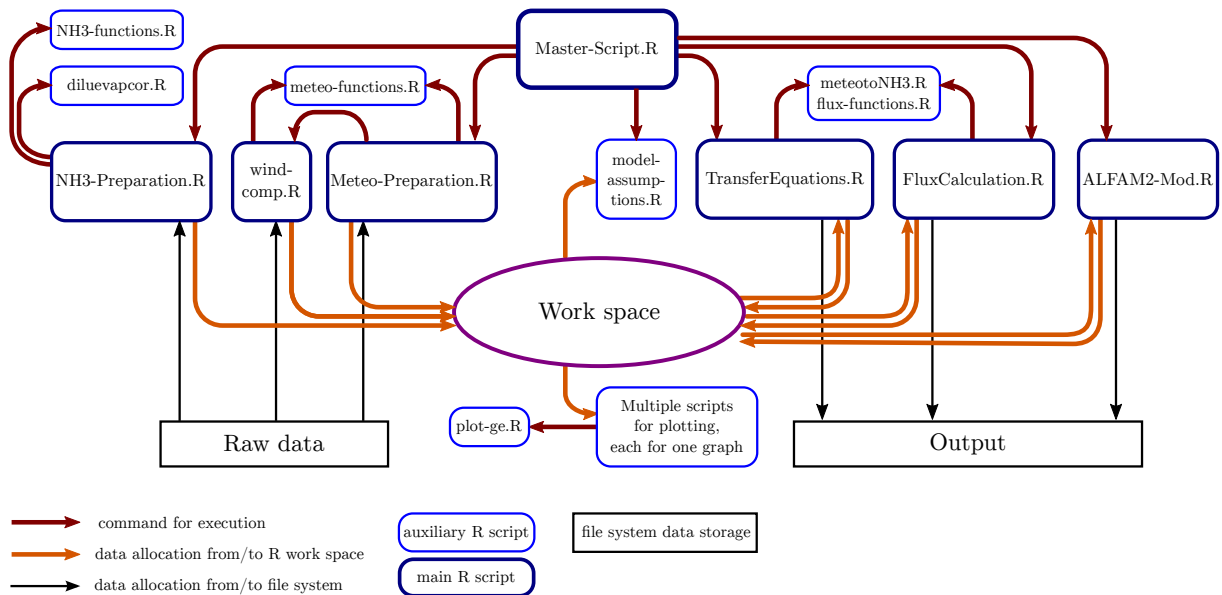
Figure 4.1: Flow chart of the network of R scripts used for calculations and statistical analysis. All calculations were executed by running the master script (MasterScript.R). Sub-scripts were called which perform all necessary data formatting, sorting, corrections and calculations. Functions being developed to execute certain special tasks were defined in auxiliary scripts, as well as statistical tests and plotting.

Wind speed data was, if needed, converted from sensor ticks into physically meaningful quantities ($\mathrm{m\,s^{-1}}$). Data points below the sensor sensitivity given by the manufacturer (Young 05103 Wind Monitor: $1\,\mathrm{m\,s^{-1}}$, Campbell Scientific Inc. 2009; A100R anemometer: $0.2\,\mathrm{m\,s^{-1}}$, Campbell Scientific Inc. 2016) were set to the sensitivity threshold value if not equal to 0. A two-weeks sensor intercomparison experiment was performed in order to derive correction factors relative to one of the Young 05103 Wind Monitors, which was chosen as a standard sensor. Psychrometer

raw data (RTD Pt100 resistance values) was transformed into temperatures and corrected for systematic logger misoperation errors that could be elucidated after the experiments. In case the measured wet temperature exceeded the dry temperature, the corresponding data points were removed from the data set. Meteorological data was measured every minute on-site and was aggregated to mean 10 min values in order to fit the periodicity of the data obtained from the meteorological station in Wynau. From dry air temperature t, saturation vapour pressure $E(t)$ was calculated using the Magnus equation (equation 1).

$$E(t) = C_1 \cdot e^{\left(\frac{C_2 \cdot t}{C_3 + t}\right)} \tag{1}$$

where:

$C_1 = 6.112\,\text{hPa}$
$C_2 = 17.62$
$C_3 = 243.12\,\text{°C}$

Actual vapour pressure e was calculated using the psychrometric equation (equation 2) from data on air pressure p as well as psychrometer dry (t) and wet temperature (t') observations, which were only available for NH_3 sampling sequences G2 to G4.

$$e = E(t) - \gamma \cdot \frac{p}{p_0}(t - t') \tag{2}$$

where:

$\gamma = 0.667\,\text{hPa}\,\text{K}^{-1}$
$p_0 = 1013.25\,\text{hPa}$

Relative humidity rH is defined as the ratio of actual and saturation vapour pressure (see equation 3).

$$rH = \frac{e}{E} \tag{3}$$

The bulk Richardson Number Ri is a measure of atmospheric stability, defined as the ratio of the buoyancy production or destruction to the production of shear by turbulent kinetic energy along a certain vertical gradient. For calculating Ri, the virtual temperature θ and the virtual potential temperature θ_v can be determined using equation 4 from observations of absolute dry air temperature T, air pressure p and actual vapour pressure e.

Adding gradients of absolute dry air temperature ΔT, horizontal wind speed Δu and height above ground Δz, Ri is defined according to equation 5.

$$\Theta = T \cdot \left(\frac{p_0}{p}\right)^{\frac{R_l}{c_p}}$$

$$\Theta_v = \Theta \cdot \left(1 + 0.38 \cdot \frac{e}{p}\right)$$

$$(4)$$

where:

$p_0 = 1000\,\text{hPa}$
$R_l = 287.058\,\text{J}\,\text{kg}^{-1}\,\text{K}^{-1}$
$c_p = 1004.834\,\text{J}\,\text{kg}^{-1}\,\text{K}^{-1}$

$$Ri = \frac{g}{\Theta_v} \cdot \frac{\Delta T \cdot \Delta z}{(\Delta u)^2}$$

$$(5)$$

where:

$g = 9.81\,\text{m}\,\text{s}^{-2}$

Ri values were calculated based on aggregated data for an entire measurement interval. In case the difference between $2\,\text{m}$ and $4\,\text{m}$ wind speeds was smaller than the sensor sensitivity of $0.3\,\text{m}\,\text{s}^{-1}$ (Young 05103 Wind Monitors), it was set to $0.3\,\text{m}\,\text{s}^{-1}$; in case the difference was negative (higher wind speeds at $2\,\text{m}$ than at $4\,\text{m}$ height), corresponding data points were removed.

4.2 Passive sampler NH$_3$ concentration data

Measured concentrations of NH_4^+ that accumulated in the passive sampler solution during the measuring interval ($c_{NH_4^+,meas}$) were corrected for dilution or evaporation during the time of exposure. An artificial PO_4^{3-} spike ($c_{PO_4^{3-},init}$) was added to the passive sampler acid solution prior to the measurements and was assumed to be quantitatively constant. Using equation 6, concentrations of NH_4^+ could be adjusted to dilution or evaporation based on the concentration of PO_4^{3-} ($c_{PO_4^{3-},meas}$) in the passive sampler solutions after the exposure.

By dividing concentrations (c) found in the passive samplers by the time that the samplers were exposed to the atmosphere above a plot (d), they were converted into concentration flux values (S, $\text{mg}\,\text{l}^{-1}\,\text{min}^{-1}$), see equation 7.

Both reference and experimental plot concentration fluxes (S^{ref} and $S^{Slu/Min/Con}$) were corrected by subtracting the mean of the background concentration fluxes S^{bg} found in the four passive samplers located at some distance to the plots over the same measurement interval to only cover plot effects (see equation 8).

$$c_{\mathrm{NH_4^+},cor} = \frac{c_{\mathrm{PO_4^{3-}},init} \cdot c_{\mathrm{NH_4^+},meas}}{c_{\mathrm{PO_4^{3-}},meas}} \qquad (6)$$

where:

c : Concentration of a species

cor : Corrected

$init$: Initial

$meas$: Measured in sample

$$S = c/d \qquad (7)$$

where:

S : Concentration of a species

c : Concentration of a species

d : Passive sampler exposure time

4.3 Calculation of transfer factors and fitting of transfer factor models

A conceptual diagram of the analysis of the data collected on the field to derive numbers for plot NH_3 losses (hypotheses 1 and 4), as well as fitting and comparison of models relating original standard comparison (SCM) method transfer factors to meteorological observations (hypotheses 2 and 3), is schematically shown in Figure 4.2.

4.3.1 Standard Comparison Method

Transfer factors (f) relate passive sampler concentration fluxes (S) to standard reference NH_3 fluxes at the ground (F), which is determined on SFR plots (Vandré and Kaupenjohann, 1998, see Chapter 3.2.2). Transfer factors were calculated for each measuring interval i within a sampling sequence j and each of the two SFR systems k according to equation 8 (also see Figure 4.2).

4.3.2 Fitting of transfer factor models

Meteorology-based models predicting transfer factors f from meteorological observations I were fitted and optimized (figure 4.2). Meteorological data was aggregated from $10\,\mathrm{min}$ values to the duration of exposure of each of the reference plot passive samplers. Wind speed, temperature, relative humidity, and virtual potential temperature were averaged. Bulk Richardson number was calculated based on aggregated values according to the description in Chapter 4.1 (see

Figure 4.2: Conceptional diagram of the analytical steps conducted on experimental field data NH_3 on volatilization. Transfer factors were calculated according to the original SCM using data collected on SFR plots. Three kinds of models explaining time series of transfer factors by observations of $2\,m$ horizontal wind speed u, $2\,m$ dry temperature t, $2\,m$ relative humiditiy rH and bulk Richardson number Ri were fitted depending on data availability and optimized. Nash-Sutcliffe coefficients for model efficiency NSE were calculated to assess the explanatory power of meteorology-based models. Finally, plot NH_3 volatilization fluxes were calculated based on both SCM and modelled transfer factors.

equation 5). Linear models without interactions were fitted according to the generic model structure displayed in equation 9. Explaining variables I were wind speed (u) and dry air temperature (t) observations at $2\,m$ height for all NH_3 sampling sequences. Relative humidity rH and bulk Richardson number Ri were used according to the availability of psychrometer or humidity probe observations. Model configurations can be found in Table 4.1. Additionally, complementary models were fitted for each sampling sequence. Therefore, combined data from all other sampling sequences was used. As during some sampling sequences, data is not available for all meteorological parameters, several complementary models were fitted based on sets of sampling sequences featuring a common availability of meteorological data (see Table 4.2). Also,

$$f_{i,j,k} = \frac{S_{i,j,k}^{ref} - <S_{i,j}^{bg}>}{F_{i,j,k}^{ref}} \tag{8}$$

where:

F : Reference plot NH_3 flux

S : Passive sampler concentration flux

f : Transfer factor

ref, bg : SFR system, background sampler

i, j, k : Indices for NH_3 sampling sequence, measuring interval, reference plot

it was evaluated if due to a possible similarity of atmospheric transport conditions present during the five sampling sequences, they can be successfully combined in an overall model. Thus, and similarly to the complementary model, overall models including meteorological records from sampling sequences of the same data availability were fitted (see Table 4.1).

$$f_{i,j,k} = b_i^0 + b_i^1 \cdot I_{i,j,k}^1 + ... + b_i^n \cdot I_{i,j,k}^n \tag{9}$$

where:

f : Transfer factor

b : Model parameter

I : Meteorological predictor variable

n : Index of the meteorological predictor variable

i, j, k : Indices for NH_3 sampling sequence, measuring interval, experimental plot

All initial models were optimized in an iterative process based on the significance of the fitted model transfer parameters and the Akaike Information Criterion AIC (Fahrmeir et al., 2013). First, the p-values for the transfer parameters were computed. The p-value represents the probability to obtain an at least as extreme value for the transfer parameter as observed under the null hypothesis, which would be a transfer parameter of 0 (no effect). Subsequently, a model without the explaining variable corresponding to the smallest p-value was fitted. After that, the AICs of both models were computed and compared: If the AIC decreased by omitting the least significant explaining variable, the optimization process was repeated. Once the AIC did not decrease any more, the model including the tentatively removed explaining variable was accepted as optimized model. The same applied to models with only one variable left.

Table 4.1: Initial model and optimized model parametrization for individual sampling sequences as well as overall models on data from multiple sampling sequences.

	Initial model	optimized model
G1	t,u	u
M1	t,u,rH	t,u,rH
G2	t,u,rH,Ri	t,u,rH,Ri
G3	t,u,rH,Ri	t
G4	t,u,rH,Ri	t
overall	t,u	t
overall-rH	t,u,rH	t
overall-Ri	t,u,rH,Ri	t

4.3.3 Calculation of fluxes

The flux of NH_3 (F) from the surface of each experimental plot k was calculated for each measuring interval i within the sampling sequence j from plot-specific passive sampler NH_3 concentration flux values (S) and transfer factors (f):

$$F_{i,j,k} = \frac{S_{i,j,k} - <S_{i,j}^{bg}>}{f_{i,j,k}} \tag{10}$$

where:

F : Experimental plot NH_3 flux

S : Passive sampler concentration flux

f : Transfer factor

bg : Background passive sampler

i, j, k : Indices for NH_3 sampling sequence, measuring interval, experimental plot

Transfer factors were either directly derived from the SCM as the mean of the two reference plots or the null model (see Chapter 4.3.4) and optimized single-sequence or complementary models (generic equation 9, also see Figure 4.2). Meteorological observations for modelling I were aggregated over the time span each individual passive sampler was exposed to the atmosphere above the plot surface as explained in Chapter 4.3.2.

NH_3 volume fluxes (F, $l\,min^{-1}$) were converted into mass fluxes of NH_3 and NH_3-N (m) by equation 11 using the molar mass of NH_3 and the atomic mass of nitrogen (M), respectively. The atomic mass of nitrogen is used instead of the molar mass, because per molecule of NH_3, only one atom of nitrogen is released. By multiplying it with the exposure time of the passive

Table 4.2: Initial and optimized parametrizations of complementary models.

	Initial model	optimized model
G1	t,u	t
M1	t,u	t
	t,u,rH	t
G2	t,u	t
	t,u,rH	t
	t,u,rH,Ri	t
G3	t,u	t
	t,u,rH	t
	t,u,rH,Ri	t
G4	t,u	u
	t,u,rH	t,u,rH
	t,u,rH,Ri	t,u,rH,Ri

sampler d and adding the values from all intervals within a sampling sequence, the mass of NH_3 or NH_3-N volatilized from the plot surface following a slurry application was calculated.

$$m_{\mathrm{NH_3/NH_3}-N} = \frac{F \cdot d}{\frac{R_n \cdot T}{p} \cdot M_{\mathrm{NH_3/NH_3}-N}} \tag{11}$$

where:

$m_{\mathrm{NH_3/NH_3}-N}$: Mass of NH_3 or NH_3-N volatilized (g)

$M_{\mathrm{NH_3/NH_3}-N}$: Molar mass of NH_3 ($17\,\mathrm{g\,mol^{-1}}$) or atomic mass of NH_3-N ($14\,\mathrm{g\,mol^{-1}}$)

F : Plot NH_3 flux ($l\,min^{-1}$)

d : Duration of the measuring interval (min)

R_n : Universal gas constant: $8.314\,46\,\mathrm{J\,mol^{-1}\,K^{-1}}$

T : Air temperature (K)

p : Air pressure (hPa)

4.3.4 Null model

As a standard model and reference for comparison of the predictive power of different models, a null model was defined as the mean of the transfer factors f within the considered sampling sequence (see equation 12).

$$F_{i,j,k} = \frac{S_{i,j,k} - <S^{bg}_{i,j}>}{\overline{f_i}} \tag{12}$$

where:

F : Plot NH_3 flux

S : Passive sampler concentration flux

f : Transfer factor

bg : Background passive sampler

i, j, k : Indices for NH_3 sampling sequence, measuring interval, experimental plot

4.3.5 ALFAM2 model

For comparison with the NH_3 losses from the plot surface measured by the SCM method as described before, the ALFAM2 model presented by Hafner et al. (2019) was applied for the specific field conditions recorded in this study. This semi-empirical model is based on a large data base of experimental observations of NH_3 emissions, containing data from 490 field plots in 6 countries (Hafner et al., 2018). Conceptually, it separates field-applied slurry in a "fast" pool in direct contact with the atmosphere and a "slow" pool, representing infiltrated slurry or fractions otherwise less available for volatilization (Hafner et al., 2019). Explanatory variables are air temperature, wind speed and precipitation rate as well as slurry application rate and slurry properites such as pH value, total slurry TAN and dry matter content. These data are available for the slurry applications performed during this study. The ALFAM2 model predicted cumulative time series of NH_3 volatilization during each of the sampling sequences, consisting of temporally explicit emission values for each measuring interval. For doing so, the ALFAM2 model which is freely available on Github as R scripts (Hafner, 2019) was integrated in the structure of already existing data analysis R scripts, see Figure 4.1.

4.4 Statistical data analysis

Assumptions on the data required for fitting the linear transfer factor models were tested mainly using visual analysis of scatter plots. Plots of residues against fitted values (homoscedasticity), residues against explaining variables as well as normal qq-plots of the residues were investigated. Standard errors and mean of the measured and modelled NH_3 volatilization were calculated for each fertilizer treatment. Using a t-test, the significance of the difference between volatilizations from different fertilizer treatments was checked on a significance level of < 0.05. The significance (< 0.05) of model parameters to predict transfer factors was assessed by running a model ANOVA

(Hastie, 2017; Fahrmeir et al., 2013). In order to determine and compare the quality of different models to predict transfer factors and volatilization fluxes, the Nash-Sutcliffe coefficient for model efficiency NSE was calculated (Nash and Sutcliffe, 1970, also see Figure 4.2):

$$NSE = 1 - \frac{\sum_{t_{start}}^{t_{end}} (Q_m^t - Q_O^t)^2}{\sum_{t_{start}}^{t_{end}} (Q_O^t - \overline{Q_O})^2} \tag{13}$$

where:

t : time

Q_m : modelled quantity

Q_O : observed quantity

This parameter compares the predictive power of a model compared to a null model (see Chapter 4.3.4). If NSE equals zero, the model is as good to predict a quantity as the mean of observations. Up to a NSE of 1, which corresponds to a perfect match between modelled and observed data, the quality of the tested model is increasing. In case NSE is lower than 0, the model is worse in predicting the observations than the mean of the observations themselves. It can, similarly to the R^2, also be understood as the fraction of observed variation of the transfer parameters explained by the model.

4.5 Plot N balance

For each treatment on Field A and B, respectively, a plot N balance was established using experimental data on the fate of fertilizer N. While N losses via NH_3 volatilization were taken from the SCM measurements of this study, N accumulation in soil pools as well as uptake and removal by biomass averaged over the treatment replicates (see equation 14) were traced using a ^{15}N direct labelling approach (Douxchamps et al., 2011). Data on N losses due to percolate leaching was supplied by the overarching PhD project (Frick et al., 2018, unpublished data). The results can be compared to the known treatment fertilization rates.

For soil and biomass samples, the fraction of total N derived from ^{15}N-labelled fertilizer had to be calculated (Douxchamps et al., 2011), which was conducted by Hanna Frick (Frick et al., 2018). Total soil N concentrations in dry soil (N_{soil}) were converted into total N stocks (N_{stock}) per soil layer and field area using data on soil bulk density ρ_B and skeletal content s using equation 15. The fraction of N derived from fertilizer (%*Ndff*) in each soil layer was calculated based on atom $^{15}Nexcess$ values of the fertilizer and the sample following equation 16.

$$\overline{N_{trace}^{fert}} = \overline{N_{loss,vol}^{fert}} + \overline{N_{loss,leach}^{fert}} + \overline{N_{harvest}^{fert}} + \overline{N_{soil}^{fert}} \tag{14}$$

where:

$\overline{N_X^{fert}}$: Treatment replicates average

N_{trace}^{fert} : Sum of fertilizer N traced

$N_{loss,vol/leach}^{fert}$: Fertilizer N losses via volatilization and leaching

$N_{harvest}^{fert}$: Fertilizer N removed by the harvest of biomass

N_{soil}^{fert} : Fertilizer N accumulation in soil N pools

$$N_{stock} = N_{soil} \cdot \rho_B \cdot \left(\frac{100 - s}{100} \right) \cdot D \tag{15}$$

where:

ρ_B : Soil layer bulk density $(\mathrm{g\,cm^{-3}})$

s : Soil layer skeletal content (%)

D : Soil layer depth (cm)

$$\%Ndff = \frac{atom\ ^{15}N\,excess_{sample}}{atom\ ^{15}N\,excess_{fertilizer}} \cdot 100 \tag{16}$$

The absolute amount of fertilizer-derived N per field area (*Ndff*) was calculated as displayed in equation 17.

$$Ndff = \frac{\%Ndff \cdot N_{stock}}{100} \tag{17}$$

Finally, amounts of fertilizer-derived N per soil layer were summed up in order to provide total numbers.

5 Results

5.1 Meteorological measurements

Weather conditions

Meteorological data collected on-field during the experiments are in line with the exceptionally dry and hot conditions recorded throughout Switzerland and Central Europe during the summer of 2018. Time series of available standard meteorological measurements during the NH_3 sampling sequences are displayed in Figure 5.1.

While the first sampling sequence (G1) was still mild, already one week later during the measurements on Field A (M1), mid day air temperatures exceeded 27 °C and never fell below 13 °C. G1 and M1 were the only sampling sequences featuring precipitation with steady rain during slurry application and the following night of G1 as well as a local thunderstorm during the last night of M1 measurements. The following experiments were entirely affected by the 2018 draught period. Mid day temperatures during G2 and G3 reached up to 32 °C, minimum temperatures were 10 °C during G2 and 18 °C during G3. The last experimental sampling sequence (G4) was the coolest, noticably in fall, with minimum temperatures as low as 3 °C and a maximum of 24 °C. Relative air humidity declined to about 35 % during the day, which reflects a high vapour pressure deficit due to high temperatures and a lack of available water for evapotranspiration during G2 - G4. During night, relative air humidity approached saturation which was underpinned by partially heavy dew formation on the fields. Similarly, observed wind speeds were lower in the night than during the day, often a night calm could be observed. Wind speeds during slurry application usually ranged around $2\,\mathrm{m\,s^{-1}}$, except for the G4 measurements with constant strong westerly winds of between 5 and $7\,\mathrm{m\,s^{-1}}$ during the day.

Data availability and corrections

Availability of meteorological data of the experiments was compromized by instrument and logger problems as well as data cleaning measures, which restricted the parametrization of meteorology-
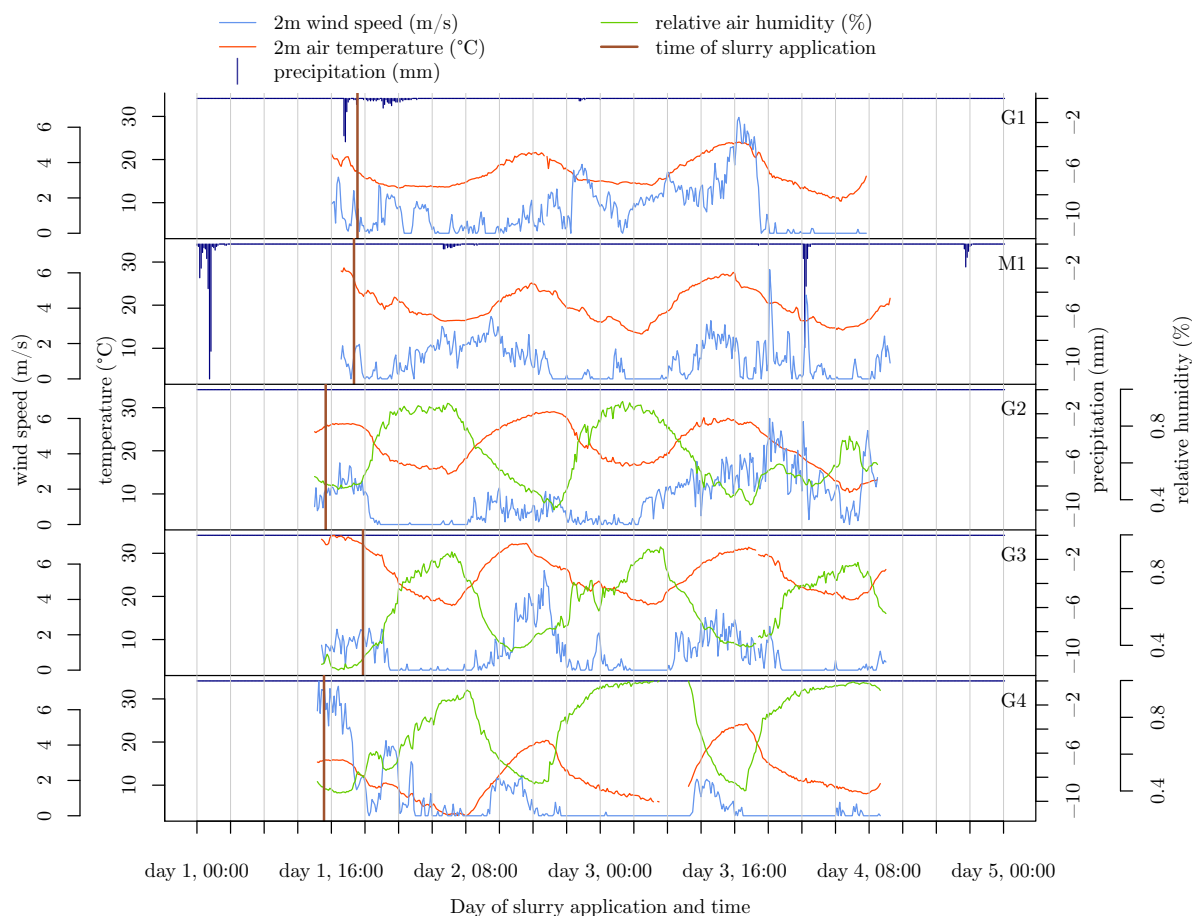
Figure 5.1: Overview of the records of wind speed, air temperature and relative humidity taken during the NH$_3$ sampling sequences on-site as well as precipitation records from the meteorological station Wynau of the Swiss Federal Office of Meteorology and Climatology MeteoSwiss. Timing of slurry application is marked as vertical brown bars.

based transfer factor models. Therefore, data required for the calculation of gradient parameters like the bulk Richardson number was only available for sampling sequences G2, G3 and G4. Data for the comparison of wind conditions on both ends of the microplot strip was only available for G1, M1 and G2. Due to psychrometer ventilation head motor failures and wrong wiring of the logger connection, data on air temperature and humidity was only partially available for sampling sequences G1 and M1. Also, due to wind sensor logger problems, data of certain wind sensors was partially missing for G1, M1, G3 and G4.

Meteorological data was cleaned and corrected as a preparation for subsequent calculations and analysis (see Chapter 4.1). 37.9 % of the wind sensor data was below the sensitivity threshold value given by the manufacturer ($1\,\mathrm{m\,s^{-1}}$ for Young 05103 Wind Monitors; $0.3\,\mathrm{m\,s^{-1}}$ for the A100R anemometer) and set to $0\,\mathrm{m\,s^{-1}}$. Additionally, in course of the calculation of the bulk Richardson number, 70.2 % of the wind speed gradients were set to the Young 05103 Wind

Monitor's accuracy of $0.3\,\mathrm{m\,s^{-1}}$ in case they fell below this value, another 2.3 % of the data points were removed due to negative gradients violating the logarithmic wind profile. During some nights, this procedure led to a correction of over 98 % of the data required for the bulk Richardson number (see Figure 5.2).
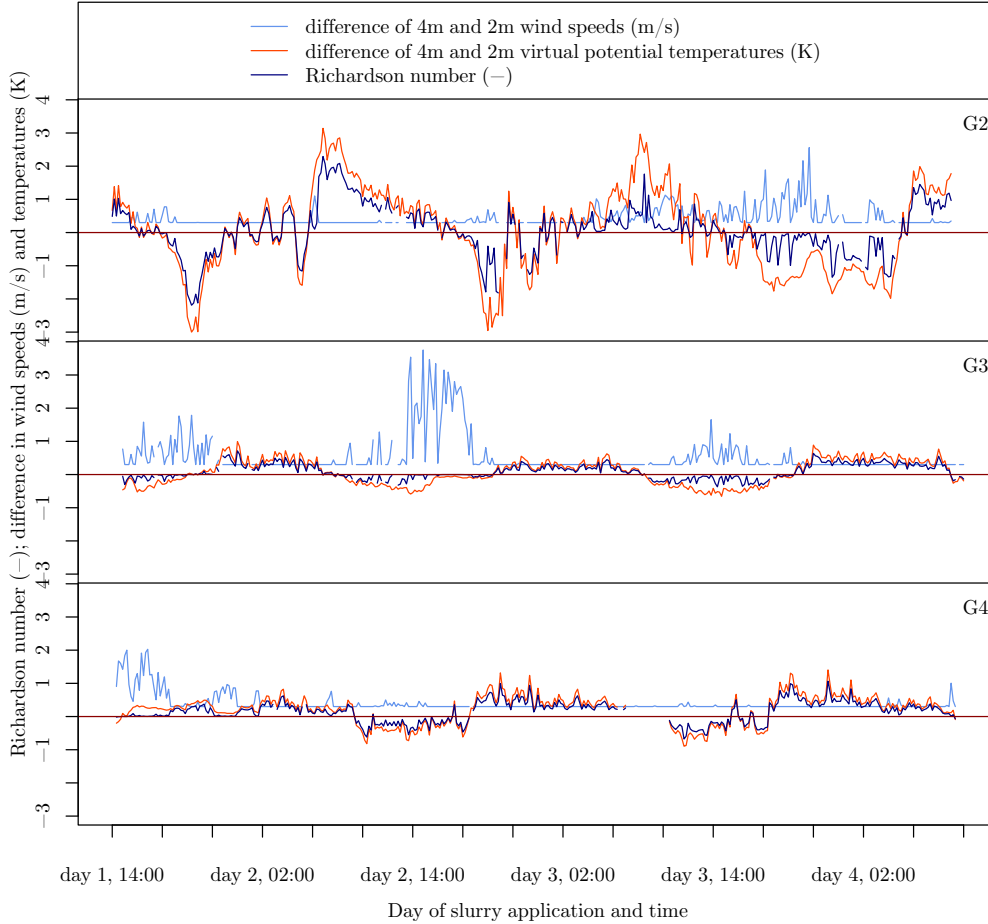
Figure 5.2: Time series of corrected wind speed and temperature gradients between measurements at 2 and 4 m height, as well as the bulk Richardson number for the sampling sequences G2, G3 and G4.

In the wind sensor intercomparison experiment, wind speeds below a threshold value of $2.5\,\mathrm{m\,s^{-1}}$ featured a good fit to the standard sensor values. For standard sensor wind speeds exceeding $2.5\,\mathrm{m\,s^{-1}}$, linear models between the standard sensor and the remaining wind sensors were fitted. These were used to correct wind speeds exceeding a threshold value corresponding to the intersection of the 1:1 line and the fitted correction model (see example Figure 5.3).

Systematic psychrometer logger aberrations determined by manual resistance measurements in the lab could be formulated as linear relationships and used for correction of the logged
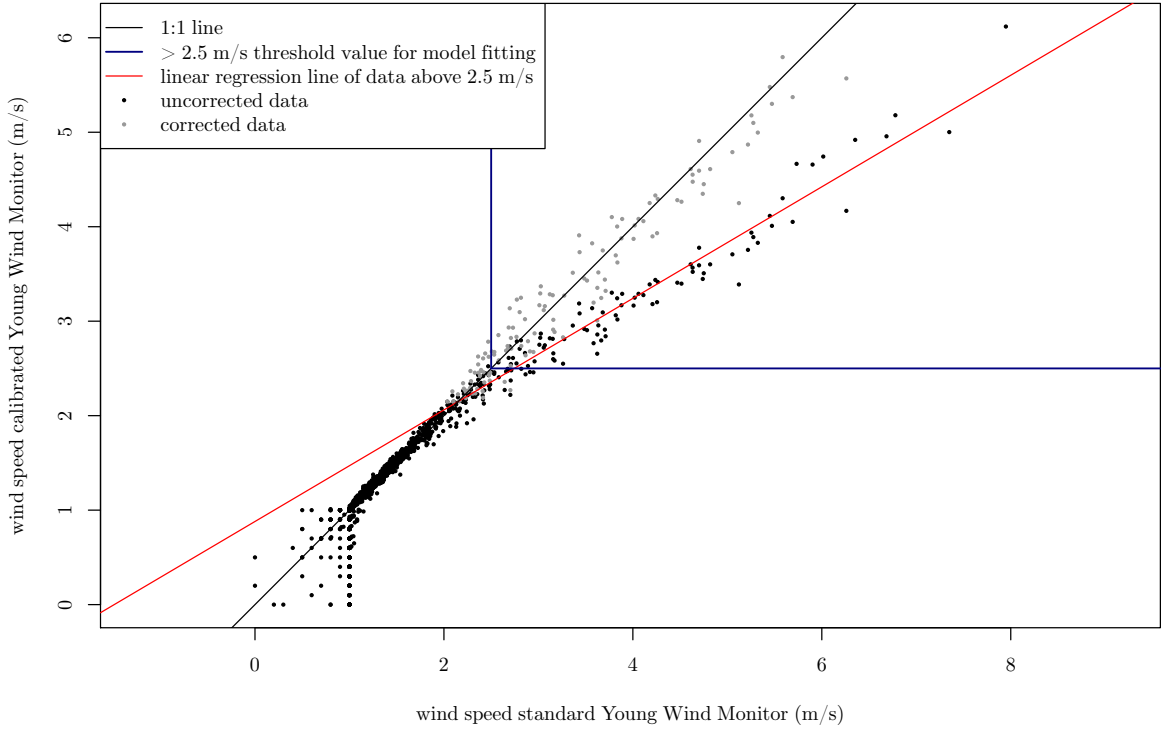
Figure 5.3: Example scatter plot of data from the wind sensor intercomparison experiment: Raw data from a Young 05103 Wind Monitor to be calibrated is plotted against reference sensor data. Additionally, the regression line based on wind speeds above $2.5\,\mathrm{m\,s^{-1}}$ and corrected data is shown.

Pt100 resistance. By multiplying the logged resistance r_{meas} by a psychrometer-specific factor C, corrected resistance values r_{cor} were obtained for further conversion into temperature values.

$$r_{cor} = r_{meas} * C \tag{18}$$

where:

Psychrometer $1 : C = 1.070\,00$

Psychrometer $2 : C = 1.072\,15$

In the data used for further calculations, data points where wet temperature exceeded dry temperature of the same psychrometer were classified as unphysical and excluded from the data set.

Variability of wind speed along the microplot strip

Local inhomogeneities of the wind field due to closeby obstackes (see Chapter 3.1) could compromise the applicability of transfer factors obtained on SFR plots for calculation of NH_3 volatilization fluxes from the experimental microplots. Along the microplot strips, no clear difference in wind speeds could be detected (see Figure 5.4). For Field A, during the sampling sequence M1, the slope of the regression line between the data recorded by the two Young 05103 Wind Monitors being placed on the opposite ends of the microplot strip (see Figure 3.11) was not significanly different from 1 (5.4, left panel), same as for all available data on Field B taken together (5.4, right panel). If data is split into subsets collected during G1 and G2 on Field B, G1 showed significantly higher wind speeds at the site close to hedges and forest, in the case of G2 it was the opposite (5.4, right panel).
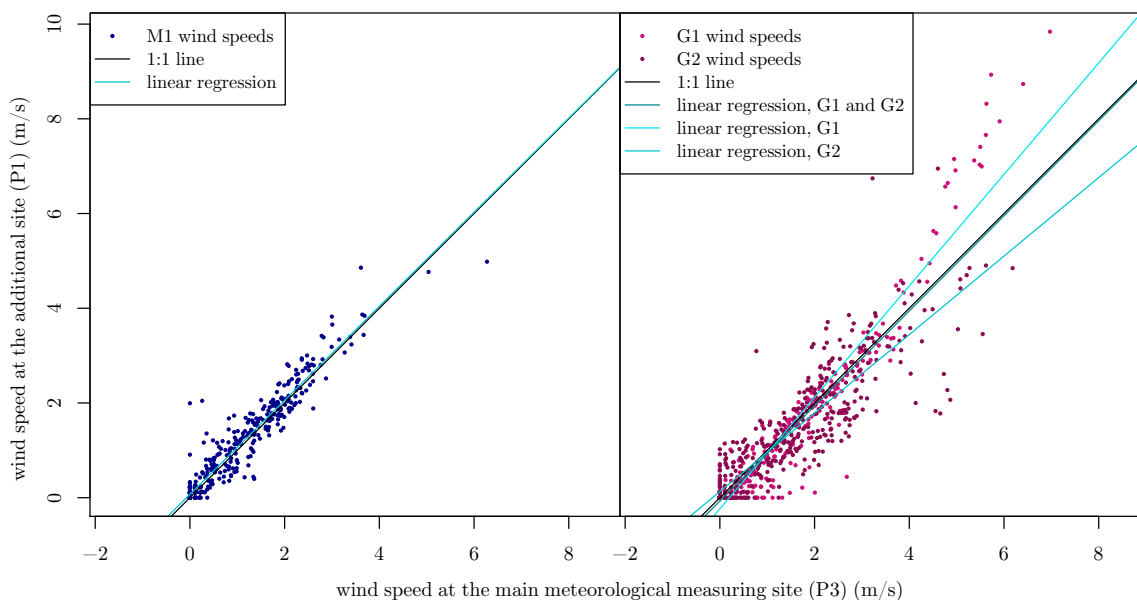
Figure 5.4: Scatter plot of corrected wind speeds taken at opposite ends of the measurement strip (figure 3.11) during M1 on Field A (left panel) and G1 and G2 on Field B (right panel), including regression lines. Regressions are all highly significant (p-value $< 2.2 \cdot 10^{-16}$). Slopes of regression lines of G1 and G2, respectively, are significantly different from zero.

5.2 Standard Comparison Method

Availability of the standard flux reference (SFR) system

During the first two sampling sequences of G1 and M1, the SFR system was, for the most part, out of order. After the first 12 hours of G1, gas flow from the gas cylinders to the tube system dropped and finally stopped entirely, even when the valve was entirely opened. Inspection by the manufacturer revealed that the construction material of the two-stage pressure valves were not suited to be used for gas mixtures containing ammonia, as it is not persistent against corrosion. One of the valves could be made available by the manufacturer for the last 40 hours of sampling sequence M1, the other one was only available from G2 on. As a consequence, for G1 and M1, data was only partially available. For G1, only the first three measuring intervals could be used for the calculation of NH_3 losses from experimental plots. Conversely, data on NH_3 transport and capture by passive samplers on SFR system plots was not collected during the first day of sampling sequence M1 on Field A. On SFR plots, the last 24 hours measuring interval of M1 was split in 6 hours subintervals and one 6 hours measuring interval was added after the end of measurements on experimental plots in order to obtain more data points for transfer factor modelling.

Passive sampler NH_3 trapping

The rate of NH_4^+ being trapped per minute in the passive sampler acid solution during the measurement intervals of the experiment (NH_4^+ concentration flux $mg\,L^{-1}\,min^{-1}$) is the starting point for the calculation of both transfer factors on SFR plots and fluxes of volatilized NH_3 from the surface of experimental plots. Time series of NH_4^+ concentration fluxes being observed on experimental plots, as shown in Figure 5.5, feature distinct temporal patterns and differences between plot treatments. Concentration fluxes for the first measuring intervals are always highest compared with the subsequent observations within the same sampling sequence. Data from plots fertilized with ^{15}N labelled slurry (Slu) could be significantly distinguished from minerally fertilized (Min) and 0 N control (Con) plots for most of the measuring intervals (see Figure 5.5). This is especially true in the very beginning of the sampling sequence (see Figure 5.5). Later in the experiment, the rate of NH_4^+ trapped by passive samplers installed on plots, as well as its variability, decreased and was similar for Slu, Min and Con plots. Concentration fluxes recorded on Slu plots, except for G1, feature a secondary maximum during the second day of measurements. Standard errors of the first measurement interval of G2 and G4 on Slu plots

were exceptionally high, being nearly three times as large as in the case of the other sampling sequences. In contrast to their distinction from Slu plots, differences between Min and Con plots were only significant for three intervals out of the five sampling sequences, two of them being the first ones directly after fertilizer application.
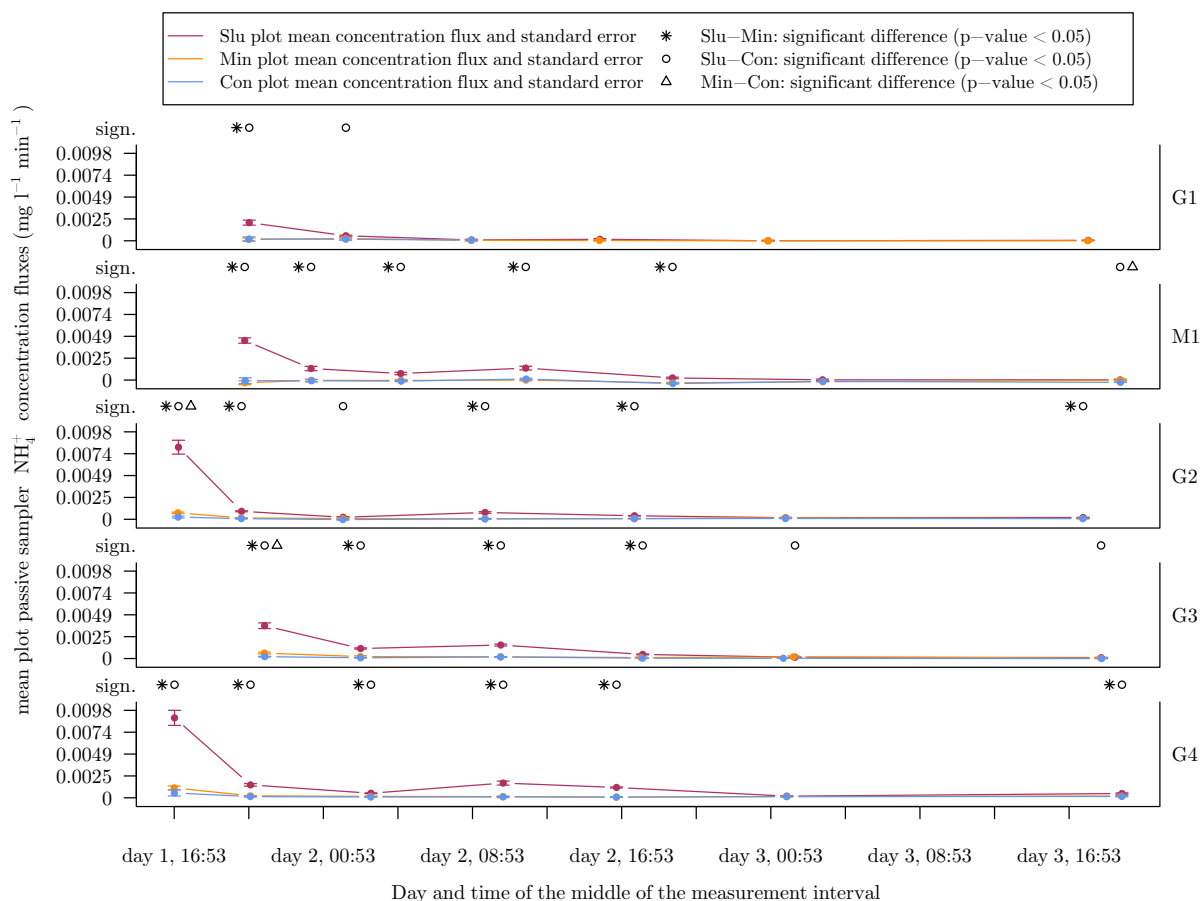
Figure 5.5: Mean corrected NH_4^+ concentration fluxes detected in the passive sampler acid solution of the replicates of Slu, Min and Con plots during the five NH_3 sampling sequences, including standard errors and the significance of the difference between mean concentration fluxes of different plot treatments

The ratio of pairs of passive sampler NH_4^+ concentration flux data from the two SFR systems continuously emitting $0.18\,\mathrm{L\,min^{-1}}$ and $0.09\,\mathrm{L\,min^{-1}}$ of the 10 % NH_3 in N_2 gas mixture (see Chapter 3.2), respectively, should be 2 if the efficiency of NH_3 transport and capture by the passive samplers is independent of the outgassing flux rate. In contrast, over all sampling sequences in which both SFR systems were in operation, the ratio was significantly higher than the theoretical value of 2 (p-value of 0.01).

Corrections of NH_4^+ concentration values

Evaporation of water from passive sampler acid solution or its dilution by precipitation or dew formation could be tracked by monitoring the concentration of a PO_4^{3-} spike in the samples (see Chapters 3.2.1 and 4.2). The data obtained indicates a small evaporation of up to 25.0% as the most frequent case, followed by evaporations of between 25.0 and 50.0% and dilutions of up to 25.0%. The median is an evaporation of 10.0%. Evaporation of up to 82.6% of the passive sampler acid solution is much less frequent. The picture is even more clear for dilutions - only a few extreme case of dilutions of more than 100%, with a single event of 257% could be documented (see Figure 5.6). Standard error of the NH_4^+ concentration data was reduced from 0.13 to 0.09 by correcting for dilution or evapotranspiration.
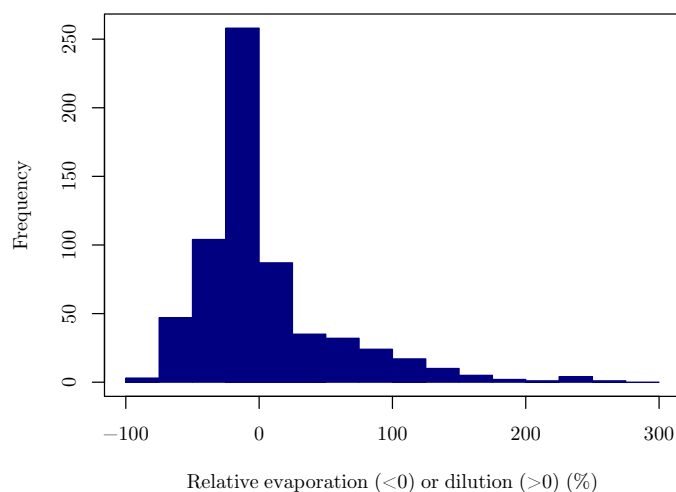
Figure 5.6: Histogram of the percentage of evaporation or dilution of the passive sampler acid solution during the measurement intervals.

Ambient concentrations of NH_3 in the air being advected towards the experimental site were tracked by four background concentration passive samplers. 95% of background sampler NH_4^+ concentration fluxes were in a range between 0 and $0.00093\,\mathrm{mg\,l^{-1}\,min^{-1}}$ with a median of $0.00028\,\mathrm{mg\,l^{-1}\,min^{-1}}$, which is about 31% of the median concentration flux from Slu plots. Consequently, correcting plot fluxes by the average measuring interval background NH_4^+ concentration flux decreased concentration fluxes of Slu, Min and Con plots by on average 42%, 90% and 95%, respectively.

Temporal dynamics of transfer factors

According to their definition, high transfer factor values indicate a high fraction of NH_3 released from the plot surface being captured by the passive samplers and vice versa. They can be looked at as a kind of capturing efficiency. Low intensities of atmospheric mixing lead to a slow transport of released NH_3 away from each plot and thus to a high fraction being trapped in the passive sampler acid solution. Transfer factors according to the SCM method varied between 0.15 and $1.57\,\text{mg}\,\text{L}^{-2}$ by about an order of magnitude (see Figure 5.7). During daytime, transfer factors were lower than transfer factors during night, which holds true for all sampling sequences with a few exceptional situations (see Figure 5.7) especially during hot summer sampling sequences. The dependence of transfer parameters on time of day is even more clear and can be statistically proven (see Figure 5.8) if measurement intervals of 24 h, which do not contain any sub-daily information, are excluded, transfer factors are normalized and plotted against the time of day.
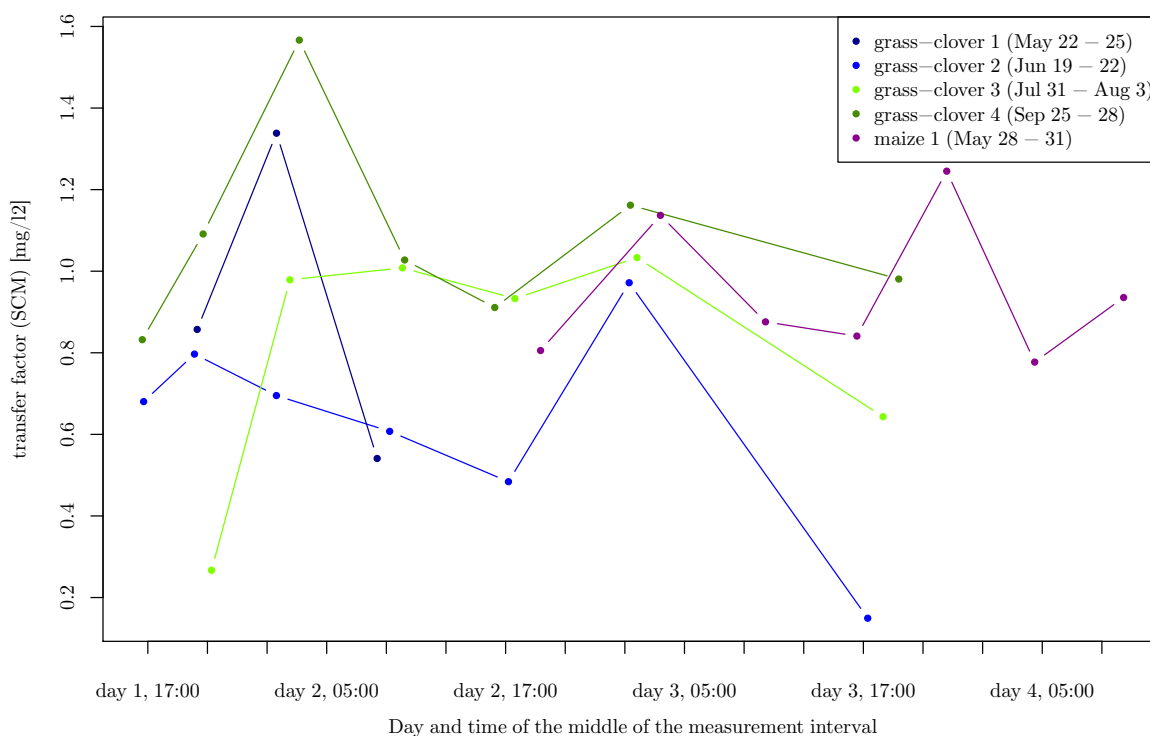
Figure 5.7: Levels of measurement interval transfer factors according to the SCM during the course of the five NH_3 sampling sequences
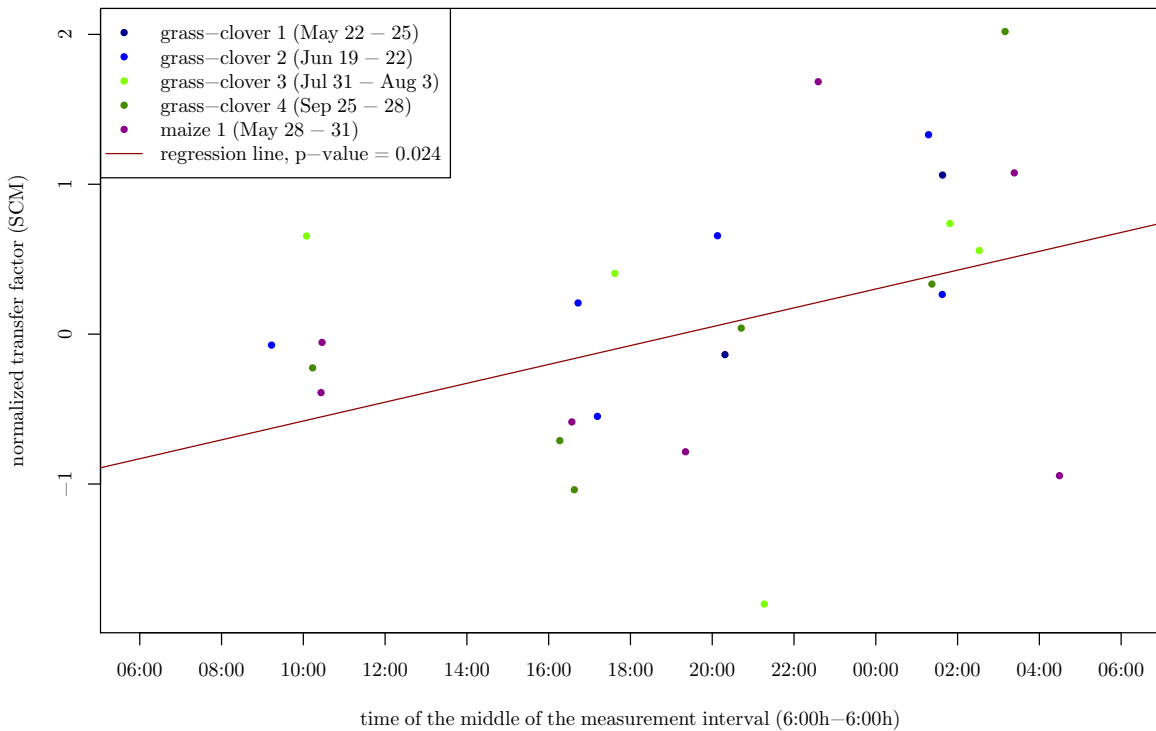
Figure 5.8: Levels of measurement interval transfer factors according to the SCM, plotted against day time from 6 am to 6 am, including a regression line of day time against transfer factors.

5.3 Model fitting and optimization

Optimization of linear models predicting transfer factors from meteorological observations resulted in quite different parametrizations, depending on the data available for one or a specific set of sampling sequences. 2 m air temperature and wind speed turned out to be part of the optimized model parametrization in the case of three single sampling sequences each (see Table 5.1). 2 m wind speed explains more of the variance of the data than 2 m air temperature, but temperature is the single optimal predictor for transfer factors if data from all sampling sequences is taken together. In the case of M1 and G3, none of the considered meteorological parameters could significantly explain transfer factors. Information on relative humidity is significantly relevant for M1 and G2, while bulk Richardson number as a proxy for atmospheric stability could only add to modelling transfer factors in G2. Interestingly, in the optimized model for G2, omitting the highly unsignificant 2 m air temperature did not result in an improvement of the AIC and even decreased p-values of the highly significant 2 m wind speed and air humidity as well as the bulk Richardson number in the reduced model. For overall models combining data from multiple sampling sequences depending on the data availability of relative humidity and bulk

Richardson number, air temperature was the only remaining and significant model parameter after model optimization (Table 5.1).

Table 5.1: Parametrization of initial and optimized models predicting transfer parameters from meteorological observations, including sampling sequence-specific and overall models. Further, p-values for optimized model parameters as well as mean residues of optimized model predictions relative to measured values are shown. t: air temperature; u: wind speed; rH: relative humidity; Ri: bulk Richardson number.

measurement sequence	G1	M1	G2	G3	G4	G1/M1/G2/G3/G4 overall model	M1/G2/G3/G4 overall model	G2/G3/G4 overall model
initial model parametrisation	t/u	t/u/rH	t/u/rH/Ri	t/u/rH/Ri	t/u/rH/Ri	t/u	t/u/rH	t/u/rH/Ri
optimized model parametrization	u	u/t/rH	u/t/rH/Ri	t	t	t	t	t
p-value for t		0.0666	0.626	0.202	0.00629*	0.000116*	0.000116*	0.000283*
p-value for u	0.0349*	0.444	0.0270*					
p-value for rH		0.0919	0.000601*					
p-value for Ri			0.184					
mean relative residues	0.32	0.06	0.22	65.79	0.13	14.98	16.94	19.05

Explanatory power of model fits

Nash-Sutcliffe model efficiency coefficients (NSE) of models predicting transfer factors from meteorological observations turned out to be highly variable for the different sampling sequences and model types. The results for optimized single-sequence, complementary and overall models are displayed in Figure 5.9. Only for sampling sequences G1, M1 and G2, NSE values of optimized models were higher than the threshold value of 0.5, above which the model is considered to be of sufficient quality to predict transfer factors. Optimized overall models fitted on data of the same data availability taken together (t/u, t/u/rH, t/u/rH/Ri) performed better than the mean of the transfer factors, indicated by NSE values above zero, but were clearly worse in predicting transfer factors than the single-sequence models. Except for G1, optimized complementary models, fitted on all data except of data from the respective sampling sequence itself, performed even worse in predicting transfer factors than the plain mean of the original transfer factors, as the NSE amounts to less than zero.
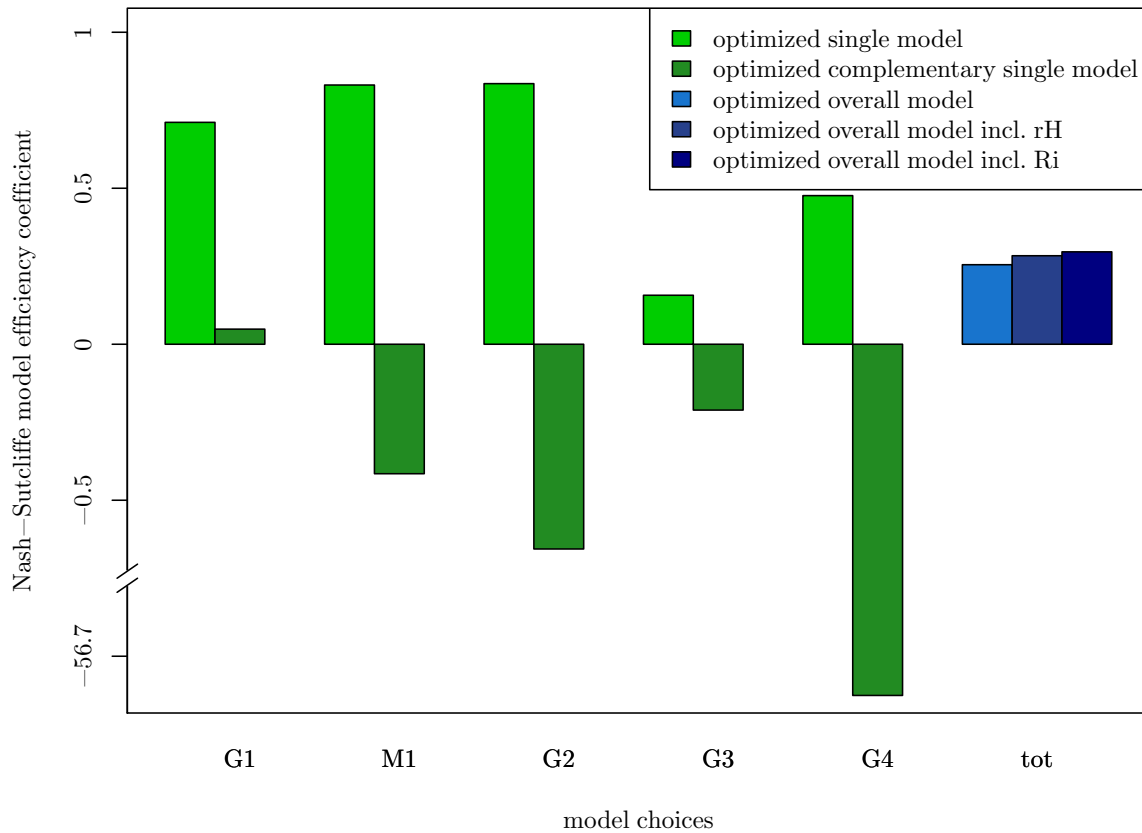
Figure 5.9: Nash-Sutcliffe model efficiency coefficients of optimized single-sequence and complementary models as well as three overall models fitted using t/u, t/u/rH or t/u/rH/Ri, respectively.

5.4 NH₃ volatilization fluxes

5.4.1 General flux patterns

Temporal aspects

Time series of NH$_3$ volatilization from experimental plots all feature a similar pattern, characterized by an initial peak during the first measurement interval and a secondary maximum during the second day of the measuring sequence (figures 5.10, 5.11). These observations can be substantiated for the five measurement sequences, as well as both for data based original SCM and the optimized single-sequence model by the following measures:

For all sampling sequences, volatilization during the first measurement interval made up a large part of the total NH$_3$-N release (figures 5.10, 5.11). Directly after slurry application, fluxes determined using the SCM exceeded the mean flux of the following measurement intervals by

factor 3.38 (G1) to factor 7.37 (G3). Between 38.9 % (G2) and 62.8 % (G1) of the total amount of released NH_3-N was volatilized within the first measurement interval. After the initial peak, NH_3 fluxes strongly decreased and faded out towards the end of the sampling sequence (Figures 5.10, 5.11). After three days of measurements, measured and modelled fluxes were still significantly different from 0 in the case of G2, G3 and G4 both for the SCM and the optimized model. Temporal trends of NH_3 volatilization did not differ between models and SCM. In contrast to the original SCM method, the (optimized) models were able to cover measuring intervals of sampling sequences G1 and M1 during which the SFR system was out of operation and thus provide complete time series. Cumulative volatilization according to the SCM could not be calculated for M1 because the SFR system was not available during the initial measurement intervals of M1. Similarly, for G1, cumulative volatilization according to the SCM is not complete as values for late volatilization more than 12 hours after slurry application are lacking. Interesting temporal features are the secondary maxima in NH_3 volatilization during the second day that occured during the third and fourth interval of all sampling sequences except of G1 (figures 5.10, 5.11). For G1 and M1, the measuring intervals during which this feature occured could not be captured by pure SCM measurements due to the SFR system failures, but is only contained in NH_3 flux data based on modelled transfer factors (figure 5.11). Secondary maxima are especially visible when displaying NH_3-N flux as a function of time of day (Figure 5.12).

Differences between fertilizer treatments

The amount of NH_3 emission from slurry (Slu) plots can be distinguished from the results of mineral fertilizer (Min) and control (Con) plots. Especially in the first interval of the sampling sequence, significantly more NH_3-N was released from the surface of Slu plots than from Min and Con plots. This is shown in time series of cumulative amounts of NH_3-N released (Figure 5.13). Only for G2, G3 and G4, the amount of NH_3-N volatilized from Slu plots during the last 24 h measurement interval was significantly different from Min and Con values, in contrast to G1 and M1. Volatilization of NH_3 from Min and Con plots was at the same level throughout most of the time of measurements. In the case of G2, G3 and G4, Min plots showed slightly elevated NH_3 fluxes in the initial measurement interval. Levels of NH_3 volatilization from Slu plots were between 4.5 and 7 times higher than from Con and Min plots. Absolute levels of NH_3-N loss ranged from $0.14\,\mathrm{g\,m^{-2}}$ (G1) to $1.04\,\mathrm{g\,m^{-2}}$ (G2) on Slu plots according to the optimized model. Min and Con plots reached $0.03\,\mathrm{g\,m^{-2}}$ (G1) to $0.22\,\mathrm{g\,m^{-2}}$ (G2) and scaled with the Slu plot values (see Figure 5.14). In the case of M1, calculations yielded negative emissions for Min and
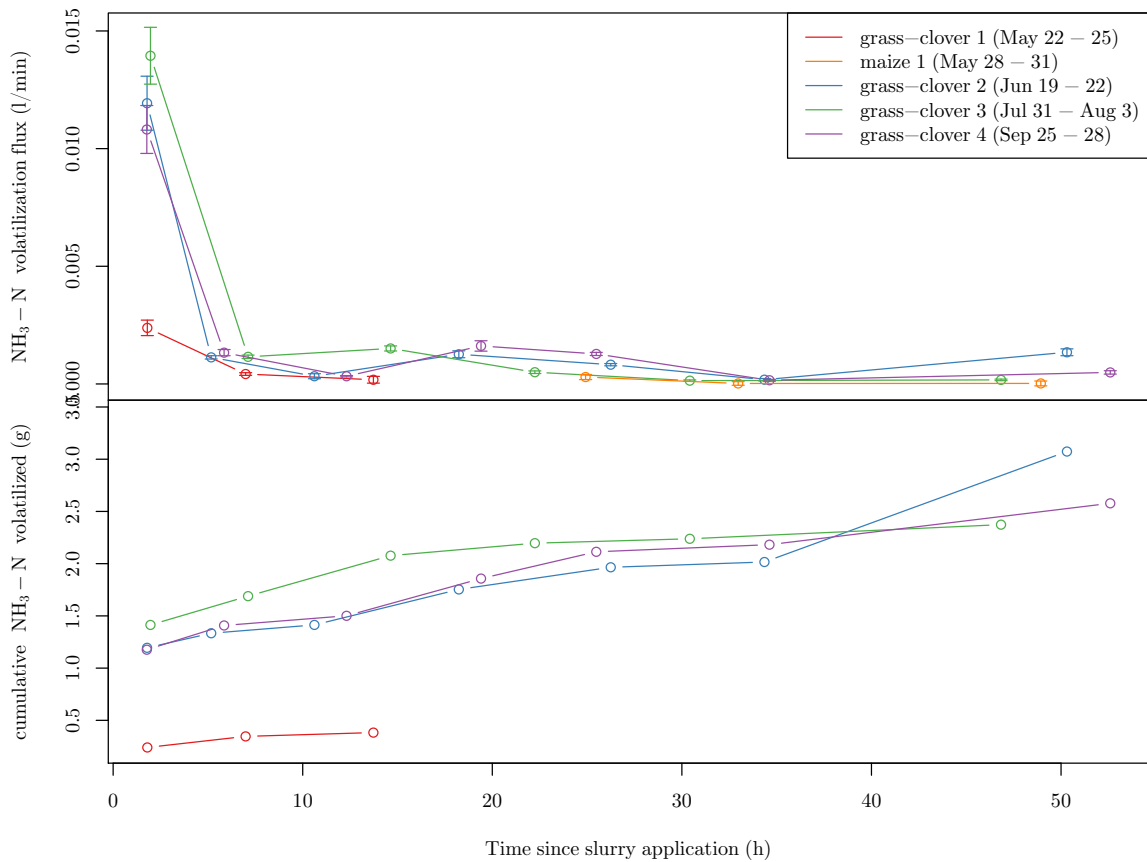
Figure 5.10: Time series of NH_3 volatilization from Slu plots according to the SCM for each NH_3 sampling sequence, fluxes per plot including replicate standard errors as error bars (upper panel) and cumulative amounts of NH_3-N volatilized per plot (lower panel) as a function of time since fertilizer application.

Con plots, which can be attributed to the correction of NH_4^+ concentrations found in the passive samplers by background measurements that exceeded the concentrations on Min and Con plots.

Total amount of NH$_3$-N volatilized

Emissions of NH_3-N from slurry plots differed strongly between sampling sequences that were conducted under different meteorologic conditions. Losses of NH_3-N for the comparison of sampling sequences were calculated based on the optimized model, as original SCM data of sampling sequences G1 and M1 is not complete due to failures of the SFR system. A comparison of total amounts of NH_3-N losses predicted by the different models and the SCM method relative to the optimized model can be found in Table 5.2.

Total volatilization of NH_3 from the surface of Slu plots covered a range of nearly an order of magnitude between $0.14\,\mathrm{g\,m^{-2}}$ (G1) and $1.04\,\mathrm{g\,m^{-2}}$ (G2, see Figure 5.14). This represents
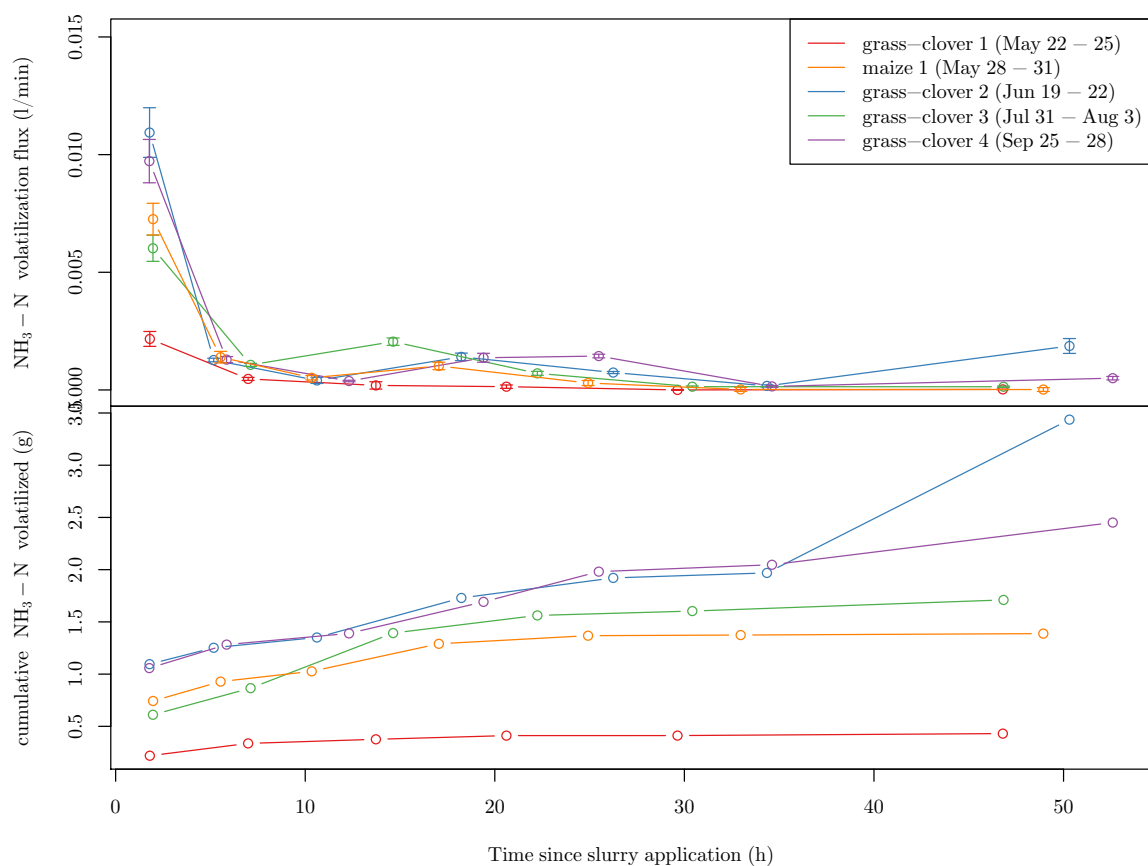
Figure 5.11: Time series of NH₃ volatilization from Slu plots according to the optimized model for each sampling sequence, fluxes per plot including replicate standard errors as error bars (upper panel) and cumulative amounts of NH₃-N volatilized per plot (lower panel) as a function of time since fertilizer application.

3.9 to 31.1 % of the NH_4^+-N (TAN) or 2.4 to 19.1 % of the total N contained in the applied slurry (see Figure 5.14). Especially the first sampling sequence G1, measured using incomplete instrumentation and featuring low temperatures and rain during the first measurement intervals, yielded very low values. Highest volatilization was recorded in late June during G2. Compared to Field B values (G1 - G4), a relatively low amount of NH₃ was measured to volatilize during the sampling on Field A (M1). This is especially true if comparing M1 to G2 or G3, all featuring hot, partially windy conditons without precipitation during the sampling sequence. Looking at the SCM values (Figure 5.10), NH₃ volatilization rates in sampling sequences G2, G3 and G4 were quite similar. Only in the last interval of G2 and in contrast to all other measurements, a late increase of NH₃ volatilization during the last measurement interval was recorded, which had large effects on the total amount of NH₃-N lost from the plot surface.
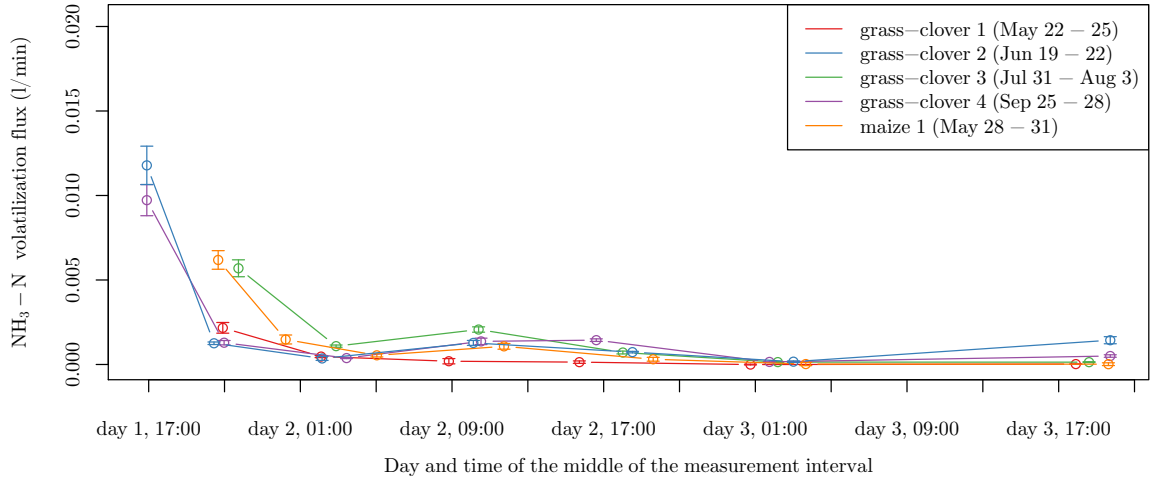
Figure 5.12: Time series of NH$_3$ volatilization from Slu plots according to the optimized model, fluxes as a function of time of day, including replicate standard errors as error bars.

Table 5.2: NH$_3$-N volatilized for the optimized model in the five sampling sequences and relative percentage of NH$_3$-N release according to the SCM, the complementary model, the null model and the ALFAM2 predictions compared to the optimized model.

NH$_3$ sampling sequence	G1	M1	G2	G3	G4
optimized model $(\mathrm{g\,m^{-2}})$	0.14	0.46	1.15	0.57	0.82
SCM (%)	89		89	139	105
complementary model (%)	109	107	56	152	42
null model (%)	115	91	69	92	92
ALFAM2 (%)	159	145	80	168	73

5.4.2 Differences between models

Single-sequence models

If models designed to predict transfer factors for the calculation fluxes and amounts of released NH$_3$-N from meteorology should be an alternative to constantly running the SFR system included in the original SCM, as proposed in the third hypothesis (chapter 2), it is necessary that they are able to yield high accuracy predictions of resultant fluxes compared to the original SCM measurements. In this experiment, meteorology-based models strongly differed in their accuracy relative to the original SCM (Figure 5.15).

The optimized meteorology-based models increased the quality of transfer factor prediction relative to the null model, which equals to the temporal mean of SCM transfer factors (see
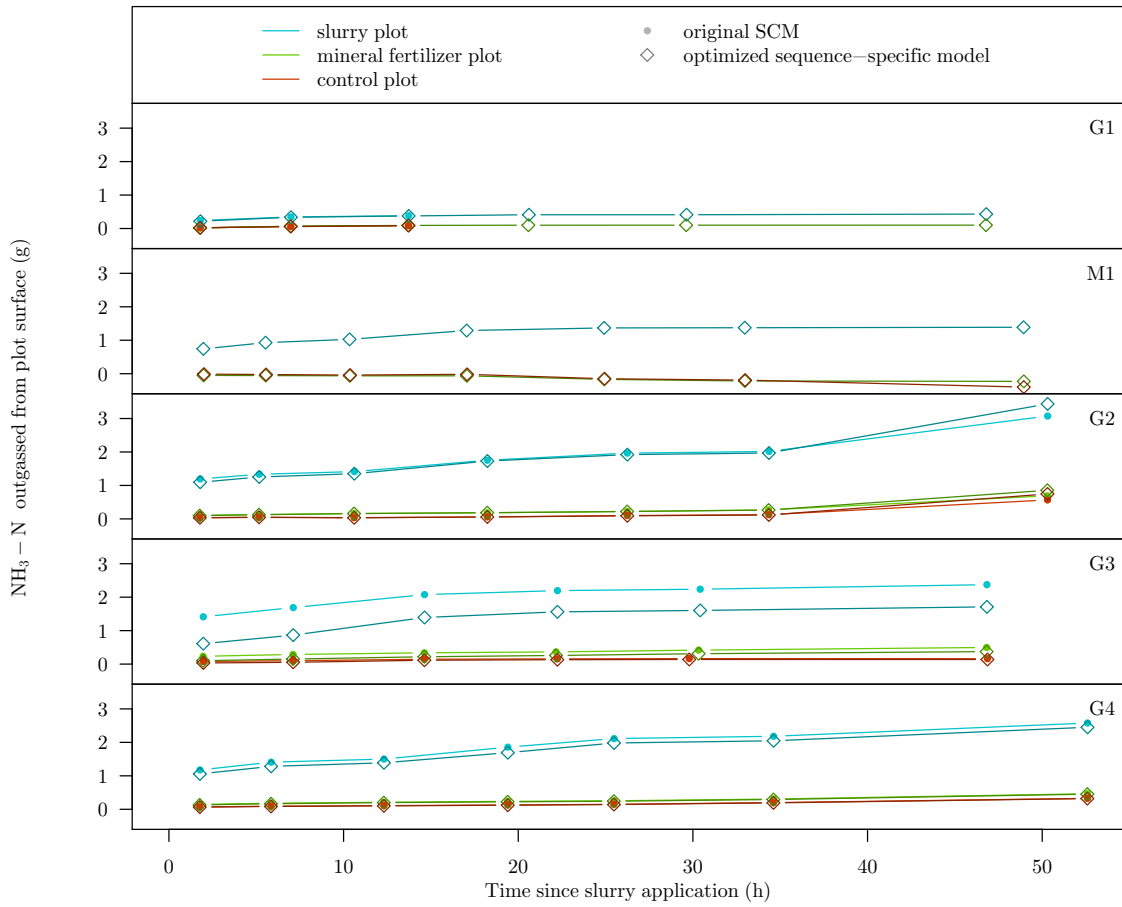
Figure 5.13: Mean cumulative amounts of NH_3 volatilized from Slu, Min and Con plots according to the optimized model compared to the SCM method for each NH_3 sampling sequence.

Chapter 5.3. NH_3 fluxes calculated based on the null model estimation for transfer factors deviated considerably from the NH_3 fluxes according to the SCM throughout all sampling sequences. In contrast, NH_3 fluxes calculated based on optmized model transfer factors deviate little from SCM fluxes. This relation was most clearly visible when comparing cumulative time series of NH_3-N released from cattle slurry amended plots during sampling sequences G3 and G4 (see Figure 5.15). All model lines run steadily in parallel. While the null model line is far away from the SCM, predictions of the optimized model were found to be more accurate.

For G2, the optimized model was, in contrast to the null model, able to map the the relatively high NH_3 flux in the last measurement interval (Figure 5.15). This can be assigned to adding information on relative humidity to the model parametrization, as the G2 optimized model only fitted on temperature and wind speed data increased the initial pulse of NH_3 volatilization in the first interval compared to the SCM method and then predicted continuous release rates at low levels until the last interval.
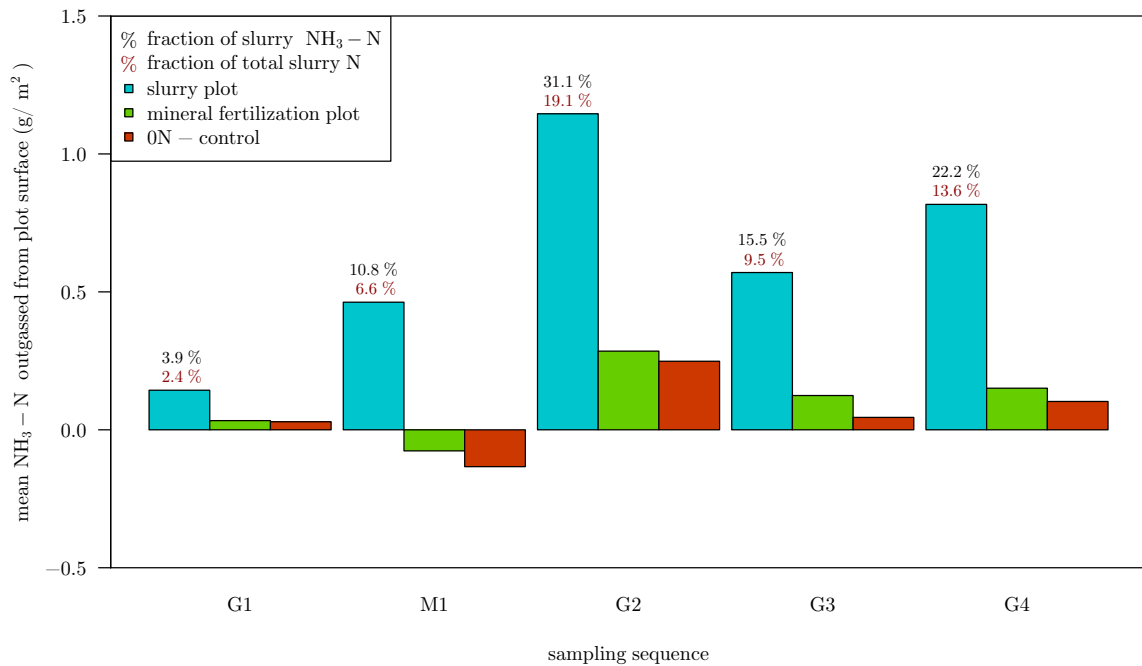
Figure 5.14: Total amounts of NH$_3$ volatilized from Slu, Min and Con plots, according to the optimized model, grouped by the five sampling sequences. Additionally, the fraction of the slurry total or NH$_4^+$-N that is represented by the NH$_3$-N losses from the Slu plots is displayed.

The first and second NH$_3$ sampling sequences, G1 and M1, were characterized by a partial lack of SCM data due to equipment failures. For G1, modelled cumulative NH$_3$-N release could be compared with SCM records during the first two measurement intervals and yielded a good fit.

During the first day of M1 measurements, the SFR system was not running and thus, no NH$_3$ flux could be calculated using the SCM method. The optimized model was fitted on meteorological and passive sampler data collected during and after the last three sampling sequences of M1. Modelled fluxes matched well the SCM data available for M1 for the last three sampling sequences. Comparing modelled NH$_3$ flux and cumulative amounts of NH$_3$-N released during G1 and M1 with original SCM data sampling sequences with continuous SFR system coverage revealed a plausible pattern of G1 and M1 NH$_3$ time series.

In general, flux calculations using transfer factor estimations from meteorology-based models seemed to underestimate the initial emissions of NH$_3$ directly after fertilizer application compared to SCM data, while emissions towards the end of the measurements are often overestimated.
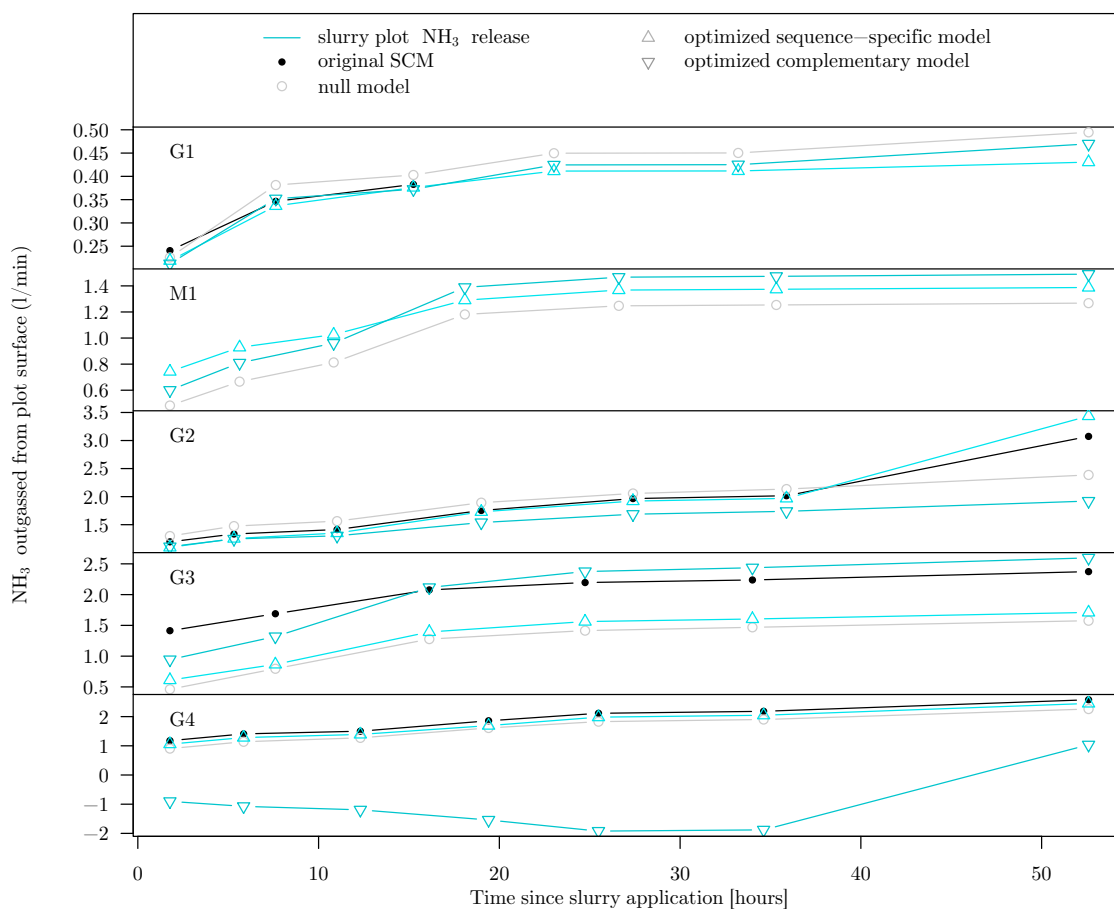
Figure 5.15: Mean cumulative amounts of NH_3 volatilized from Slu plots according to the SCM as well
as the Null models, initial fully parametrized models and optimized models for each of the
five sampling sequences.

Complementary models

In this experiment, complementary models were, with the exception of G3, not able to reach
an accuracy to predict transfer factors similar to that of the optimized single-sequence models.
Only in G3, NH_3 fluxes calculated based on the complementary model turned out to be closer to
the SCM fluxes than the optimized model. In contrast to that, for the other sampling sequences,
complementary models were worse in predicting NH_3 fluxes than optimized models, and G2 and
G4 even worse than the null model. The complementary model fitted for G4, including data from
G2 and G3 in order to be able to integrate rH and Ri predicts unphysical negative NH_3 fluxes
for most measurement intervals and thus is an exceptionally bad predictor (see Figure 5.9).

5.4.3 Comparison of SCM and ALFAM2

A comparison of the NH$_3$ losses as measured by the original SCM, the enhanced SCM using a meteorology-based model and a prediction calculated by using the ALFAM2 model (Hafner et al., 2019) reveals that measurements and model predictions show very similar patterns. The deviation of ALFAM2 predicted values from SCM measurements are in the same range as the deviations of results based on the optimal model from the original SCM for all sampling sequences. There is no tendency visible indicating systematic over- or underestimations of NH$_3$ emissions by ALFAM2 compared to SCM (also see Table 5.2). This is supported by a pairwise t-test between SCM and ALFAM2 cumulative NH$_3$ losses, resulting in a p-value of 0.52, indicating no significant difference in true means. For optimal model compared to ALFAM2 datas, the pairwise t-test p-value is 0.71.
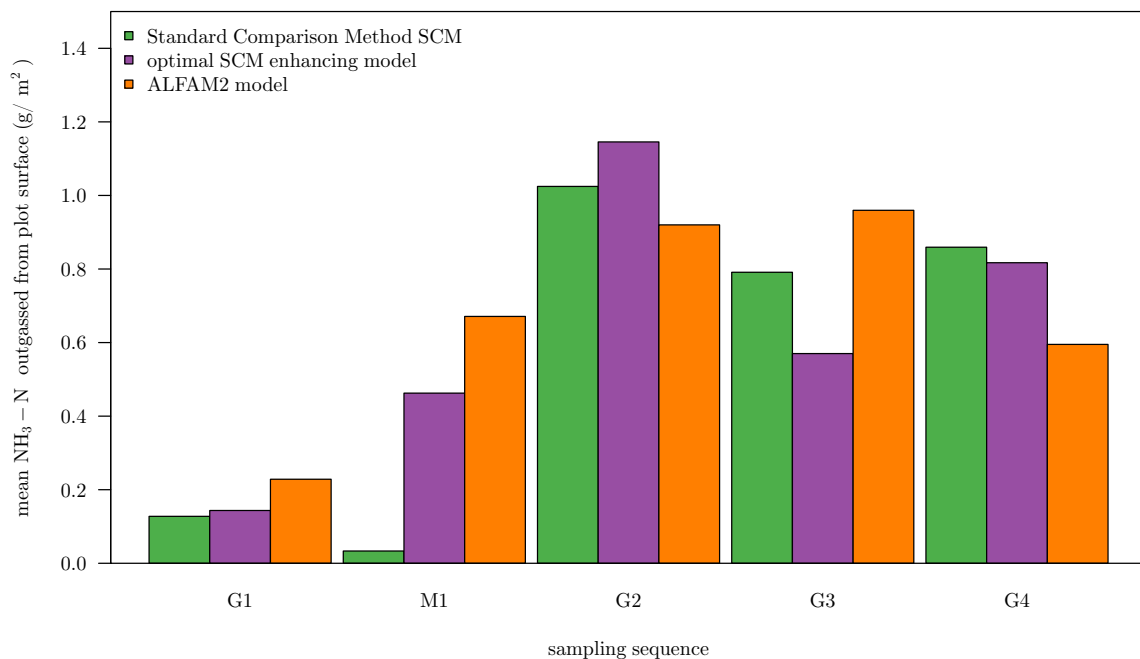
Figure 5.16: Total amounts of NH$_3$ volatilized from Slu plots according to the SCM as well as the optimized meteorology-based models, compared with prediction by the ALFAM2 model (Hafner et al., 2019), grouped by the sampling sequences.

5.5 Plot N balance

The contribution of measurements of the volatilization of NH$_3$ after fertilization to closing the plot N balance differs between field sites in the experiment. Volatilization data for sampling sequences G2 - G4 is directly taken from SCM measurements, while for G1 and M1, data based

on the optimized model was used, which also include the volatilization of NH_3 during times of SFR system failure. Adding data on N losses via volatilization to the average plot N balance reduced the amount of fertilizer N not captured by measurements of biomass uptake and removal, leaching and soil storage in the case of both Slu and Min treatments on Field B (see Table 5.3). In contrast, for Field A, considering NH_3 volatilization rather downgrades the accuracy of the N balance. For Slu plots, the sum of recoveries from all N pathways traced including volatilization exceeds the amount of fertilizer N applied by 5.1 % (Table 5.3). Compared to that, without considering NH_3 volatilization, the remaining data on fertilizer N recoveries from soil and plant pathways sum up to 98.5 %) of the fertilizer N applied. On Min plots, volatilization data is erroneous, featuring negative values. If these data would be considered, they would increase the gap between the amount of fertilizer N spread and recoveries in soil and plant samples.

Table 5.3: Partial and Total, average N balance of fertilized plots in absolute and percental numbers relative to the amount of fertilizer N applied. The partial N balance is based on recovery data obtained by tracing soil and plant pathways of N fate; the total N balance additionally includes N loss via volatilization of NH_3. Data on N leaching (*italic*) was not directly measured but was inferred based on multiple indications as discussed in Chapter 6.4.

Fate of fertilizer N	Field A				Field B			
	Slu		Min		Slu		Min	
	$\frac{g}{m^2 \cdot a}$	%	$\frac{g}{m^2 \cdot a}$	%	$\frac{g}{m^2 \cdot a}$	%	$\frac{g}{m^2 \cdot a}$	%
Appl. fertilizer N	6.00	100.0	3.68	100.0	24.00	100.0	14.71	100.0
Biomass	1.25	20.9	1.59	43.3	3.80	15.8	5.59	38.0
Leaching	0.00	0.0	0.00	0.0	0.00	0.0	0.00	0.0
Remaining in soil	4.66	77.6	0.82	22.2	15.63	65.1	5.37	36.5
Partial N balance	5.91	98.5	2.41	65.5	19.43	80.9	10.96	74.5
Volatilization	0.40	6.6	−0.11	−3.1	2.41	10.1	0.50	3.4
Total N balance	6.31	105.1	2.30	62.4	21.84	91.0	11.46	78.9
Total N balance gap	−0.31	−5.1	1.39	37.6	2.14	9.0	3.25	22.1

Comparing recoveries in different compartments on plots managed according to Slu and Min treatments show that a larger fraction of the mineral fertilizer was taken up by plants than of the cattle slurry. Further, Min treatment results in a lower percentage of fertilizer N remaining in the soil close to the end of the cropping season. Overall, together with NH_3 volatilization, the gap not covered by the plot nitrogen balance is larger for Min than for Slu plots. These results are valid for both Field A and B.

Nevertheless, Field A features different patterns of N pathways than Field B. Compared to Field B, plant uptake as well as the soil remainder on Field A Slu plots is clearly higher. This results in a higher total recovery on Field A despite the lower recorded NH_3 volatilization rates. Plant uptake on Min plots is, similar to the Slu plots, higher on Field A than on Field B, but the part that remained in the soil is lower. NH_3 volatilization is close to zero. This resulted, in contrast to Slu plots, in a lower recovery on Field A than on Field B Min plots.

6 Discussion

6.1 Ammonia volatilization

In this study, NH_3 volatilization from replicated microplots amended with cattle slurry and ammonium nitrate as well as control plots was measured using the SCM method (Vandré and Kaupenjohann, 1998). Measuring and analyzing NH_3 volatilization during and after these five fertilization events, one on a field cropped with silage maize (Field A) and four on a grass-clover field (Field B, see Figure 5.16), this study supplied data to the PhD thesis on manure management within the NitroGäu framework (Frick et al., 2018).

While for three sampling sequences on Field B, measurements could be conducted without major technical problems, the first measurement on Field B and the measurement on Field A were suffering from equipment failures, which led to incomplete NH_3 emission time series and thus an underestimation of the total amount of NH_3 loss by the original SCM. This could be compensated for by predicting transfer factors using a meteorology-based model, which is discussed later (see Chapter 6.2). Comparing gaseous N losses through NH_3 volatilization from cattle slurry and ammonium nitrate applications shows that volatilization of NH_3 is much greater from slurry than from mineral ammonium nitrate fertilizer (see Figures 5.13, 5.14), which corresponds to the expectations (Sommer and Hutchings, 2001; Meisinger and Jokela, 2000; Louro et al., 2013; Van der Weerden and Jarvis, 1997; Whitehead and Raistrick, 1990; Bouwman et al., 2002) and supports the first hypothesis (chapter 2).

Emission factors for NH_3 volatilization from cattle slurry reported in the literature cover a wide range of values as they are strongly influenced by a multitude of environmental conditions and slurry properties (Meisinger and Jokela, 2000; Sommer et al., 2003). Emission factors reach from 2.3 % of the TAN applied on the field (Pietzner et al., 2017) to nearly 100 % (Sintermann et al., 2012). Frequently, values are between 25 and 50 % (Häni et al., 2016; Louro et al., 2013; Sintermann et al., 2012; Génermont et al., 1998). Compared to that, observed emission factors in our experiment (between 3.9 and 31.1 % of TAN according to the optimized model, see Figure 5.14) are in the lower range of literature values. Absolute levels of NH_3 volatilization of 1.28 -

$10.2\,\mathrm{kg\,ha^{-1}}$ according to the SCM or 1.40 - $11.5\,\mathrm{kg\,ha^{-1}}$ according to the optimized model in our study are in the magnitude of the results of other experiments on the lower end of the scale (Misselbrook et al., 2005; Thompson and Meisinger, 2005; Gericke et al., 2011; Spirig et al., 2010; Vandré and Kaupenjohann, 1998). For example, Spirig et al. (2010) measured similar low volatilization of NH_3, which was attributed to a low dry matter content of the applied slurry which favoured infiltration, as well as low N content and low water vapour saturation deficit of the air. However, many other studies resulted in volatilization levels of up to $75\,\mathrm{kg\,ha^{-1}}$ (Misselbrook et al., 2005; Thompson and Meisinger, 2005).

A re-evaluation of swiss NH_3 volatilization measurements and emission factors, conducted by Häni et al. (2016), revealed that newer measurements systematically resulted in lower emissions as compared to earlier experiments, which could be explained by methodological shortcomings of the earlier studies revealed by posterior analysis. Except for advection of NH_3 between the replicate plots, these problems do not apply to the SCM method and the instruments we used, but contribute to a systematic overestimation of older NH_3 losses. Additionally, most values for emission factors and NH_3 emissions were established for splash plate broadspreading as reference slurry application method. Splash plate broadspreading is reported to yield higher NH_3 volatilization losses than the banded application using trail hoses as imitated in this study. These two aspects additionally support our comparably low values.

In the literature, volatilization of NH_3 after field application of ammonium nitrate is very low, almost negligible (Chambers, Dampney, et al., 2009; Van der Weerden and Jarvis, 1997; Sommer and Jensen, 1994; Whitehead and Raistrick, 1990), reporting emission factors between 0.8 and $1.6\,\%$ of the ammonium nitrate N applied. This is in contrast to the observations in our experiment, where NH_3 volatilization from plots amended with mineral fertilizer accounts for 0.6 to $6.25\,\%$ of the ammonium nitrate N applied, with values of between 4.20 to $6.25\,\%$ for the measurement campaigns without technical issues. Similarly, though NH_3 losses from the $0\,N$ control plots were observed to be lower than those from minerally fertilized plots, NH_3 volatilization was still observable through elevated concentrations of NH_4^+ in the passive samplers compared to background passive sampler values. This contradicts the expectation of zero NH_3 volatilization from non-fertilized plots.

Elevated NH_4^+ concentration levels in passive sampler solutions collected on minerally and non-fertilized plots (see Figure 5.5) could potentially be explained by cross-contamination by advection of NH_3-rich air from neighboring plots amended with cattle slurry. This might be caused by an insufficient distance of only $5\,\mathrm{m}$ between the microplots in our experiments. This

aspect has been, for example, mentioned in Wulf et al. (2002). An evaluation by Gericke et al. (2011) showed that under constant wind, a downstream influence up to a distance of 3 times the plot size is significant, where 25 % of the source strength could still be detected. In our case, this would be at a distance of 6 m from the Slu plots, which illustrates the likeliness of plot level cross-contamination. This is supported by the observed temporal pattern of NH_3 volatilization on Min and Con microplots, being similar to the one observed on Slu plots (see Figure 5.10), which implies that the underlying effect features the same dynamics as NH_3 volatilization from field applied slurry, or that the observations are directly coupled with it. Con and Min plots are, due to the semi-randomized block design of the plot arrangement (chapter 3.1.3, Figure 3.5), equally distant from Slu plots and should be similarly affected by plot level cross-contamination. If Con plot emissions are substracted from Min plot values before the calculation of emission factors, resulting emission factors of ammonium nitrate applied to Min plots are in the range of above mentioned literature values, except for the G3 case in which the ammonium nitrate emission factor is still at 3 %. This further supports potential cross-contamination as a reason for elevated calculated NH_3 losses from Min and Con plots.

Another explanation adding up to the cross-contamination could be effects of the re-wetting of the soil in the microplots by application of ammonium nitrate as aqueous solution on Min plots and stream water on Con plots. Effects of soil rewetting on NH_3 fluxes and the responsible mechanisms have not yet been systematically explored (Kim et al., 2012). Studies reported a 7 day response following rewetting, increasing NH_3 emissions by a factor of 5 to 10 compared to pre-rain conditions (Kim et al., 2012). Rochette et al. (2009) observed slight increases in NH_3 emissions from fertilized plots after light irrigation.

Contamination of background passive samplers during M1 could also be the reason for unphysical, negative results for NH_3 emissions from Min and Con plots of the original SCM and the optimized meteorology-based model (see Figure 5.13). Background passive sampler NH_3 concentration data for M1 are significatly greater than the records from the remaining measurements G1 to G4. Field A, on which M1 measurements took place beginning from the 28th May 2018, was fertilized on the 19th May 2018 using cattle slurry on the part not directly required for our experiment. NH_3 emissions can continue at, for the total amount of NH_3 loss, n levels after the first peak for at least 10 days (Génermont and Cellier, 1997) or several weeks (Rochette et al., 2009) after slurry application. It is likely that background passive samplers were influenced by residual NH_3 volatilizing from the surface, exceeding NH_3 emissions from Min and Con plots that were excluded from the farmer's amendment with cattle slurry. This could have led to an over-

correction of NH$_3$ concentrations being trapped in the passive sampler solution on microplots. Consequently, the values for NH$_3$ volatilization from Slu plots would be affected as well and are likely to underestimate true NH$_3$ losses from Field A. On the other hand, rain leads to dilution and faster infiltration of the liquid phase of surface-applied slurry and hence less potential for volatilization of NH$_3$ (Sommer et al., 2003; Hafner et al., 2019). At the meteorological station of Wynau in a distance of 9.2 km (see Chapter 4.1), rainfall of 22.2 mm was recorded in the afternoon of the 19th May 2018. Another 16.3 mm followed on the 22nd May 2018. Rain on the 19th May 2018, potentially after slurry application, could have had the effect of reducing NH$_3$ emissions. Nevertheless, it is not certain if the observations in Wynau can be transferred to our field site, as heat thunderstorms in the afternoon or evening are typically very local in extent.

A comparison with the predictions of the ALFAM2 model (Hafner et al., 2018) for NH$_3$ emissions from cattle slurry, calculated for the specific field conditions recorded during the measurement campaigns, shows that ALFAM2-modelled NH$_3$ losses do not significantly differ from original and modelled SCM measurements (see Figure 5.16). This additionally supports the empirical realism of the SC method as described by Vandré and Kaupenjohann (1998) and of our implementation on the field. The comparably low cumulative emissions of G1 relative to the remaining sampling sequences could be reproduced by the ALFAM2 predictions and can be attributed to the rainfall during the night and morning following the fertilizer application (see Figure 5.1). Also, these results show that even if NH$_3$ volatilization could be only recorded by the original SCM during the first 18 hours after fertilizer application, most of the total NH$_3$ losses could be captured. On the other hand, for the measurements of M1, comparison with the ALFAM2 predictions indicate that the original SCM could only capture a small residual part of the total NH$_3$ losses. However, the meteorology-based model as discussed in Chapter 6.2 could predict total cumulative emissions that come close to the ALFAM2 predictions and thus ensure the availability of NH$_3$ loss data for M1.

Comparing (modified) SCM and ALFAM2 results, it can be reasonable to use advanced, but simple semi-empirical models such as the ALFAM2 model for obtaining data on the volatilization of NH$_3$ from cattle slurry, as they are able to provide comparable information at lower costs and effort. The ALFAM2 model is a quite new development and no independent verification is available yet. Nevertheless, the large underlying data base as well as the simple but apparently effective structure seems to be promising. This gives rise to the outlook that an extension of the ALFAM2 data base (Hafner, 2019) has the potential to further improve the model. On the one hand, calibrating or verifying the model on data from regions other than temperate north-western

Europe would allow to extend its scope. On the other hand, adding more field data from the present area of application, as well as further experimental verification, could further strengthen confidence in ALFAM2's quality, especially when it comes to the model parameters for pig slurry. Furthermore, it would be promising to establish a robust data foundation on NH_3 emissions from other kinds of organic fertilizers than pig and cattle slurry, such as biogas digestate, composts, mulches and others. These alternative organic fertilizers can be expected to be increasingly used in agriculture due to a proposed shift towards using bio-energy, cover crops and organic farming approaches. This leads to a further demand for knowledge on their enviromnental implications, such as emissions of NH_3, to be used for example in life cycle assessments of agricultural production.

Time series of NH_3 emissions are characterized by initial peaks, followed by a strong decrease in magnitude in the second measurement interval and a fading out of emissions during the following days. This is in line with most measurements of NH_3 volatilization from animal slurry reported in the literature (for example Génermont and Cellier, 1997; Sommer and Hutchings, 2001; Thompson and Meisinger, 2005; Gericke et al., 2011). The fact that the fragments of NH_3 volatilization time series captured during G1 and M1 (figure 5.12), as well as time series of passive sampler NH_3 concentration flux (figure 5.5), nicely fit to the records of the remaining field campaigns indicates that these data are equally realistic and usable for prediction of the cumulative NH_3 loss. Also, the secondary peak in NH_3 volatilization from Slu plots we observed at the third and fourth measurement interval during some field campaigns (M1, G2, G3, G4, see Figures 5.5 and 5.12) is documented in the course of some NH_3 emission event records (Thompson and Meisinger, 2005; Sommer and Hutchings, 2001; Pain et al., 1989). According to Sommer and Hutchings (2001), this secondary emission peak, usually occuring during the morning of the day after slurry application, can be explained by the typical diurnal dynamics of radiation input, temperature and wind speed as major factors influencing NH_3 volatilization from animal slurry. In the SCM, fluxes of NH_3 from an experimental plot's surface are calculated from the rise of NH_4^+ concentrations in passive sampler acid solution observed during the exposure of passive samplers to the ambient air above a plot and the transfer factor that is determined simultaneously using the SFR system (chapters 3.2, 3.2.2). Additionally to the secondary peak of plot NH_3 fluxes in time series of concentration fluxes during all sampling sequences except for G1 (figure 5.5), transfer factors during day time feature comparably low values (figure 5.7), which translates into a low fraction of NH_3 emitted by the SFR tube system being recovered in the respective passive samplers (chapter 4.3.1, equation 8). This is due to a high efficiency of atmospheric mixing and

transport away from the plot surface and further amplifies the secondary peak observed in NH_4^+ concentration fluxes when calculating NH_3 volatilization fluxes (equation 10).

6.2 Modelling of SCM transfer factors

Prediction of SCM transfer factors relating NH_4^+ concentrations in the passive sampler acid solution to plot NH_3 fluxes by parametrizing linear models with wind speed and air temperature records as well as relative humidity and bulk Richardson number upon availability was only successful in the case of some sampling sequences (also see Hypothesis 2, Chapter 2). Models were fitted per sampling sequence as well as for combined data from multiple sampling sequences, depending on data availability and optimized as described in Chapter 4.4. Quality of the model fits was assessed by calculating the Nash-Sutcliffe model efficiency coefficient NSE (Nash and Sutcliffe, 1970; see Chapter 4.4). A model NSE higher than 0.65 can be considered as a threshold value for an acceptable model efficiency (Ritter and Muñoz-Carpena, 2013; Moriasi et al., 2007). This value is outreached by optimized single models for sampling sequences G1, M1 and G2 (see Figure 5.9). In contrast, the NSE value for G3 (0.16) is clearly below the threshold. For G4, the optimized single model NSE of 0.48 is just under the relaxed threshold value of 0.5 as proposed by Moriasi et al. (2007). Likewise, the NSE of the overall model (0.25) is clearly below the 0.5 and 0.65 threshold values (figure 5.9). Supportingly, model residuals relative to the original transfer factors of the insufficiently efficient models (Table 5.1) are considerably higher than of the G1, M1 and G2 models, with the exception of the G4 case where relative residuals are smaller than for G1 and G2 models, while NSE is below 0.5.

The outcome of the optimization process as described in Chapter 4.4 consists of quite different sets of optimal parameters (see Table 5.1). While wind speed and air temperature are the most frequent parameters, which corresponds to the expectations (Sommer et al., 1991; Sommer et al., 2003; Sommer et al., 2005), none of these two parameters is part of all optimal model parametrizations nor always significant. Relative humidity and bulk Richardson number could only contribute to the model efficiency of M1 and G2 (relative humidity) and G2 (bulk Richardson number). Further, in the case of M1 and G3, none of the parameters of the optimal model were significant, which means that a ANOVA test resulted in parameter p-values higher than 0.05 (Fahrmeir et al., 2013). For G2, only half of the four optimal parameters proved to be significant. It was not possible to identify one or two variables that played a major role in determining the transport characteristics for all sampling sequences. These findings show that the importance of meteorological quantities determining the transport efficiency varied between the sampling

sequences. They further imply that for some sampling sequences, near-surface transport could not be characterized by the selected meteorological quantities of this experiment. Together, this might explain why the overall model resulted in quite poor NSE values.

Taking together these observations, we only had partial success in fitting an efficient and significanlty parametrized model for single sampling sequences, as was hypothesized (chapter 2), and failed to find a sufficiently good overall model fit that integrates all data recorded during the five sampling sequences. This illustrates the apparent diversity of near-surface transport regimes being present during our experiments. The chosen set of meteorological parameters was only for some sampling sequences (G1, M1, G2) appropriate to describe most part of the features of the transport of gaseous NH_3 from the plot surface or the SFR system to the passive sampler solution as indicated by the NSE. But even in these optimal models yielding an acceptable NSE, parametrizations are not thoroughly significant. While for G1, the only parameter of the optimal fit is significant, none of the optimal parameters of M1 and only half of the four parameters of the optimal G2 fit significantly contribute to explaining the observed patterns in SCM transfer factors (see Table 5.1). It is probable that we failed to select the right set of parameters to describe atmospheric transport efficiency, or that an empirical linear model is not appropriate to represent the underlying processes of turbulent transport.

Atmospheric transport is mainly determined by the intensity of turbulent mixing and advection. Wind speed directly contributes to advection and turbulent kinetic energy by the production of shear (Foken and Napo, 2016). Higher air temperature alone, and similarly air humidity, do not directly lead to increased turbulence, but can come along with stronger gradients and more available energy for the development of bouyancy fluxes, which indirectly adds to the turbulence intensity. Thus, it is surprising that wind speed turned out to be part of the optimal model parameter set only in the case of three single sampling sequences, thereof two significantly. In contrast, four single model parameter sets contain air temperature, which in one case is significant. In the G2 case, relative humidity is the most significant factor (see Table 5.1), together with wind speed. This leads to the assumption that transfer factors as determined for the SCM do not only contain information on the pure atmospheric, turbulent and advective transport. Also other processes taking place on the way from the gas cylinder pressure valve and flowmeter to the passive sampler, modifying the fraction of released NH_3 being recovered and determined in the acid solution, can potentially have an substantial effect and can be influenced by, for example, air humidity. Gericke et al. (2011) mention the effect of dew formation on the SFR tube system and subsequent dissolution of gaseous NH_3 in the dew droplets, which may lead

to its interception and thus reduction of the amount of NH_3 reaching the passive sampler. In our case, dew formation in the night and morning hours was frequently observed on the SFR system as well as on the passive sampler mesh screens (see Chapter 3.3). This may have caused a reduction of transfer factor values (equation 9), followed by an overestimation of true NH_3 fluxes from experimental plot surfaces. This is only the case if a larger percentage of NH_3 is intercepted by dew on the SFR system and the respective passive samplers taken together than on experimental plot passive sampler mesh screens. This can be assumed as the SFR system adds additional surface for dew formation and subsequent NH_3 interception along the transport path of NH_3 on reference plots compared to the rather direct soil-to-passive sampler transport path on experimental plots.

The attempt to include the bulk Richardson number did not result in major improvements of the predictive power of the transfer factor models, as it is only part of the optimal parameter set in the G2 case, but is not significant (p-value < 0.05). This can be explained by the dynamical sublayer as proposed by Foken and Napo (2016) in accordance with Monin and Obukhov (1954). This lowest part of the turbulent layer, where NH_3 transport and exchange processes from the plot surface to the passive sampler took place in this experiment, is not influenced by atmospheric stability but is rather nearly neutral all the time. This means that trying to improve a model describing processes within the dynamic sublayer by including a measure of atmospheric stability is not reasonable given the existing micrometeorological theory on the near-surface atmosphere.

6.3 Replacement of the SFR system by model predictions

By comparing NSE values of single-sequence optimal models and optimal models fitted on combined data from a complementary set of sampling sequences, the ability of these complementary models to predict SCM transfer factors was assessed in order to answer the third hypothesis of this study (chapter 2). As Figure 5.9 reveals, all complementary model NSE values are substantially lower than their single-sequence counterparts. With exception of G1, all of them are even below zero. This means that they are worse in predicting SCM transfer factors than the null model, which is a simple mean of the original data. Also the G1 complementary model NSE value is far distant from the threshold value of 0.5 or 0.65, respectively (see Chapter 6.2; Ritter and Muñoz-Carpena, 2013; Moriasi et al., 2007). It is interesting that the complementary model for the M1 sampling sequence on Field A, which was fitted on data from Field B, is still better than the two complementary models fitted on Field B data for G2 and G3 on the same field. Apparently, differing surface conditions (grass-clover vs. maize field) and surrounding obstackle

structures were not the main factors causing the difference between data from both fields. This shows that based on the field conditions observed during our measurement campaigns, it was not possible to find models that represent common features relevant for the efficiency of atmospheric NH_3 transport represented by the SCM transfer factors. The easiest explanation for this finding would be that the meteorological conditions during the four sampling sequences on Field B and the one Field A sequence were too different for representation in a common model. At least the G2 and G3 sampling sequences on Field B, as well as M1, were all characterized by relatively high temperatures, a day/night wind regime and no precipitation during the main part of the measurements (figure 5.1). Nevertheless, they resulted in very different single-sequence model parametrizations. This makes it unlikely that the differences are reflected in the meteorological parameters investigated in this study. Rather, other processes that could not be observed due to the chosen instrumentations and parameter set are likely to have caused the differences. An alternative version of this explanation would be that one of the five sampling sequences investigated is very much different from the others, which leads to contradictary information entering the model optimization and fitting process. Looking at optimized single-sequence model parametrizations (Table 5.1) and NSE values (see Figure 5.9), G3 is most likely to be the sampling sequence in question. In this case, the high p-value of air temperature as the remaining variable after model optimization, as well as the NSE indicate that the relation between any kind of meteorological information provided and transfer parameters is ambiguous. Trying to fit complementary models while excluding G3 data might help to clarify this question.

Another option for explanation is that the datasets used for fitting both single-sequence and complementary models do not comprise enough data points to obtain a representative model fit. The ALFAM2 model was fitted on data from nearly 6000 measurement intervals, aiming to provide a generalizable model for estimating NH_3 emissions at least for the source area of the data. Even if this present study rather aimed to find a model for the site-specific conditions of NH_3 transport, another more comparable empirical model developed by Menzi et al. (1998) is based on data from 15 field experiments, each comprising 6-12 sampling sequences. Also, the process-based model developed by Génermont and Cellier (1997) used data in 15-min intervals from a two-week period. This shows that longer time series of SFR system data might be important to obtain more representative and significant model parametrizations.

Further, a linear model based on measurements of mean quantities might not be appropriate to model SCM transfer factors as a measure of NH_3 transport efficiency. The transfer factors of the SCM method integrate multiple processes that can not be distinguished without further

investigation. This encompasses turbulent transport from the surface to the passive sampler, advection of air from outside the plot area, dissolution in the passive sampler acid solution and interception of NH_3 on its way from the flowmeter to the passive sampler solution as discussed in Chapter 6.2. The dependence of these processes on environmental and meteorological conditions differs. While dissolution and interception of NH_3 is non-linearly temperature-dependent according to Henry's law (Smith, Harvey, et al., 2007), advection is linearly dependent on the horizontal wind speed. The eddy diffusivity determining the effectiveness of turbulent transport is strongly stability-dependent (Foken and Napo, 2016). As the processes considered here are taking place in the dynamic sublayer (see discussion in Chapter 6.2), stratification is not relevant here. Considering the substantial uncertainties of both theoretical parametrizations (for example bulk coefficients or universal functions) and measurements needed to describe the relevant processes, linear parametrization might still be a more useful alternative than arranging a complex process-based model based on uncertain theory.

6.4 Plot N balance

Measurements of NH_3 volatilization during the five fertilizations of this experiment contributed to closing the plot N balance and tracing the fate of N after its application (Frick et al., 2018) on Field B (Hypothesis 4, Chapter 2). This is confirmed by reduced average plot N balance gaps of Slu and Min treatments after consideration of volatilization losses (see Table 5.3). It did not result in a complete closure of the plot N balances for Field B, as there is still a significant gap between the amounts of N applied and recovered or traced by the measurements. On Field A, adding data on NH_3 volatilization rather resulted in an slight enlargement of the N balance gap (Table 5.3), which will be discussed in the end of this Chapter. Compared to commonly observed total plant and soil ^{15}N recoveries (Bosshard et al., 2009; Douxchamps et al., 2011) of between 31 % (Bosshard et al., 2009) and 82 % for faeces and manure as organic fertilizer, respectively, an average to high amount of ^{15}N could be recovered in this study.

On Field B, regrowth of grass-clover biomass in the time between the last cut just before the last fertilizer application G4 (25th September 2018) and the soil sampling for total residual N values on the 16th October 2018 may well have caused lower total recoveries than on Field A plots. The N absorbed by plant growth in this period was not recorded as biomass harvest and thus not included in the N balance as presented here, as a follow-up biomass sampling did not take place until spring 2019. This might have contributed to the gap in ^{15}N recoveries on Field B.

Due to the heavy drought during the summer of 2018, the soil water balance was negative during the entire time period considered. Due to a lack of available water, transport of fertilizer N with percolate water from the surface below the rooting depth is unprobable - rather, soil water was moved upwards by capillary lift. Further, analyis of the data on NO_3^- interception by the SIA samplers (Frick 2019, unpublished data) showed no effect of the plot fertilizer treatment and featured low and highly variable values for the resulting leaching of NO_3^- below the rooting depth, which supports the assumption that leaching is not relevant for this plot N balance.

Plant N use efficiency of mineral N fertilizer was found to be higher compared to slurry as an organic fertilizer, indicated by the higher fractions of fertilizer N absorbed by plants on Min plots (Table 5.3). This corresponds to the current understanding of soil N dynamics and fertilizer use and values obtained in this study (20.9 % on Field A, 15.8 % on Field B, see Table 5.3) are close to the values found by Muñoz et al. (2003). N in organic fertilizers such as slurry is partially organically bound and thus not available for plant uptake, it first requires mineralization (Jensen, 2013; Robertson and Groffman, 2015). The remaining organic matter, including the bound N, becomes increasingly recalcitrant and thus stable against decay (Jensen, 2013), which makes a portion of the organic fertilizer N virtually unusable for plant uptake or only over very long time spans. High N use efficiencies on Min plots might also be a result of lower amounts of total N applied in the Min treatment compared to the Slu treatments, as the amount of N fertilizer was adjusted to the TAN of the parallel slurry treatment. Plants on Min plots could have been comparatively limited in growth by low availability of N relative to plants on Slu plots, resulting in more efficient N uptake (Peng et al., 2006; Tilman et al., 2011).

The fraction of not directy available organic N applied to Slu plots in large part remains in the soil and results in a shift of fertilizer N partitioning between above-ground biomass and soil pools when compared with Min plots. This is reflected in the data of this experiment, as mineral fertilizer N was mainly recovered in the plant biomass, while slurry N was predominantly found back in the soil column below the experimental plots (Table 5.3). In theory, total numbers of soil and aboveground biomass recovery should not be influenced by shifts in soil-plant partitioning due to different availabilities of fertilizer N. This in contrast to this study's findings, as recoveries of slurry-derived ^{15}N were found to be considerably higher than recoveries of ^{15}N originating from mineral fertilizer (Table 5.3). This also contradicts the results found by Bosshard et al. (2009) and Thomsen and Jensen (1994), who consistently found higher ^{15}N recoveries of previously added mineral than organic fertilizer. Multiple aspects suggest that potentially, a systematic overestimation of ^{15}N on Slu plots might explain these findings: On Slu plots, infiltration of the

applied ^{15}N-labelled slurry is likely to be incomplete as until deep soil sampling, bands of dried slurry could be observed on the plot surfaces. In case particles of this ^{15}N enriched material ended up in the soil samples, resulting ^{15}N recoveries are probable to erroneously have increased resulting total soil and plant ^{15}N recoveries for Slu plots. This is further supported by numbers provided in a review by Chalk et al. (2019) from multiple field studies: Reported total plant and soil ^{15}N recoveries after the application of ^{15}N-labelled manure are consistently lower than the ones in this study. Similarly high recoveries as we found were only reported for fertilizers with a higher solid content such as sheep manure or solid feces only. Calculating ^{15}N recoveries in soil pools is very much dependent on correct measures of the soil sceletal fraction, which might cause further uncertainties in the calculation of the residual soil ^{15}N recovery. The soil skeletal fraction may be spacially heterogeneous and was only roughly estimated in the field (see Chapter 3.3). Additonally, stones in soil samples sieved to $< 2\,mm$ may have compromized the homogeneities of the subsamples used for analysis on the mass spectrometer. These potential sampling and measurement errors are generally independent of the plot location or fertilizer treatment and thus likewise increase the uncertainty of all treatments.

Also, the fact that on Field A, adding data on NH_3 losses resulted in an enlargement of the N balance gap (Table 5.3) rather than closing it, as intended, might also be related to uncertainties and systematic errors in measuring ^{15}N recoveries: While for Min plots on Field A, as mentioned, NH_3 volatilization was calculated to be negative due to potential background concentration correction errors, measured NH_3 volatilization from Slu plots overcompensated the N balance gap. In case ^{15}N recoveries on Slu plots is overestimated as discussed above, this inconsistency might vanish and turn into a case of especially high total recovery of fertizer ^{15}N.

6.5 Methodological aspects

With NH_3 being an aggressive gas (Davies, 2006), handling of pressurized gas mixtures containing NH_3 requires special equipment. Armatures like the flow meters and the two-stage pressure valves were custom-assembled for the purpose of this experiment, and the gas mixture had to be especially prepared. This made acquisition of material quite expensive, final costs were comparable to the rental fees for a sonic anemometer wind tracking system needed for a backwards-Lagrangian modelling approach (Gericke et al., 2011; Loubet et al., 2018). Additionally, storing, transporting and handling $50\,L$ gas cylinders in the field requires caution and raised difficulties. Fluctuations in gas flux released from the gas cylinders, as reported by Vandré and Kaupenjohann (1998) and Gericke et al. (2011), could not be observed during this study, even if the pressure of the gas

mixture dropped with increasing depletion of the gas stocks. Obviously, the fluctuations were avoided by choosing a gas mixture of $10\,\%$ NH_3 in N_2 and by pressure control valves providing a constant output pressure for regulating the flux using the flow meter's input needle valves.

Along the $80\,m$ plot strip, presence of trees and a hedgerow of up to $20\,m$ height in the south and east (chapter 3.1.2) on average did not cause significant divergences of wind speed (figure 5.4) during two sampling sequences on Field B (G1, G2) and Field A (M1). Nevertheless, if sampling sequences on Field B are considered separately, slight divergences between both ends of the plot strip could be observed. While for G1, the western end of the measurement strip featured slightly higher wind speeds than the eastern end, the opposite could be observed for G2. According to this finding, on average, it can be assumed that conditions of turbulence were homogenous for all plots, which is a precondition for applying the SC method to infer NH_3 emissions from plot passive diffusion sampler measurements. During the experiments, it was not checked if meteorological conditions diverged between the experimental plots and the SFR system which was located $10\,m$ closer to the forest edge than the experimental plots. In such a close proximity to obstackles, influence of the flow distortion can strongly differ depending on the distance to the obstackle (Foken and Napo, 2016), especially in a leeward situation. Underestimation of the wind speed on SFR system plots compared to experimental plots could lead to an underestimation of NH_3 release rates from experimental plots (Lavrsen Kure et al., 2018).

Theoretically, and as claimed by Vandré and Kaupenjohann (1998), the amount of NH_3 trapped in the passive samplers should be proportionate to the amount released, independent of the release rate. However, it seems that at higher release rates the efficiency in trapping NH_3 in the passive sampler's acid solution is higher, which is indicated by the ratio between passive flux sampler NH_4^+ concentrations from low and high outflux SFR systems (chapter 5.2) exceeding the expected value of 2. Wulf et al. (2002) explains similar observations by the technical difficulty to maintain constant NH_3 flux from the gas cylinders into the SFR system. This explanation is unlikely for the experiments in this study as no irregularities in gas flux could be observed and combinations of pressure relief valves and flowmeters were used interchangeably for high and low flux levels. Thus, this effect must be caused by conditions of turbulent transport as well as diffusion and resolution of NH_3 in the passive sampler solution that does not conform to the assumptions. NH_3 capturing efficiency is not correlated with differing atmospheric transport conditions caused by the location of reference plots in the field, as high and low flux level reference plots were not always on the same positions, and as the effect is observable for all sampling sequences. Even an

incomplete mixing of the ambient air with the NH_3 enriched air released from the SFR system tubes on its way to the passive samplers, which would have the effect of over- or underestimating the overall amount of NH_3 released from the reference plots, does not lead to differences in NH_3 capture between SFR systems. This is because turbulent mixing, incomplete or not, should be similar for both SFR system replicates irrespective of the NH_3 release rate as their geometries are the same. It can be speculated that NH_3 gas reacted with dew in and on the SFR system tubes, passive samplers and directly adjacent grass, as reported by Gericke et al. (2011). This could potentially have had a disproportionate effect on the amount of NH_3 reaching the passive samplers on low flux reference plots.

The correction of passive sampler NH_4^+ data for evaporation and dilution during the exposure time reduced variance of the data. This indicates that local inhomogeneities in potential evaporation might be jointly resposible for great differences between treatment replicates, and the method chosen to compensate for these effects improved the quality of the data. However, the method used to track evaporation and dilution during the measurements still has to be validated, especially as the range of values obtained for evaporation and dilution is quite high (5.6) and to my knowledge, there is no report on similar methods in the literature up to now. In Pacholski (2016), the change in volume of sampler solution is used for correcting for dilution and evaporation, which was not applicable in this study due to the construction of the passive samplers. It could not be assured to remove the acid solution volumetrically from the passive samplers. Potential sources of error are contamination of the sampler solutions by dust or dirt containing the tracer molecule HPO_4^{2-} and lab measurement errors.

Similarly to the observations reported in Wulf et al. (2002) and Svensson (1994), a relation between transfer factors and time of day could be observed (see Figures 5.7, 5.8), also reflected in NH_3 volatilization rates (see Figure 5.12). As discussed in Wulf et al. (2002), this can be assigned to the temperature dependency of NH_3 solubility and the equilibrium between NH_3 and NH_4^+ in aqueous solutions according to Henry's law, which also applies to cattle slurry.

Determination of the bulk Richardson number turned out to suffer from the arrangement of the two-level psychrometer measurements of air temperature and humidity. The differences in these parameters between $2\,m$ and $4\,m$ height were quite small and partially fluctuating in sign. This resulted in high-amplitude variations in the bulk Richardson number time series, compromizing their information content. Potentially, the quality would have improved if the distance between instrument heights would have been maximized, for example with an arrangement at $0.5\,m$ and

4 m height, profiting from the logarithmic height-dependence of most meteorological parameters in the boundary layer (Foken and Napo, 2016).

7 Conclusions

After five applications of ^{15}N-labelled cattle slurry, ammonium nitrate and from a $0\,N$ control treatment, I collected data on the volatilization of NH_3 by applying the Standard Comparison Method (SCM). This was possible by combining the SCM with a modelling approach to predict transfer factors from meteorological observations. Linear models fitted for individual measurement sequences could for the most part successfully predict transfer factors of the same measurement sequence, helped to close data gaps due to failures of the Standard Flux Reference (SFR) system and ensured the availability of complete data on NH_3 volatilization for all sampling sequences. Obtained NH_3 fluxes and cumulative losses were comparable to values reported in the literature and to the recent ALFAM2 model. Thus, it was possible to contribute quantitative information on the loss of NH_3-N after five slurry applications to the superordinate research project, which is aiming to establish a soil-system N balance on the two experimental sites over a period of 2.5 years (Frick et al., 2018). This study shows that tracing the fate of fertilizer N in the field by combining a ^{15}N isotope enrichment method (Douxchamps et al., 2011) with a micrometeorological approach to quantify gaseous NH_3 losses can result in relatively complete and accurate recoveries of fertilizer N. Nevertheless, a complete closure of the N balance of fertilization plot experiments remains challenging due to the various factors and technical difficulties that can influence fertilizer distribution, sampling representativeness and unforeseen effects that come with exposing an experimental setup to field conditions. The chosen approach to find a common, meteorology-based parametrization based on multiple measurement sequences and being able to replace SCM transfer factors failed in this experiment. As measuring sequences were unique in their combinations of transfer factors and meteorological conditions as can be seen in the different parametrizations of optimized single-sequence models, type and amount of calibration data was not sufficient to represent the meteorological processes driving NH_3 transport from the plot surface to the passive sampler solution.

Overall, despite its conceptional simplicity, the SCM method turned out to be less flexible and more costly than expected. As the similarity of measured results and ALFAM2 predictions indicates, it can be reasonable to use advanced, but simple semi-empirical models such as the

ALFAM2 model for obtaining data on the volatilization of NH_3 from cattle or pig slurry, as they are able to provide comparable information at lower costs and effort. Calibrating the ALFAM2 model for other kinds of organic fertilizers, such as biogas digestate, mulches and composts, and strengthening its empirical base might extend its scope and reduce the need for complex micrometeorological methods in multiplot field experiments. Otherwise, it can be also expected that techniques such as inverse dispersion models further improve in their experimental simplicity and applicability. This would bring about the ability to simplify research on the environmental implications of agricultural production, such as emissions of NH_3. Such a profound base of knowledge would globally simplify and accelerate the search for sustainable alternatives in farming and their evaluation, which is urgently needed.

Bibliography

Amt für Geoinformation (2019). *Web GIS client Kanton Solothurn.* URL: `https://geo.so.ch/map/?t=boden`.

Appl, Max (1982). 'The Haber-Bosch process and the development of chemical engineering'. *A century of chemical engineering. Plenum, New York*, pp. 29–53.

Asman, W and Sutton Mand Schjørring, J (1998). 'Ammonia: emission, atmospheric transport and deposition'. *The New Phytologist* 139.1, pp. 27–48.

Baldocchi, D, Hincks, B, and Meyers, T (1988). 'Measuring biosphere-atmosphere exchanges of biologically related gases with micrometeorological methods'. *Ecology* 69.5, pp. 1331–1340.

BayCEER (2019). *Environmental Observation System BayEOS.* URL: `http://www.bayceer.uni-bayreuth.de/bayeos/index.php?lang=en`.

Bischoff, WA (2008). 'Development and applications of the self-integrating accumulators: a method to quantify the leaching losses of environmentally relevant substances'.

Bosshard, C, Sørensen, P, Frossard, Emmanuel, Dubois, D, Mäder, P, Nanzer, S, and Oberson, A (2009). 'Nitrogen use efficiency of 15 N-labelled sheep manure and mineral fertiliser applied to microplots in long-term organic and conventional cropping systems'. *Nutrient cycling in agroecosystems* 83.3, pp. 271–287.

Bouwman, AF, Boumans, LJM, and Batjes, NH (2002). 'Estimation of global NH3 volatilization loss from synthetic fertilizers and animal manure applied to arable lands and grasslands'. *Global Biogeochemical Cycles* 16.2, pp. 8–1.

Bundesamt für Energie (2018). *Windpotentialanalyse für Windatlas.ch: Jahresmittelwerte der modellierten Windgeschwindigkeit und Windrichtung - Bericht zur Aktualisierung des Windatlas von 2016.* Tech. rep.

Campbell Scientific Inc. (2009). *Wind Monitors User Guide.* Campbell Scientific Ltd. Loughborough, UK. URL: `www.campbellsci.co.uk`.

Campbell Scientific Inc. (2016). *A100LK Anemometer Instruction Manual.* Campbell Scientific Ltd. Loughborough, UK. URL: `www.campbellsci.co.uk`.

Chalk, Phillip M, Inácio, Caio T, and Chen, Deli (2019). 'Tracing the dynamics of animal excreta N in the soil-plant-atmosphere continuum using 15N enrichment'.

Chambers, B, Dampney, P, et al. (2009). 'Nitrogen efficiency and ammonia emissions from urea-based and ammonium nitrate fertilisers.' *Proceedings-International Fertiliser Society*. 657. International Fertiliser Society.

Davies, M (2006). 'Corrosion by ammonia'. *ASM Handbook* 13, pp. 727–735.

Denmead, OT (1983). 'Micrometeorological methods for measuring gaseous losses of nitrogen in the field'. *Gaseous loss of nitrogen from plant-soil systems*. Springer, pp. 133–157.

Di, HJ, Cameron, KC, and McLaren, RG (2000). 'Isotopic dilution methods to determine the gross transformation rates of nitrogen, phosphorus, and sulfur in soil: a review of the theory, methodologies, and limitations'. *Soil Research* 38.1, pp. 213–230.

Dittert, K, Goerges, T, and Sattelmacher, B (1998). 'Nitrogen turnover in soil after application of animal manure and slurry as studied by the stable isotope 15N: a review'. *Zeitschrift für Pflanzenernährung und Bodenkunde* 161.4, pp. 453–463.

Douxchamps, S, Frossard, E, Bernasconi, SM, Van der Hoek, R, Schmidt, A, Rao, IM, and Oberson, A (2011). 'Nitrogen recoveries from organic amendments in crop and soil assessed by isotope techniques under tropical field conditions'. *Plant and soil* 341.1-2, pp. 179–192.

Eckelmann, W, Sponagel, H, Grottenthaler, W, Hartmann, K-J, Hartwich, R, Janetzko, P, Joisten, H, Kühn, D, Sabel, K-J, and Traidl, R (2006). 'Bodenkundliche Kartieranleitung. KA5'.

Erisman, JW, Galloway, JN, Seitzinger, S, Bleeker, A, Dise, NB, Petrescu, AM, Leach, AM, and Vries, W de (2013). 'Consequences of human modification of the global nitrogen cycle'. *Philosophical Transactions of the Royal Society B: Biological Sciences* 368.1621, p. 20130116.

European Parliament, Council of the European Union (2006). 'Directive 2006/118/EC of the European Parliament and of the Council of 12 December 2006 on the protection of groundwater against pollution and deterioration'. *Official Journal of the European Union* 372, pp. 19–31.

Fahrmeir, L, Kneib, T., Lang, S, and Marx, B (2013). *Regression: models, methods and applications*. Springer Science & Business Media.

Federal Office of Topography swisstopo (2019). *Maps of Switzerland - Swiss Confederation*. URL: `https://map.geo.admin.ch/`.

Ferm, M (1998). 'Atmospheric ammonia and ammonium transport in Europe and critical loads: a review'. *Nutrient Cycling in Agroecosystems* 51.1, pp. 5–17.

Flesch, TK, Wilson, JD, Harper, LA, Crenna, BP, and Sharpe, RR (2004). 'Deducing ground-to-air emissions from observed trace gas concentrations: a field trial'. *Journal of Applied Meteorology* 43.3, pp. 487–502.

Flesch, TK, Wilson, JD, and Yee, E (1995). 'Backward-time Lagrangian stochastic dispersion models and their application to estimate gaseous emissions'. *Journal of applied meteorology* 34.6, pp. 1320–1332.

Foken, T and Napo, CJ (2016). *Micrometeorology*. Vol. 2. Springer.

Frick, H, Oberson, A, Frossard Eand Wettstein, HR, and Bünemann, EK (2018). 'Tracing the fate of 15N-labelled animal manure in the environment'.

Galloway, JN (1998). 'The global nitrogen cycle: changes and consequences'. *Environmental pollution* 102.1, pp. 15–24.

Génermont, S and Cellier, P (1997). 'A mechanistic model for estimating ammonia volatilization from slurry applied to bare soil'. *Agricultural and Forest Meteorology* 88.1-4, pp. 145–167.

Génermont, S, Cellier, P, Flura, D, Morvan, T, and Laville, P (1998). 'Measuring ammonia fluxes after slurry spreading under actual field conditions'. *Atmospheric Environment* 32.3, pp. 279–284.

Gericke, D, Pacholski, A, and Kage, H (2011). 'Measurement of ammonia emissions in multi-plot field experiments'. *Biosystems engineering* 108.2, pp. 164–173.

Guthrie, S, Giles, S, Dunkerley, F, Tabaqchali, H, Harshfield, A, Ioppolo, B, and Manville, C (2018). 'The impact of ammonia emissions from agriculture on biodiversity'.

Hafner, SD (2019). *ALFAM2-data*. `https://github.com/sashahafner/ALFAM2-data`.

Hafner, SD, Pacholski, A, Bittman, S, Burchill, W, Bussink, W, Chantigny, M, Carozzi, M, Génermont, S, Häni, C, Hansen, MN, et al. (2018). 'The ALFAM2 database on ammonia emission from field-applied manure: Description and illustrative analysis'. *Agricultural and Forest Meteorology* 258, pp. 66–79.

Hafner, SD, Pacholski, A, Bittman, S, Carozzi, M, Chantigny, M, Génermont, S, Häni, C, Hansen, MN, Huijsmans, J, Kupper, T, et al. (2019). 'A flexible semi-empirical model for estimating ammonia volatilization from field-applied slurry'. *Atmospheric environment* 199, pp. 474–484.

Häni, C, Sintermann, J, Kupper, T, Jocher, M, and Neftel, A (2016). 'Ammonia emission after slurry application to grassland in Switzerland'. *Atmospheric environment* 125, pp. 92–99.

Hansen, B, Thorling, L, Schullehner, J, Termansen, M, and Dalgaard, T (2017). 'Groundwater nitrate response to sustainable nitrogen management'. *Scientific reports* 7.1, p. 8566.

Hastie, Trevor J (2017). *Statistical models in S*. Routledge.

Hunkeler, D., Sonney, R., Paratte, D., Tallon, L., Gerber, C., and Purtschert, R. (2015). *Nitratprojekt Gäu-Olten: Hydrochemische Erkundung des Grundwasserleiters und Bestimmung der Altersstruktur*. Report.

Jensen, LS (2013). 'Animal manure fertiliser value, crop utilisation and soil quality impacts'. *Animal manure recycling: Treatment and management*, pp. 295–328.

Jokela, WE and Randall, GW (1987). 'A Nitrogen-15 Microplot Design for Measuring Plant and Soil Recovery of Fertilizer Nitrogen Applied to Corn 1'. *Agronomy journal* 79.2, pp. 322–325.

Kim, DG, Vargas, R, Bond-Lamberty, B, and Turetsky, MR (2012). 'Effects of soil rewetting and thawing on soil gas fluxes: a review of current literature and suggestions for future research'. *Biogeosciences* 9.7, pp. 2459–2483.

Lavrsen Kure, J, Krabben, J, Vilms Pedersen, S, Carozzi, M, and Sommer, S (2018). 'An Assessment of Low-Cost Techniques to Measure Ammonia Emission from Multi-Plots: A Case Study with Urea Fertilization'. *Agronomy* 8.11, p. 245.

Lockyer, DR (1984). 'A system for the measurement in the field of losses of ammonia through volatilisation'. *Journal of the Science of Food and Agriculture* 35.8, pp. 837–848.

Loubet, B, Carozzi, M, Voylokov, P, Cohan, J. P., Trochard, R, and Génermont, S (2018). 'Evaluation of a new inference method for estimating ammonia volatilisation from multiple agronomic plots'. *Biogeosciences* 15.11, p. 3439.

Louro, A, Sawamoto, T, Chadwick, D, Pezzolla, D, Bol, R, Báez, D, and Cardenas, L (2013). 'Effect of slurry and ammonium nitrate application on greenhouse gas fluxes of a grassland soil under atypical South West England weather conditions'. *Agriculture, ecosystems & environment* 181, pp. 1–11.

Meisinger, JJ and Jokela, WE (2000). 'Ammonia volatilization from dairy and poultry manure'. *Proceedings from managing nutrients and pathogens from animal agriculture*, pp. 334–354.

Menzi, H, Katz, PE, Fahrni, M, Neftel, A, and Frick, R (1998). 'A simple empirical model based on regression analysis to estimate ammonia emissions after manure application'. *Atmospheric Environment* 32.3, pp. 301–307.

MeteoSchweiz (2019). *Klimabulletin Jahr 2018*. Tech. rep. Meteoschweiz.

Misselbrook, TH, Nicholson, FA, Chambers, BJ, and Johnson, RA (2005). 'Measuring ammonia emissions from land applied manure: an intercomparison of commonly used samplers and techniques'. *Environmental Pollution* 135.3, pp. 389–397.

Monin, AS and Obukhov, AM (1954). 'Basic laws of turbulent mixing in the surface layer of the atmosphere'. *Contrib. Geophys. Inst. Acad. Sci. USSR* 151.163, e187.

Moriasi, DN, Arnold, JG, Van Liew, MW, Bingner, RL, Harmel, RD, and Veith, TL (2007). 'Model evaluation guidelines for systematic quantification of accuracy in watershed simulations'. *Transactions of the ASABE* 50.3, pp. 885–900.

Muñoz, Gabriela R, Powell, J Mark, and Kelling, Keith A (2003). 'Nitrogen budget and soil N dynamics after multiple applications of unlabeled or 15 Nitrogen-enriched dairy manure'. *Soil Science Society of America Journal* 67.3, pp. 817–825.

Nash, JE and Sutcliffe, JV (1970). 'River flow forecasting through conceptual models part I—A discussion of principles'. *Journal of hydrology* 10.3, pp. 282–290.

Oelmann, M, Czichy, C, Scheele, U, Zaun, S, Dördelmann, O, Harms, E, Penning, M, KAUP, EM, Bergmann, A, and Steenpaß, C (2017). 'Quantifizierung der landwirtschaftlich verursachten Kosten zur Sicherung der Trinkwasserbereitstellung'. *UBA Texte* 43, p. 2017.

Pacholski, A (2016). 'Calibrated passive sampling-multi-plot field measurements of NH3 emissions with a combination of dynamic tube method and passive samplers'. *Journal of visualized experiments: JoVE* 109.

Pacholski, A, Cai, G, Nieder, R, Richter, J, Fan, X, Zhu, Z, and Roelcke, M (2006). 'Calibration of a simple method for determining ammonia volatilization in the field–comparative measurements in Henan Province, China'. *Nutrient Cycling in Agroecosystems* 74.3, pp. 259–273.

Pain, BF, Phillips, VR, Clarkson, CR, and Klarenbeek, JV (1989). 'Loss of nitrogen through ammonia volatilisation during and following the application of pig or cattle slurry to grassland'. *Journal of the Science of Food and Agriculture* 47.1, pp. 1–12.

Peng, Shaobing, Buresh, Roland J, Huang, Jianliang, Yang, Jianchang, Zou, Yingbin, Zhong, Xuhua, Wang, Guanghuo, and Zhang, Fusuo (2006). 'Strategies for overcoming low agronomic nitrogen use efficiency in irrigated rice systems in China'. *Field Crops Research* 96.1, pp. 37–47.

Pietzner, B, Rücknagel, J, Koblenz, B, Bednorz, D, Tauchnitz, N, Bischoff, J, Köbke, S, Meurer, K, Meißner, R, and Christen, O (2017). 'Impact of slurry strip-till and surface slurry incorporation on NH3 and N2O emissions on different plot trials in Central Germany'. *Soil and Tillage Research* 169, pp. 54–64.

R Core Team (2018). *R: A Language and Environment for Statistical Computing*. R Foundation for Statistical Computing. Vienna, Austria. URL: https://www.R-project.org.

Ritter, A and Muñoz-Carpena, R (2013). 'Performance evaluation of hydrological models: Statistical significance for reducing subjectivity in goodness-of-fit assessments'. *Journal of Hydrology* 480, pp. 33–45.

Robertson, GP and Groffman, PM (2015). 'Nitrogen transformations'. *Soil microbiology, ecology and biochemistry.* Elsevier, pp. 421–446.

Robertson, GP and Vitousek, PM (2009). 'Nitrogen in agriculture: balancing the cost of an essential resource'. *Annual review of environment and resources* 34, pp. 97–125.

Rochette, P, Angers, DA, Chantigny, MH, MacDonald, JD, Gasser, MO, and Bertrand, N (2009). 'Reducing ammonia volatilization in a no-till soil by incorporating urea and pig slurry in shallow bands'. *Nutrient Cycling in Agroecosystems* 84.1, pp. 71–80.

Schneidemesser, E, Kurtzner, R, Münster, A, Staudt, E, Saar, D, Schaap, M, and Banzhaf, S (2016). *Agriculture, Ammonia, and Air Pollution.* Tech. rep. Institute for Advanced Sustainability Studies.

Schweizerische Eidgenossenschaft (1998). „*Gewässerschutzverordnung vom 28. Oktober 1998 (GSchV)*", *SR 814.201.*

Sintermann, J, Dietrich, Ks, Häni, C, Bell, M, Jocher, M, and Neftel, A (2016). 'A miniDOAS instrument optimised for ammonia field measurements'. *Atmospheric Measurement Techniques* 9.6, pp. 2721–2734.

Sintermann, J, Neftel, A, Ammann, C, Häni, C, Hensen, A, Loubet, B, and Flechard, CR (2012). 'Are ammonia emissions from field-applied slurry substantially over-estimated in European emission inventories?' *Biogeosciences* 9.5, pp. 1611–1632.

Sintermann, J, Spirig, C, Jordan, A, Kuhn, U, Ammann, C, and Neftel, A (2011). 'Eddy covariance flux measurements of ammonia by high temperature chemical ionisation mass spectrometry'. *Atmospheric Measurement Techniques* 4.3, pp. 599–616.

Skalar Analytical, BV (2005). 'The SANplus segmented flow analyser: soil and plant analysis'. *Skalar Analytical BV: The Netherlands.*

Smil, Vaclav (2004). *Enriching the earth: Fritz Haber, Carl Bosch, and the transformation of world food production.* MIT press.

Smith, Francis L, Harvey, Allan H, et al. (2007). 'Avoid common pitfalls when using Henry's law'. *Chemical engineering progress* 103.9, pp. 33–39.

Sommer, SG, Génermont, S, Cellier, P, Hutchings, NJ, Olesen, Jørgen E, and Morvan, T (2003). 'Processes controlling ammonia emission from livestock slurry in the field'. *European Journal of Agronomy* 19.4, pp. 465–486.

Sommer, SG and Hutchings, NJ (2001). 'Ammonia emission from field applied manure and its reduction'. *European journal of agronomy* 15.1, pp. 1–15.

Sommer, SG and Jensen, C (1994). 'Ammonia volatilization from urea and ammoniacal fertilizers surface applied to winter wheat and grassland'. *Fertilizer research* 37.2, pp. 85–92.

Sommer, SG, McGinn, SM, and Flesch, TK (2005). 'Simple use of the backwards Lagrangian stochastic dispersion technique for measuring ammonia emission from small field-plots'. *European Journal of Agronomy* 23.1, pp. 1–7.

Sommer, SG, Olesen, JE, and Christensen, BT (1991). 'Effects of temperature, wind speed and air humidity on ammonia volatilization from surface applied cattle slurry'. *The Journal of Agricultural Science* 117.1, pp. 91–100.

Spirig, C, Flechard, CR, Ammann, C, and Neftel, A (2010). 'The annual ammonia budget of fertilised cut grassland–Part 1: Micrometeorological flux measurements and emissions after slurry application'. *Biogeosciences* 7.2, pp. 521–536.

Svensson, L (1994). 'Ammonia volatilization following application of livestock manure to arable land'. *Journal of agricultural engineering research* 58.4, pp. 241–260.

Thompson, RB and Meisinger, JJ (2005). 'Gaseous nitrogen losses and ammonia volatilization measurement following land application of cattle slurry in the mid-Atlantic region of the USA'. *Plant and soil* 266.1-2, pp. 231–246.

Thomsen, Ingrid K and Jensen, Erik S (1994). 'Recovery of nitrogen by spring barley following incorporation of 15N-labelled straw and catch crop material'. *Agriculture, ecosystems & environment* 49.2, pp. 115–122.

Tilman, David, Balzer, Christian, Hill, Jason, and Befort, Belinda L (2011). 'Global food demand and the sustainable intensification of agriculture'. *Proceedings of the National Academy of Sciences* 108.50, pp. 20260–20264.

Van der Weerden, TJ and Jarvis, SC (1997). 'Ammonia emission factors for N fertilizers applied to two contrasting grassland soils'. *Environmental Pollution* 95.2, pp. 205–211.

Vandré, R and Kaupenjohann, M (1998). 'In situ measurement of ammonia emissions from organic fertilizers in plot experiments'. *Soil Science Society of America Journal* 62.2, pp. 467–473.

Whitehead, DC and Raistrick, N (1990). 'Ammonia volatilization from five nitrogen compounds used as fertilizers following surface application to soils'. *Journal of Soil Science* 41.3, pp. 387–394.

Wilson, JD, Thurtell, GW, Kidd, GE, and Beauchamp, EG (1982). 'Estimation of the rate of gaseous mass transfer from a surface source plot to the atmosphere'. *Atmospheric Environment (1967)* 16.8, pp. 1861–1867.

Wulf, S, Maeting, M, and Clemens, J (2002). 'Application technique and slurry co-fermentation effects on ammonia, nitrous oxide, and methane emissions after spreading'. *Journal of environmental quality* 31.6, pp. 1795–1801.

Yang, W, Zhu, A, Zhang, J, Xin, X, and Zhang, X (2017). 'Evaluation of a backward Lagrangian stochastic model for determining surface ammonia emissions'. *Agricultural and Forest Meteorology* 234, pp. 196–202.

Ziesemer, J (2007). 'Energy use in organic food systems'. *Natural Resources Management and Environment Department Food and Agriculture Organization of the United Nations, Rome.*

Eidesstattliche Erklärung

Hiermit versichere ich, Michael Cormann, Matrikelnummer 1234516, diese vorliegende Masterarbeit

Application of ^{15}N labelled slurry in a microplot field study: Ammonia volatilization and plot N balance

selbstständig und ohne fremde Hilfe angefertigt zu haben. Ich habe dabei nur die in der Arbeit angegebenen Quellen und Hilfsmittel benutzt. Die aus den verwendeten Quellen wörtlich oder inhaltlich entnommenen Stellen wurden als solche kenntlich gemacht.

Diese Masterarbeit wurde in gleicher oder ähnlicher Form noch keiner anderen Prüfungsbehörde vorgelegt und auch noch nicht veröffentlicht.

Ich bin mir des Weiteren bewusst, dass eine falsche Erklärung rechtliche Folgen haben kann.

Bayreuth, den 29. Januar 2020 ....

Michael Cormann